Graduate School Form 30
(Revised 08/14)

PURDUE UNIVERSITY
GRADUATE SCHOOL
Thesis/Dissertation Acceptance

This is to certify that the thesis/dissertation prepared

By Kuk Hyun Ahn

Entitled
IMPACT OF ANTHROPOGENIC ACTIVITIES ON HYDROCLIMATOLOGICAL VARIABLES

For the degree of Doctor of Philosophy

Is approved by the final examining committee:

Venkatesh M. Merwade

Laura C. Bowling

Rao. S. Govindaraju

C. S. P. Ojha

To the best of my knowledge and as understood by the student in the Thesis/Dissertation Agreement, Publication Delay, and Certification/Disclaimer (Graduate School Form 32), this thesis/dissertation adheres to the provisions of Purdue University's "Policy on Integrity in Research" and the use of copyrighted material.

Venkatesh M. Merwade

Approved by Major Professor(s): _____

Approved by: Dulcy M. Abraham 10/10/2014

Head of the Department Graduate Program Date

IMPACT OF ANTHROPOGENIC ACTIVITIES ON HYDRO-CLIMATOLOGICAL VARIABLES

A Dissertation

Submitted to the Faculty

of

Purdue University

by

Kuk Hyun Ahn

In Partial Fulfillment of the

Requirements for the Degree

of

Doctor of Philosophy

December 2014

Purdue University

West Lafayette, Indiana

To my parents and family

ACKNOWLEDGEMENTS

I would like to express my gratitude for my advisor, Dr. Venkatesh M. Merwade, for his immeasurable guidance and encouragement throughout my graduate studies. I would also like to extend sincere thanks to my thesis committee members, Dr. Rao Govindaraju, Dr. Laura Bowling and Dr. C.S.P. Ojha, who have provided insights and helpful comments for improving the quality of my research. I especially wish to thank Dr. Bryan C. Pijanowski for his significant input in landuse data, and Dr. Jacques W. Delleur for the travel grant. I also like to thank all my colleagues and friends: Dr. Eunjin Han, Dr. Kwangmin Kang, Dr. Younghun Jung, Dr. Sanjiv Kumar, Dr. Sultan Ahmed, Nikhil Sangwan, Adnan Rajib, Siddharth Saksena, Jessica Holberg, John Newton, Becca Essig, G. Mallya, Richa Ojha, Meenu Ramadas and Dr. Y. Hoque. I am grateful to Jun Myoung Choi for his encouragement and kindness. I will never forget sharing my graduate life with all of you. Last but most crucially, I am truly grateful to my family – father, mother, two sisters, two brothers-in-law, my nephew and pretty nieces. I would not have been able to complete my graduate studies without their unlimited support and encouragement.

TABLE OF CONTENTS

LIST OF TABLES

LIST OF FIGURES

ABSTRACT

Ahn, Kuk-Hyun. Ph.D., Purdue University, August 2014. Impact of anthropogenic activities on hydro-climatological variables. Major Professor: Venkatesh M. Merwade

The natural environment has been significantly affected by anthropogenic activities. Between 1700s and 2000s, agricultural land area had quintupled and the extent of natural vegetation was globally reduced by half. Furthermore many scientists argue that the recent rise in CO_2 levels in the atmosphere is mainly due to anthropogenic activities. Anthropogenic activities may also play a crucial role in the change of the hydro-climatologic variables. In this study, impact of anthropogenic activities on two representative hydro-climatologic variables, temperature and streamflow, is investigated. The variations in temperature occur over larger spatial and time scale, and hence the United States is adopted for studying the impact on temperature. The continental United States includes most of the existing climate types in its large size and geographic variety. On the other hand, streamflow is affected by local environmental factors, including land cover condition and dam construction, and thus it is investigated based on a small regional area.

The three objectives of this study are to: (1) evaluate the impact of anthropogenic activities on temperature in the continental U. S., and compare the impact of anthropogenic activities with natural variability using the AR4 climate models, (2) quantify the change in streamflow by considering both the natural factors and anthropogenic activities, and (3) investigate the impact of land cover change on extreme streamflow.

The first objective is to detect the changes in temperature in the continental United States (CONUS) and attribute these changes to anthropogenic activities by applying the Detection and Attribution methodology. The CONUS is divided into ten regions by using the *K*-mean clustering method. For each region, the Mann-Kendall trend analysis is used to examine the magnitude of change in observed temperature data as well as the data from eight climate models and an ensemble from all climate model outputs. Then the optimal fingerprint method is used to analyze the impact of anthropogenic activities on temperature changes. The results show the trends in the observed temperature of the entire CONUS over the 20th century lie inside the range expected from natural internal climate variability. In the regional analysis, the western U.S. is affected the most from the anthropogenic activities, based on both the results from the optimal fingerprint based detection and attribution analysis, and from comparison of trend between observed and simulated data using the Mann-Kendall test.

In the second objective, the roles of climate impact and anthropogenic activities on streamflow are evaluated using historical streamflow records, in conjunction with trend analysis and hydrologic modeling. In this study, four U.S. states, including Indiana, New York, Arizona and Georgia area used to represent various level of human activity based on population change and diverse climate conditions. Four hydrologic modeling methods, including linear regression, hydrologic simulation, annual balance, and Budyko analysis are then used to quantify the amount of climate impact and anthropogenic activities on streamflow. In conclusion, the results indicate that the impact of anthropogenic activities is higher on streamflow at most gauging stations in all four states compared to climate impact.

The third objective is to investigate the effect of land cover change on the duration and severity of high and low flows by using the Soil Water Assessment Tool (SWAT) model and copulas. High and low flows are defined in terms of percentiles of streamflow. Two watersheds, which have different dominant land covers within the Ohio River basin, are employed to carry out this study. The results show that land cover change explicitly affects the duration and severity of both high and low flows. Increase in the forest area leads to a decrease in the duration and severity in high flow; its significant impact is observed in extreme high flows.

Overall, the results presented in the dissertation indicate that the impact of anthropogenic activities plays an important role in the hydrologic system and certainly should be considered for a better understanding of the hydrologic system.

CHAPTER 1. INTRODUCTION

1.1 Background and Motivation

The natural environment has been significantly affected by anthropogenic activities (Goudie, 2013). Between 1700s and 2000s, agricultural land area quintupled and the extent of natural vegetation was globally reduced by half (Pongratz et al., 2008; Scanlon et al., 2007). Furthermore many scientists argue that the recent rise in CO_2 levels in the atmosphere is mainly due to anthropogenic activities (Ghosh and Brand, 2003). Burning fossil fuels like coal and petroleum is the main cause of increased CO_2. It is recognized that deforestation is the second major cause of increased CO_2. While the amount of carbon released from fossil fuels increased dramatically from 6.15 gigatonnes (33.5 gigatonnes of CO_2) in 1990 to 9.14 gigatonnes in 2010, land use contributed much less; its CO_2 emission level decreased from 1.45 gigatonnes in 1990 to 0.87 gigatonnes in 2010 (Peters et al., 2011). In addition, the impact of anthropogenic activities on the environment can vary with time and from one region to another. For instance, the total cleared area of the Amazon Rainforest went from 202,000 to 672,000 km^2 in thirty years from 1970 to 2000 (Klink and Moreira, 2002) while a majority of land cover in the midwestern U.S. was converted to crop land between 1850 and 1950 (Whitney, 1996).

Anthropogenic activities can also play a crucial role in affecting the hydrologic cycle. Hydrologic cycle mainly includes: precipitation, evapotranspiration, groundwater or groundwater flow, and river runoff. According to Ye et al. (2003), summer (high) flows at the outlet of the Vilui valley have been reduced by up to 55% and winter (low) flows have been increased by up to 30 times due to the construction of a large dam in the Lena River basin. In hydrologic cycle, the alternation of one element can have a huge impact on the whole process. For example, evapotranspiration is decreased by the conversion of natural vegetation into agricultural land and this leads to increased fresh water availability (Gordon et al., 2003). Similarly, urbanization can lead to both increased runoff and decreased groundwater flow (Yang et al., 2010).

Up to now, a significant number of studies have focused on the impact of anthropogenic activities to the hydrologic cycle at the global scale (Santer et al., 1995; Zhang et al., 2007). However, it is critical to note that even small changes in hydrologic processes or variables at global scale can seriously affect the hydrology of a smaller region (Leemans and Eickhout, 2004). For example, precipitation amount in one region can increase, but then the precipitation amount in other region may decrease. This offsetting effect may not be explicit when looking at the global scale. Therefore, this study aims to investigate the impact of anthropogenic activities on hydrologic variables at regional scale rather than global scale.

1.2 Research Objectives

The **overarching goal** of this study is to investigate the impact of anthropogenic activities on hydro-climatologic variables. Understanding how hydrologic systems are affected by anthropogenic activities is invaluable from the viewpoint of water resources management. This study uses test beds at different scales to look at the effect of anthropogenic activities on climate and hydrologic variables. Specifically, larger (continental scale) study area is used for studying the impact on climatologic variables while relatively smaller area (basin or watershed scale) is employed for studying the impact on hydrologic variables. The three objectives pursued in this dissertation are described below:

(1) **Detection and attribution of temperature changes in the continental United States**: In this objective, the change of temperature in the continental U.S. is investigated and its causes are scrutinized. The majority of total precipitation (60 ~ 65 %) on the land surface returns to the atmosphere in the form of evapotranspiration (ET) (Postel et al., 1996). Because ET is directly influenced by temperature, changes in ET can have direct impact on regional water resources (Gordon et al., 2003). Hence, the detection and attribution of temperature change is a necessary pre-requisite for regional water resource assessment.

(2) **Quantification of the relative impact of climate and human activities on streamflow**: Compared to a climate variable such as temperature, streamflow is directly affected by anthropogenic activities. In addition, streamflow is also directly influenced by climate variable such as precipitation. Therefore, the second objective is to quantify the change in streamflow by considering both natural factors and anthropogenic activities.

(3) **The effect of land cover change on high and low flows**: Land cover change caused by humans plays an important role in hydrologic cycle at the basin and regional scale. Therefore, understanding how the hydrologic system is affected by land cover change is important for the overall management of water resources. The third objective is to investigate the effect of land cover change on the duration and severity of high and low flows.

1.3 Organization of this Dissertation

This dissertation consists of five chapters. Chapters two to four describe the three major topics of this dissertation. These chapters are presented in a self-contained manner, i.e. each chapter has an abstract, introduction, description of study area and data, methods, results, and summary sections. However, they are all linked under the umbrella of the

impact of anthropogenic activities. The overall conclusions and remarks synthesizing all chapters are presented in Chapter five.

CHAPTER 2. DETECTION AND ATTRIBUTION OF TEMPERATURE CHANGES IN THE UNITED STATES

2.1 Abstract

Temperature plays a major role in the overall hydrologic cycle through evaporation and transpiration. Therefore, understanding the changes in temperature and the underlying causes is important for the overall management of water resources. The objective of this study is to detect the changes in temperature in the continental United States (CONUS) and attribute these changes to anthropogenic activities by applying the Detection and Attribution (D&A) methodology. The CONUS is first divided into ten regions by using the K-mean clustering method. For each region, the Mann-Kendall (MK) trend analysis is used to examine the magnitude of change in temperature in observed data as well as the data from eight climate models and an ensemble from all climate model outputs. For the next step, the optimal fingerprint method is used to analyze the impact of anthropogenic activities on temperature changes. The results show the trends in the observed temperature of the entire CONUS over the 20th century lie inside the range expected from natural internal climate variability. In the regional analysis, the western U.S. is affected the most from the impact of anthropogenic activities, based on both the results from the optimal fingerprint based detection and attribution analysis, and from comparison of trend between observed and modeled data using the MK test. The methodology used in this study is also enables to correctly highlight the significance of the appropriate delineation for the regional area.

2.2 Introduction

There is a growing interest within the hydrology community to study how hydrologic variables are affected by external forces including human activities. Many scientists have preferred to use the Detection and Attribution (D&A) method which provides a robust tool to decipher the complex causes of climate change. According to Hidalgo et al., (2009), detection is defined by climatological or hydrologic variables, which are evaluated in order to determine the presence of influence from natural variability to the observed changes, while attribution is a process to investigate the causes of observed changes in the climatological or hydrologic variables if the observed changes are unexplainable with natural variability.

The optimal fingerprint based D&A methodology can reduce high-dimensional climate time series to a low or single dimension with the principal role. This methodology has been employed to detect changes of several climatic variables— temperature (Allen and Stott, 2003; Hegerl et al., 1996; Santer et al., 2011), sea level pressure (Gillett et al., 2003), precipitation (Zhang et al., 2007), precipitation extremes (Min et al., 2011), and ocean heat content (Barnett et al., 2001). However, most of these studies were focused on the climatological variables at the global scale.

Even though global scale studies of detection and attribution provide meaningful information, small changes in some variables at a global scale can seriously affect hydroclimatology within a region. Leemans and Eickhout (2004) argued that even small

increases in global mean temperatures will considerably impact many species, ecosystems and landscapes and there could be large regional differences. Accordingly, some recent studies use the D&A approach for addressing regional scale issues (e.g., Barnett et al., 2008; Hidalgo et al., 2009; Mondal and Mujumdar, 2012).

A number of recent studies have also performed D&A for hydrologic or meteorological variables in the western U.S. (Barnett et al., 2008; Bonfils et al., 2008; Hidalgo et al., 2009). Bonfils et al. (2008) examined significant changes in river flow, winter temperature, and snow pack, using the D&A methodology; significant changes were detected with 5 percentages significant levels in all variables used in their study. Furthermore, Barnett et al. (2008) investigated the late winter/early spring changes in hydrologically relevant temperature variables, focusing on the mountain ranges of the western U. S. They also found that significant changes occurred in the mid-1980s. Two studies reported to having identified meaningful changes in temperature-related variables due to anthropogenic activities: Hidalgo et al. (2009) studied the nature of observed shifts in the timing of streamflow, while Pierce et al. (2009) took January-February-March (JFM) temperatures over the western U.S into consideration.

As described above, a vast amount of the D&A work in the U.S. has been focused on the western region owing to observed changes in temperatures in the region. According to Andreadis and Lettenmaier (2006), these significant changes in temperature in the western U.S. have led to intensification in drought duration and severity. Since change in temperature is fairly-well correlated with the occurrence of natural disasters (Van Aalst,

2006), the analysis of change in temperature and the investigation for its causes using the D&A approach is necessary for other regions in the U.S. In addition, as all the previous research was conducted by using the data from 1950 to 1999, the impact of anthropogenic activities on the hydrologic cycle past 1949 is not well understood. Therefore, research on the trends of a longer period of records in the CONUS is needed.

The objective of this study is to perform Detection and Attribution analysis of temperature as a representative climate variable in the CONUS. Temperature plays a major role in the overall hydrologic cycle through evaporation and transpiration. For example, change in evaporation can influence water availability and /or surface runoff. Thus analyzing the changes in temperature and investigating their underlying causes is valuable in understanding the changes to the hydrologic cycle in a region.

2.3 Study Area and Data

2.3.1 Study Area

The impact of anthropogenic activity can be described in various ways. One way to look at anthropogenic influence is the increase in population which leads to changes in landuse, thus eventually affecting the temperature. According to Li et al. (2013), land cover change and anthropogenic activity play crucial role in temperature change and contribute to the observed warming. The U.S. Census Bureau explains that U.S. population almost quadrupled during the 20th century, from approximately 76 million in 1900 to 316 million in 2000 (Bureau, 2005). Therefore, the CONUS is selected for this study. The

land area of the CONUS is 2,959,064 square miles (7,663,941 km2); it includes most of the existing climate types and geographic variability within its area. To the east of longitude 100° W., the climate ranges from humid continental in the north to humid subtropical in the south, including the southern tip of tropical Florida. The Great Plains west of 100° W. longitude are semiarid. The rest of the country also shows dynamic climate differences: a large part of the Western mountains are alpine; the climate is arid in the Great Basin, desert is present in the Southwest; coastal California represents Mediterranean; and it is oceanic in coastal Oregon and Washington. Extreme weather is not uncommon—the states bordering the Gulf of Mexico are prone to hurricanes (Lubowski et al., 2009).

2.3.2 Observed Data

The University of Delaware Air Temperature (UDelT) period —1900 to 1999 (100 years) — is employed in this study. The UDelT was originally based on a 0.5 degree by 0.5 degree latitude/longitude grid, and was compiled from several sources including the Global Historical Climatology Network (GHCN2) (Peterson and Vose, 1997). Firstly, this UDelT is spatially interpolated onto T85 resolution. T85 is approximately 1.4 degree resolution, giving 256 x 128 regular longitude/latitude global horizontal grids. According to Collier and Zhang (2007) and Meehl et al. (2006), regional biases were somewhat improved at T85 resolution. The newly-constructed data has 436 interpolated points covering the entire CONUS. Figure 2.1 represents the annual average temperature in the aforementioned 100 year span (1900 ~ 1999) using the newly-constructed data.

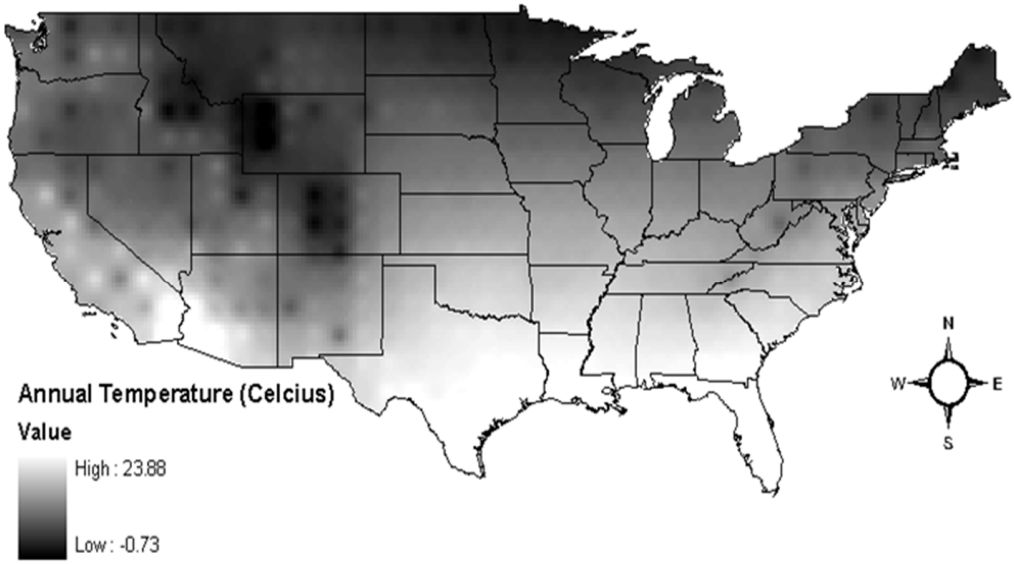

Figure 2.1 Annual average Temperature in the Continental U.S

2.3.3 Climate Model Data

Eight models are employed among the climate model data offered by IPCC Fourth Assessment Report (Intergovernmental Panel on Climate Change, 2007). Two scenarios—20C3M, considering the human influence through the 20th century and the control run, a scenario intact from the impact of anthropogenic activities—are used to describe near surface air temperature (TAS) in each climate model. In other words, the 20C3M scenario is used for regenerating the climate conditions of the 20th century (1900 ~ 1999); whereas the control scenario re-enact the preindustrial climate condition. Since the control scenario does not describe the climate of a specific time, there are various temporal domains corresponding to the General Circulation Models (GCMs)—the

longest is 500 years, and the shortest is 240 years. Table 2.1 summarizes the GCMs used in this study.

Table 2.1 The summary of GCMs used in this study

Name of the Model	Model Abbreviation	Scenario	Origin	Initial Resolution	Final Resolution	No. of Years
BCCR: BCM2	BCM2	20C3M	Bjerknes Centre for Climate Research, Norway	128 × 96	256 × 128	100
BCCR: BCM2		CONTROL		128 × 96	256 × 128	250
CCCMA: CGCM3_1-T63	CGCM3	20C3M	Canadian Center for Climate Modelling and Analysis, Canada	128 × 96	256 × 128	100
CCCMA: CGCM3_1-T63		CONTROL		128 × 96	256 × 128	350
CNRM: CM3	CNRM	20C3M	Centre National de Recherches Meteorologiques, France	128 × 96	256 × 128	100
CNRM: CM3		CONTROL		128 × 96	256 × 128	500
NIES:MIROC3_2_MED	NIES	20C3M	National Institute for Environmental Studies, Japan	128 × 96	256 × 128	100
NIES:MIROC3_2_MED		CONTROL		128 × 96	256 × 128	500
MRI: CGCM2_3_2	MRI	20C3M	Meteorological Research Institute, Japan	128 × 96	256 × 128	100
MRI: CGCM2_3_2		CONTROL		128 × 96	256 × 128	350
NCAR: PCM	PCM	20C3M	National Centre for Atmospheric Research, USA	128 × 96	256 × 128	100
NCAR: PCM		CONTROL		128 × 96	256 × 128	350
UKMO: HADCM3	HADCM3	20C3M	UK Met. Office, UK	96 × 73	256 × 128	100
UKMO: HADCM3		CONTROL		96 × 73	256 × 128	341
UKMO: HADGEM1	HADGEM	20C3M	UK Met. Office, UK	129 × 144	256 × 128	100
UKMO: HADGEM1		CONTROL		129 × 144	256 × 128	240

2.4 Methodology

First, the CONUS is categorized into different regions by the K-mean clustering method. After the regions are determined, data from nine climate models (8 GCMs and one ensemble) are generated using a statistical downscaling procedure and multi-model

ensemble method. As the next step, the human-made signals and the natural variability noises are calculated for each region by using the temperature data and the fingerprint method. The details of each step in the methodology are provided in the following sub-sections.

2.4.1 Regionalization

The CONUS is divided into regions by using the *K*-mean clustering method (Wilks, 2006), which divides N observations into K clusters by minimizing the mean of within-cluster sum of squares of selected variables (MacKay, 2003; Xu and Wunsch, D., 2005) The following five variables are applied to cluster the areas: average temperature, standard deviation of temperature, latitude, longitude and slope for a span of 100 years. The variables are selected to represent the spatial and temporal variations as well as the statistical properties and trends in the data. After having various K values under consideration and scrutinized, the categorization of ten clusters is selected as the optimal *K* value, using Bayesian Information Criterion (BIC). The BIC takes into account the number of regional areas that have to be estimated to achieve this particular degree of fit, by imposing a penalty for increasing the number of a regional area. Lower values of the index indicate the preferred model, that is, the one with the fewest parameters that still provides an adequate fit to the data.

$$\mathrm{BIC} = -2\ln(L) + K\ln(N) \qquad (2\text{-}1)$$

Where, K is the number of clusters, L is the maximized log likelihood function for the estimated model, and N is the number of data points.

Although most of the analysis is conducted by using the clusters under the five variables listed above, some of the results are also analyzed for their sensitivity to the regionalization by creating multiple clusters using different combinations of some of the five variables.

2.4.2 Downscaling Methodology

The spatial resolution of the global climate models' output is unsuitable for analyzing the data at regional scales. In addition, data from GCMs are occasionally biased (Quintana Seguí et al., 2010). To overcome the limitations of spatial resolution and bias, the data are subjected to Bias Correction and Spatial Downscaling (BCSD) as described by Wood et al. (2004). While the quantile mapping method (QM; Boé et al., 2007; Déqué et al., 2007) is applied in the original BCSD, nested bias correction (NBC; Johnson and Sharma, 2012) based on auto-regression is employed in this study. For the stage of bias correction, Coarse Observation Temperature (COT) is additionally required and computed by an arithmetic mean of observation adjusted to initial resolution in each climate model. For instance, the COT for the PCM is calculated by the average of the 12 nearest points of UDelT while the COT of the HADCM3 is estimated by the average of 16 close locations of UDelT. T85 resolution is employed as Fine Observation Temperature (FOT). After

bias correction is implemented for each GCM by using an individual COT and the NBC method, the data are downscaled spatially to the FOT resolution by using the methodology described in Wood et al., (2004).

2.4.3 Creating Multi-model Ensemble

Recent studies have shown that multi-model ensemble-averaged estimates perform better in analyzing climate outputs compared to any individual model (Mondal and Mujumdar, 2012; Pierce et al., 2009; Santer et al., 2007). This ensemble GCM and the use of the first component EOF in the fingerprint method are all associated with reducing the noise (Barnett et al., 2008; Santer et al., 1995). Reliability Ensemble Averaging (REA; Giorgi and Mearns, 2002), which is one of the most popular among the weighted ensemble methods, is employed to calculate the ensemble scenario in this study. The original REA method is composed of historical and future projection terms. However, the future projection term can be omitted owing to the fact that only historical data are used in this study. The REA can be finally derived by using Equation (2-2).

$$w_i = \left| \frac{\varepsilon_T}{abs(B_i)} \right| \qquad (2\text{-}2)$$

where, i is the ith GCM, B_i is defined as the difference between simulated and observed mean temperature for 100 years, and ε_T is estimated by the difference between the maximum and minimum values of the 30 year moving average.

While each GCM has a control scenario, the ensemble model does not. Thus, the Monte Carlo simulation method is employed to establish the control for the ensemble model. First, eight—the same number as the GCMs used in this study—S_{noise} are calculated after randomly selecting the segment periods regardless of the GCMs in the control scenario. The control scenario of the multi-model ensemble is then generated using the average of S_{noise} values from eight GCMs. The length of segment data is decided by continuously increasing from 11 to 100 years, equivalent to the other control scenarios of the GCM. The total length of the control of the multi-model ensemble is assumed to be 500 years, which is the length of the longest control scenarios. Then the magnitude of noise for the multi-model ensemble is reversely calculated by decreasing the number (45, 45, … 5), which is given by the ratio of 500 years over the length of segment data.

2.4.4 Optimal Fingerprint-based Detection and Attribution

The optimal fingerprint method of detection and attribution is commonly used to evaluate the causes of complex climate change. A fingerprint can be defined as a low or single dimension series that has a principal role in high-dimensional climate time series. Santer et al. (1995) stipulated that a fingerprint applied in 20C3M scenarios is a signal strength induced by human influences. Just as in signal strength, a fingerprint employed in control

scenarios is regarded as a noise strength representing the natural fluctuation. Signal strength and noise strength are defined in Equations (2-3) and (2-4), respectively.

$$S_{\text{signal}} = \text{trend}[F(x) \cdot D(x,t)] \quad (2\text{-}3)$$

$$S_{\text{noise}} = \text{trend}[F(x) \cdot C(x,t)] \quad (2\text{-}4)$$

The Equation 2.3 and 2.4 indicate trends of the hydrologic vector projected into the fingerprint for each of the climate runs year by year. $F(x)$ is the fingerprint obtained from the climate model corresponding to the location x. The fingerprint can be obtained by the first component of the Empirical Orthogonal Function (EOF) of data. $D(x,t)$ is the standard normalized observed temperature at location x for time t. $C(x,t)$ is the standard normalized control temperature at location x for time t. Previous studies have utilized the least squares linear trend; however, Sen's slope (Sen, 1968; Theil, 1950) is used in this study to calculate the trend due to its robust linear regression that chooses the median slope among all lines through pairs of two-dimensional sample points. Accoring to Wilcox (2001), Sen's slope is more accurate than simple linear regression for skewed and heteroscedastic data, and competes well against simple least squares even for normally distributed data. To obtain reliable results, it is necessary to first review the similarity of fingerprints between observed data and synthetic data (Mondal and Mujumdar, 2012).

After each strength is calculated, the degree of principal influence is examined using Sen's slope. A relatively lengthy period of data is acquired in the noise, whereas only one

hundred years of data is employed in the signal. Thus, signal is estimated by the trends of increasing length L (L = 11, 12... 100), namely an overlapping approach while noise is evaluated by the trends of non-overlapping L-length segments of the control time-series. Under the aforementioned methodology, the noise has multiple outcomes. The magnitude of noise is estimated using these multiple results by Equation (2-5) (Santer et al., 1995).

$$\varepsilon = [\frac{1}{n-1}\sum_{c=1}^{n} S_{noise,c}{}^{2}]^{\frac{1}{2}} \qquad (2\text{-}5)$$

where, the expectation of S_{noise} is assumed to be zero and n is the segment number of the control time-series.

As the last step, detection is computed by using the Signal to Noise Ratio (SNR)—the signal strength divided by the magnitude of noise. The Year of Detection (YOD) stipulates that SNR stays at or above a 5 or 10 % significant level in the study.

2.5 Results

2.5.1 Regionalization from *K*-mean Clustering

The CONUS is divided into ten regions by using the K-mean clustering methodology as shown in Figure 2.2. The ten regions along with the number of temperature points in parenthesis in each region is as follows: The Northeast (NE, 26), The East (EA, 52), The

Southeast (SE, 38), The Mid-south (MS, 45), The Midsection (MI, 46), North Central (NC, 46), The Rocky Mountains (RM, 58) The Southwest-B (SB, 42), The Southwest-A (SA, 28) and The Northwest (NW, 55). There are totally 436 temperature points used in this study.

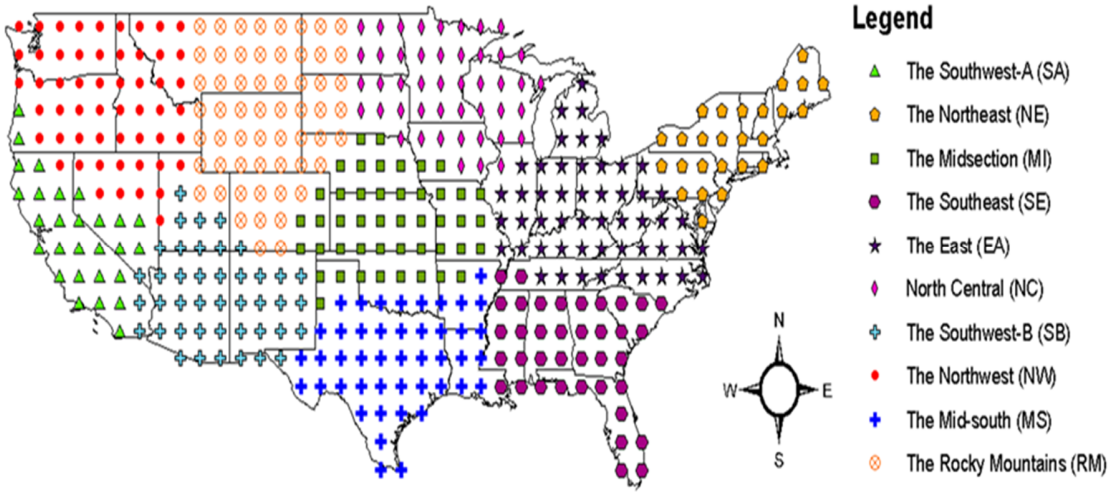

Figure 2.2 *K*-mean clustering results

2.5.2 Temperature Data

2.5.2.1 The Results of Downscaling Methodology

The downscaling method is applied not only for the control runs, but also for 20C3M scenarios. Downscaling is conducted by using data from 1900 to 1939 (40 years) as test period, and the data from 1940 to 1999 (60 years) as training period. Figure 2.3 represents the annual average temperatures of the GCMs in the training period. Because the issue of stationary can arise in statistical downscaling (Ghosh and Mujumdar, 2008;

Mondal and Mujumdar, 2012), the similarity of trend between the simulated and observed data is employed as one of the indices to compare the accuracy. The similarity of trend in the two groups of data is calculated by comparing observed and downscaled data using a linear regression slope. While mean Normalized Mean Square Error (mean-NMSE; Zhang and Govindaraju, 2000) is used to investigate the accuracy in the test and training periods, mean Mean Absolute Error (mean-MAE; Hyndman and Koehler, 2006) is employed for judging the trend accuracy. Table 2.2 shows the average biases in the eight GCMs used in this study. Even though the disparity of accuracy between the methodologies can be negligible in both periods, BCSD with NBC has much higher accuracy in the similarity of trend.

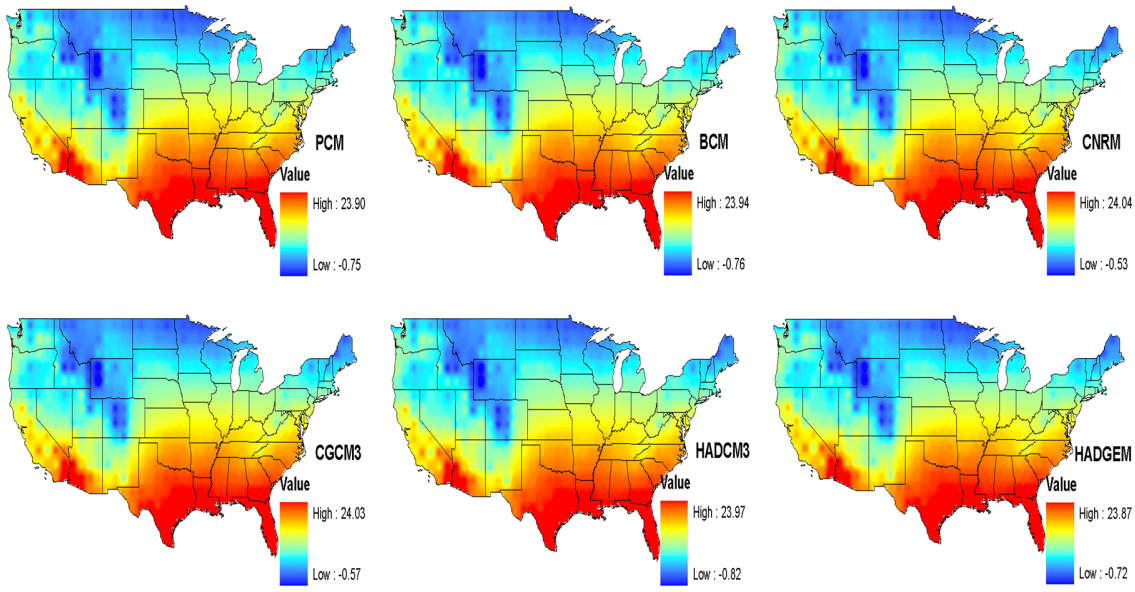

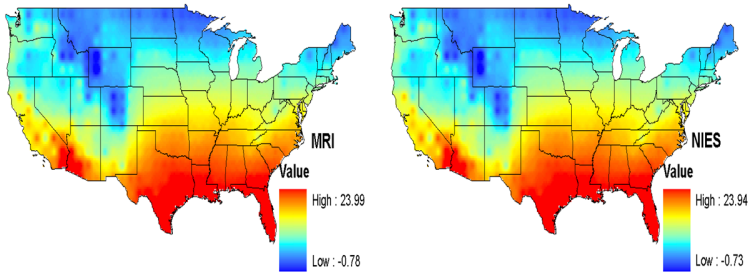

Figure 2.3 The annual average temperature (°C) in the training period (1940 ~ 1999) (a) PCM (b) BCM (c) CNRM (d) CGCM3 (e) HADCM3 (f) HADGEM (g) MRI, and (h) NIES

Table 2.2 The average biases in eight GCMs used in this study

	Test period	Train period	Trend ($\times 10^{-2}$)
BCSD with QM	0.869	0.892	0.753
BCSD with NBC	0.887	0.849	0.632

2.5.2.2 Multi-model ensemble

The weights of each GCM are calculated using Equation (2-2). Figure 2.4 shows the REA weights corresponding to the locations and the GCMs. The higher weights indicate higher accuracy when compared to the observed data. There is no single GCM which is superior in all regions. A GCM which is more accurate in one region receives a higher weight in that region. For example, the CGCM3 shows the highest weight in the northeastern part of the U.S. Therefore, CGCM3 is weighted at approximately 0.25 instead of the average of 0.125. The CNRM has the highest weight in the southwestern part of the U.S., whereas PCM has the highest weight in the Rocky Mountain area. One of the primary characteristics to cause different weights is that non-identical GCMs can simulate

different regional changes even under the same anthropogenic forcing scenario (Giorgi and Francisco, 2000; Giorgi and Mearns, 2002; Kittel et al., 1997). These results can be another reason the ensemble model should be employed.

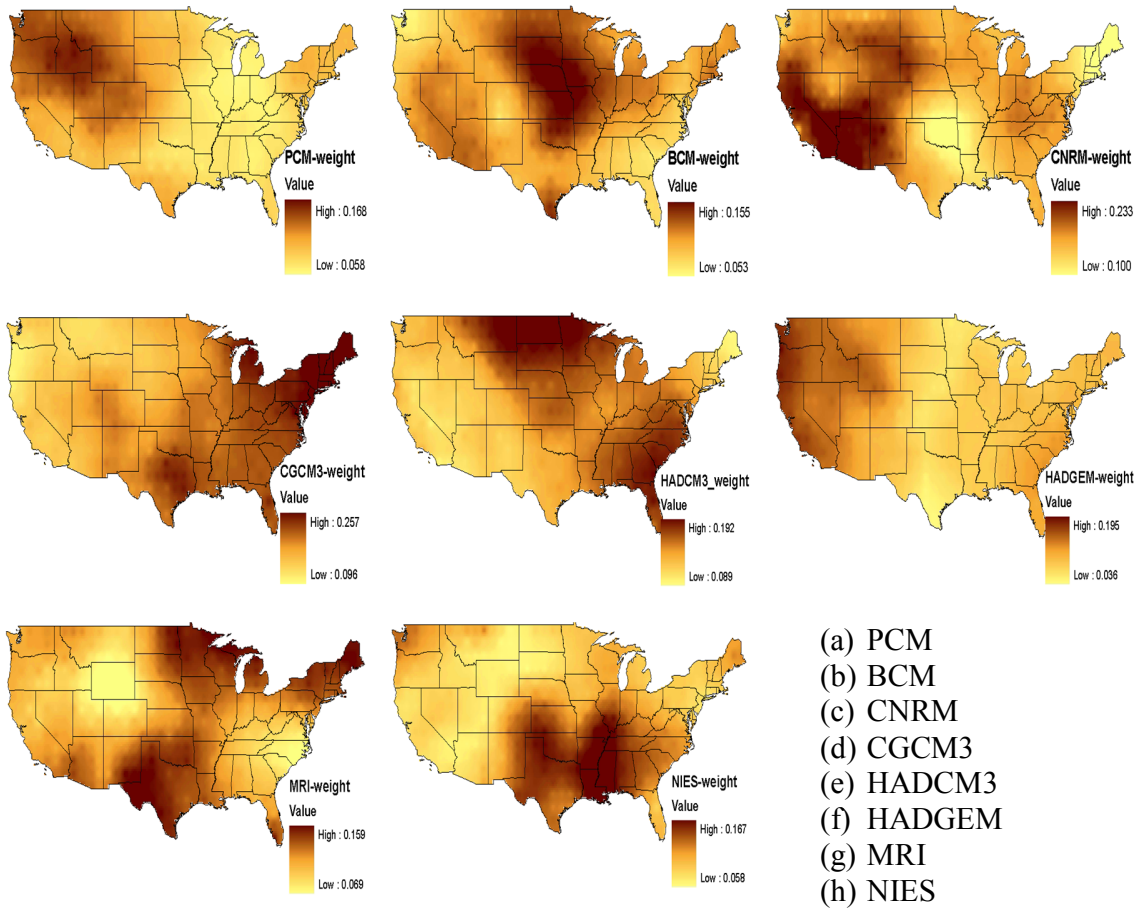

Figure 2.4 The weights of GCM corresponding to the locations (a) the weights of PCM (b) the weights of BCM (c) the weights of CNRM (d) the weights of CGCM3 (e) the weights of HADCM3 (f) the weights of HADGEM (g) the weights of MRI, and (h) the weights of NIES

2.5.3 Preliminary Analysis

2.5.3.1 Trend in Observed Temperature

Since the 20C3M scenario imitates the actual temperature, observed data must be investigated before dealing with the GCM datasets. The average change in temperature in the entire CONUS and each study region in 100 years (1900-1999), including its p-values for 95% confidence interval are presented in Figure 2.5. An increase of 0.23 degrees Celsius in average temperature is observed in the CONUS, while the southwest area (SA and SB) show the biggest temperature increase. Two regions, namely MS and SE, show a significant decrease in the average temperature from 1900-1999, with MS region showing the greatest decrease (-0.32 degrees Celsius). However, only three regions—the RM, the SB, and the SA—show a significant increase in temperature from 1900-1999. The results show identical temperature changes in the COMUS as found in previous studies by Hansen et al., (2001), Karl et al. (1996), and Lu et al. (2005).

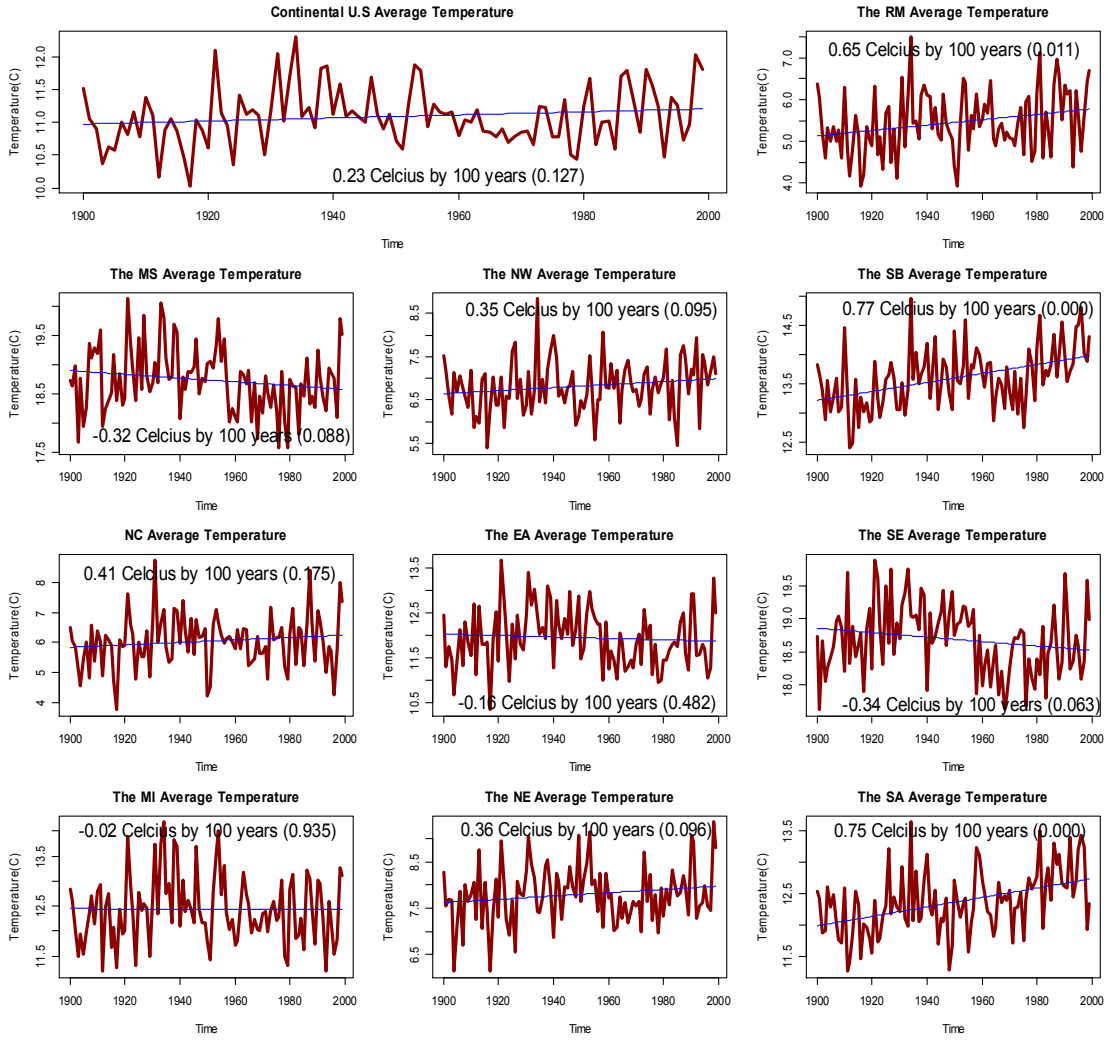

Figure 2.5 The temperature changes depending on the regional areas. Temperature time-series in 100 years is shown and the change amount in 100 years and its p-value are denoted in each figure.

To examine the temperature changes of individual stations, the Mann-Kendall test (Kendall, 1955; Mann, 1945) is employed. Out of 436 stations, a total of 135 stations show significant increase in temperature; whereas 51 stations show significant decrease in temperature at a 95% confidence level (Figure 2.6).

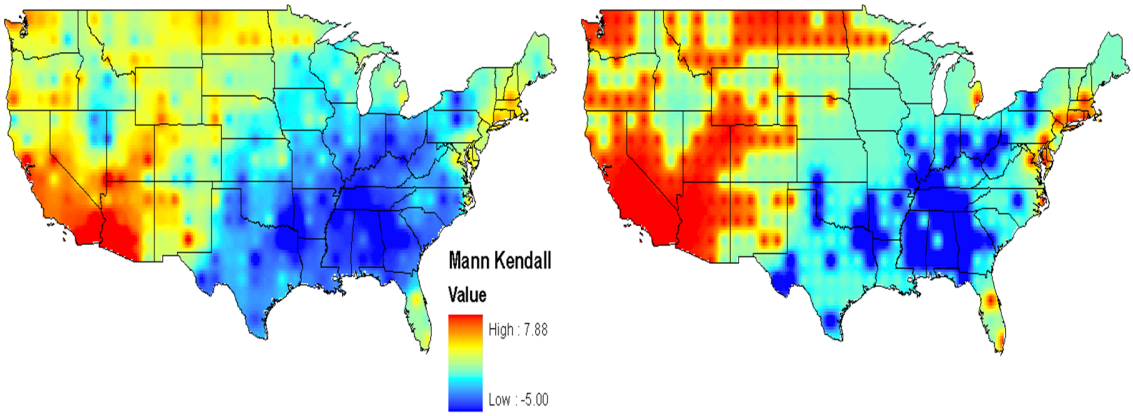

Figure 2.6 Trend Analysis results using Mann-Kendall test (a) The magnitude of Mann-Kendall results (b) The locations which show the significant change in temperature with 95 % confidence level (the red- increasing trend, the blue- decreasing trend)

Figure 2.6 shows that the majority of the stations showing significant increase in temperature are located in the RM, NW, SA and SB regions. Conversely, the stations showing significant decrease in temperature are located in the MS, EA, and SE regions. The numbers of stations presenting the trends in each region are presented in Table 2.3.

Table 2.3 The number of significant changes corresponding to the regions: negative sign indicates the decreasing trend

Groups	Total Points	Increasing		Decreasing	
		5% significant	1% significant	5% significant	1% significant
The RM	57	33	20	0	0
The MS	45	0	0	-13	-7
The NW	55	26	15	0	0
The SB	42	30	25	0	0
NC	46	3	2	-16	-4
The EA	52	3	2	-16	-4
The SE	38	2	2	-17	-10

The MI	46	3	2	-3	-1
The NE	26	6	4	-2	-1
The SA	28	24	21	0	0
Total	436	130	93	-67	-27

2.5.3.2 Accuracy Assessment of Model Output Temperatures

The accuracy of the 20C3M scenario of GCMs that are downscaled also needs to be verified. After the 100 years are divided into the test period (1900 - 1939) and the training period (1940 - 1999), their accuracies are compared. The differences between observed and downscaled values are computed after the average temperatures corresponding to the locations are calculated in each period. The results are shown in Figure 2.7; each box includes the results of 436 locations. The accuracies in the test period are relatively higher than the ones in the training period. What is notable in the test period is that the medians of the majority GCMs have negative bias. Conversely, the medians of the most GCMs are positively biased in the training period. Although commonly shown, this difference is particularly observed in CNRM. As a bigger difference can result in a more overestimated trend of temperature, it is viable to say that the downscaled data in this study is sufficiently accurate with the calculated differences of less than 0.3 degree Celsius.

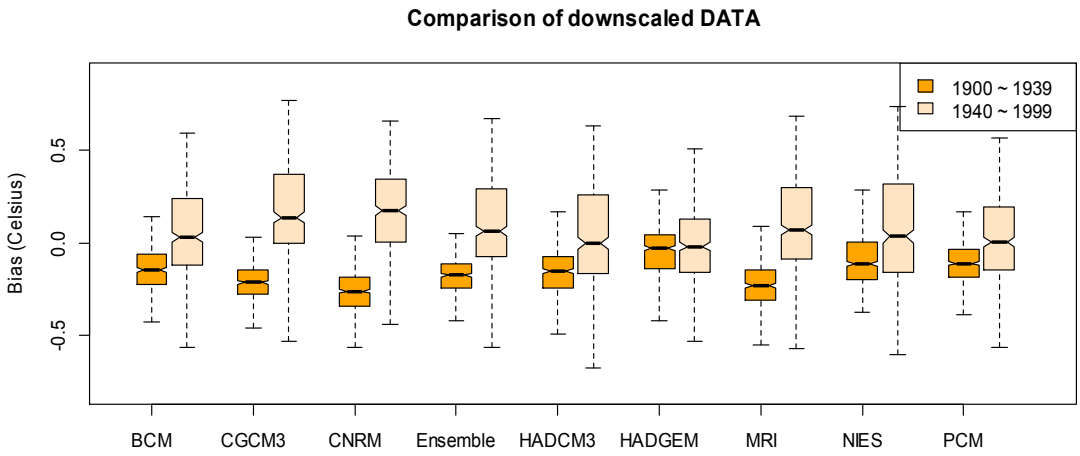

Figure 2.7 The accuracy of GCMs compared to observed data

The accuracy of downscaled data plays a fundamental and crucial role in this study. In particular, the bias of internal variability (INV) is a serious problem, because it significantly affects the results of the fingerprint method (Hegerl and Zwiers, 2011). Spectral analysis is commonly used to investigate the INV problem in numerous studies (Hegerl, 2007; Hegerl and Zwiers, 2011; Knutson et al., 2013). Spectral analysis confirms that that the INV of 20C3M scenarios correspond with the observed variability, while the INV of control scenarios do not (Hegerl et al., 1996; Santer et al., 1995). Figure 2.8 represents the power spectral density (Percival and Walden, 1993) of temperature including the observed and downscaled data, which is computed using average annual temperature of each region. The 95% confidence intervals of observed data are also shown in Figure2.8. It is clear from Figure 2.8 that spectral density of all GCMs does not lie inside the 95% confidence interval of the observed data; a great amount of scatter among all GCMs at higher frequency is observed, which indicates uncertainty in the

models at this frequency. On the other hand, the majority of the models fall within the 95% confidence interval at a lower frequency; the deviations in the model data are relatively small. Therefore, it is viable to use the data in this study with considerable adjustment in the model data to improve the accuracy of GCMs as Knutson et al., (2013) argued in their research.

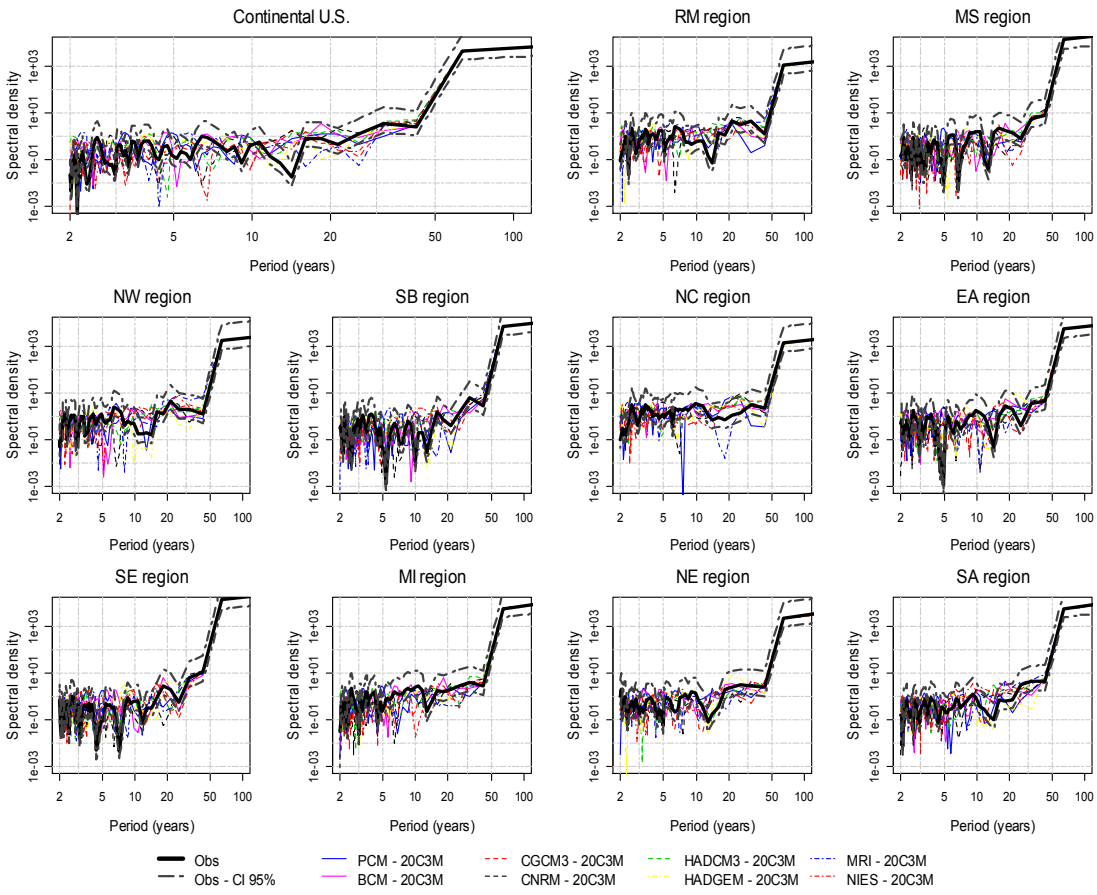

Figure 2.8 Power spectral densities for regional average of observed temperature and GCMs: the grey dotted line is 95 % confidence level of observed data

2.5.3.3 Comparison of trend between observed and modeled temperatures

As mentioned in Section 2.3, the control scenario indicates the natural variability while the 20C3M scenario represents the temperatures of the 20th century. If the trend in the observed data is similar to that of the control scenarios, this demonstrates that the data is less affected from anthropogenic activities. Conversely, if a region is affected by anthropogenic activities, the trend in its observed data will follow the trend found in one of the 20C3M scenarios. In this study, the trends of the average temperature corresponding to the regional areas are investigated using the MK test. First, the MK test is applied to the control scenarios employing the non-overlapping method at a specific temporal interval. For example, a control scenario for BCM has data for 250 years, which produces two values for the MK test corresponding to each 100 year period. By using the data from the GCMs control scenarios, a histogram is constructed for the regions on the CONUS. This histogram represents the distribution of possible changes in natural variability. Then, the MK test is applied to 100 years of observed data and the 20C3M scenarios. This produces a single MK value for each GCM and the observed data. The results are shown in Figure 2.9.

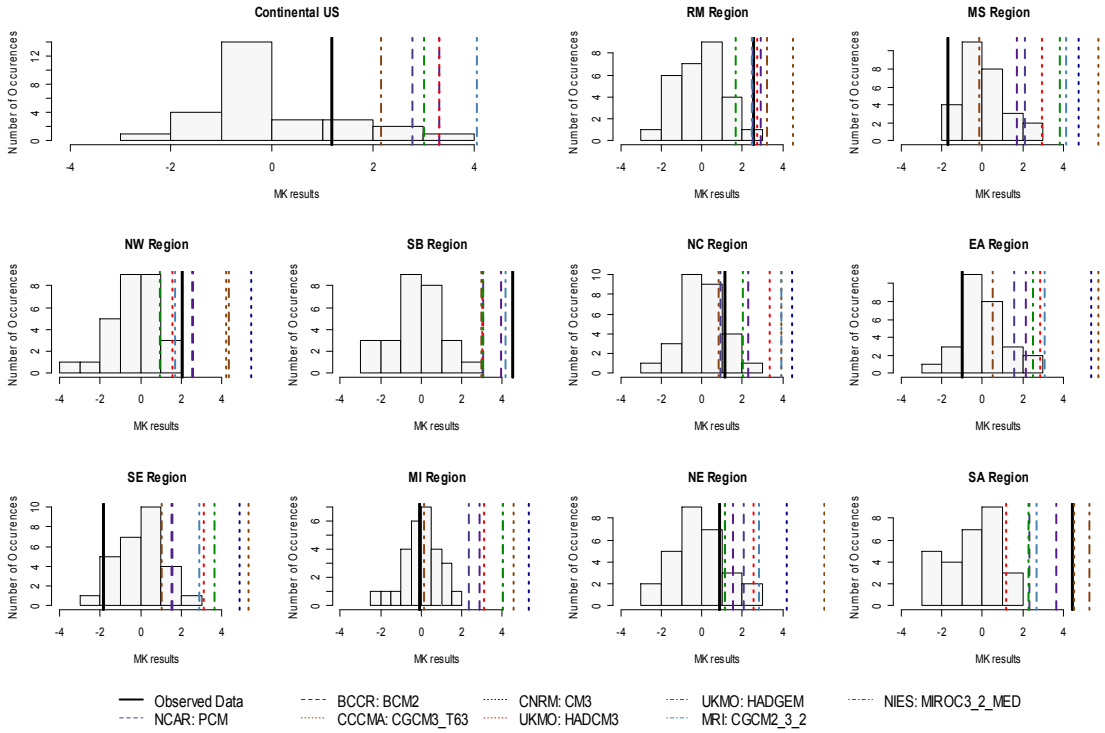

Figure 2.9 The trend of the natural variability and the temperatures of the 20th century: the histogram represents the natural variability, the black line is for the trend of observed temperature in the 20th century and each line represents the trend of modeled temperature in 20C3M scenario

Figure 2.9 describes that the majority of the regions follow natural variability. Similarly, a number of regions, for example, the states of RM, NW, SB, SE and the SA, show trends that are significant at 95% confidence level. However, the trends in NW, SA and SB regions lie outside the distribution of natural variability, and are closer to the trends of 20C3M scenarios. In other words, the trends in the these states are affected by external forces.

2.5.4 Fingerprint of GCMs

The value of the fingerprints F(x), as defined in Equation 2-3, are obtained for the study areas by using the downscaled data of the GCMs. The fingerprints, which define the leading EOF at each study location, are considered as the relative weight corresponding to individual locations. Figure 2.10 shows the results of the fingerprints for the three study regions—CONUS, RM, and SB. According to Figure 2.10, the fingerprints illustrate high similarity for the GDMs for the given regions. This confirms that the fingerprints acquired by the nine GCMs including REA are not demonstrating conflicting results, and thus reliable fingerprint results can be obtained from most GCMs.

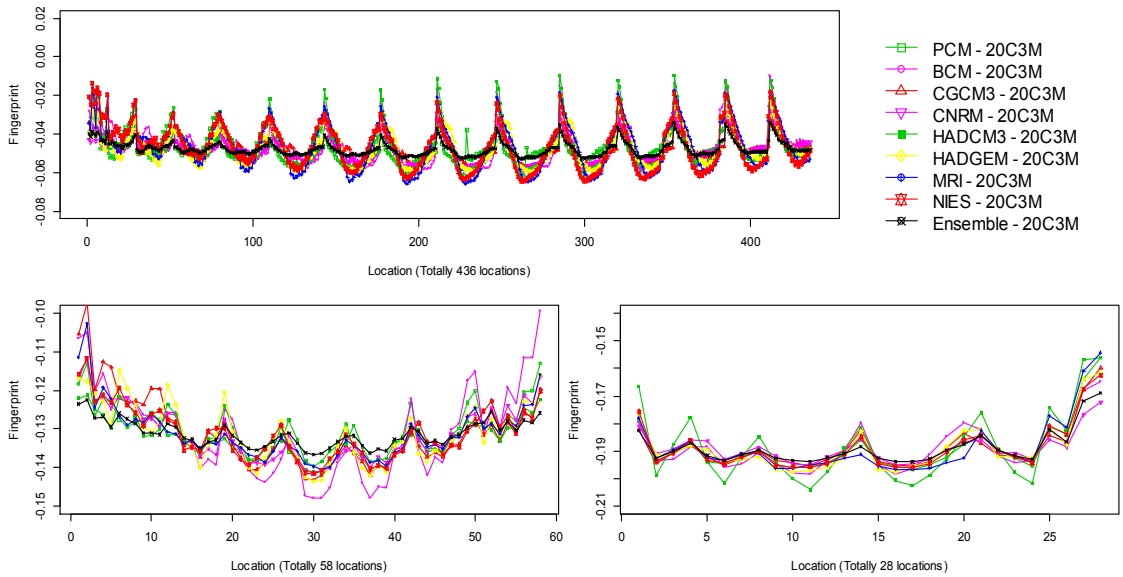

Figure 2.10 The fingerprints corresponding to the locations: x-axis is location (a) is for the continental U.S., (b) shows the Rocky Mountains (RM), and (c) the Southwest-B (SB)

The fingerprint obtained for each region is then used to compute signal strength for each GCM with Equation 2-3. The signal strengths for Rocky Mountains are shown in Figure 2.11. The signal strength from each GCM including the REA is non-zero, which means the temperature is affected by anthropogenic activities. As shown in Figure 2.11, the signal strengths from the multi-model ensemble scenario (REA) are the closest to those of the observed temperature. The result supports the argument of the previous studies in terms of the usefulness of multi-model ensemble-averaged estimates.

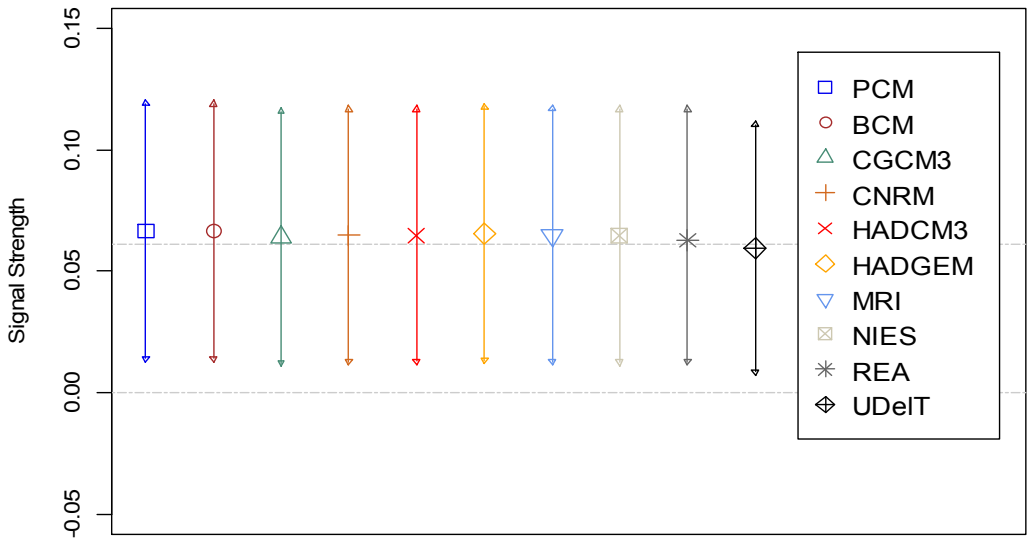

Figure 2.11 Detection plot for annual temperature in the Rocky Mountains. The average of signal strengths and their 95 % confidence intervals are designated

2.5.5 Year of Detection (YOD)

The signal to noise ratio (SNR) is calculated after signal strengths are estimated by Sen's slope. To reflect the characteristics of each GCM, a corresponding control scenario is employed in place of the pooled control scenario (Santer et al., 1995). The SNRs are computed for the regions including CONUS; Figure 2.12 shows SNR results for the SA region as an example to compare the results of the western U.S. with Bonfils et al. (2008). In the SA region, as shown in Figure 2.5, there is an average regional temperature increase of 0.75 ^{o}C (p-value = 0.000) in the 20th century. In addition, as shown in Figure 2.6b, 86% of the stations in the SA region display significant increase in temperature trends. According to the SNR results in Figure 2.12 from each GCM for the SA region, it is notable that seven out of nine models demonstrate significant results by crossing the 90% confidence interval (or detection) line, and that the changes mostly occurred in the early 1980s. Bonfils et al. (2008) identified 1983 as the YOD with 5% significant level by using the PCM data; however, the results from PCM—the YOD with 5% significant level is 1989—are slightly different. It is mainly due to the difference in the period of the data used in the analysis (Santer et al., 2007); Bonfils et al. used fifty years of data (1950-1999), whereas 100 years of data are used in this study.

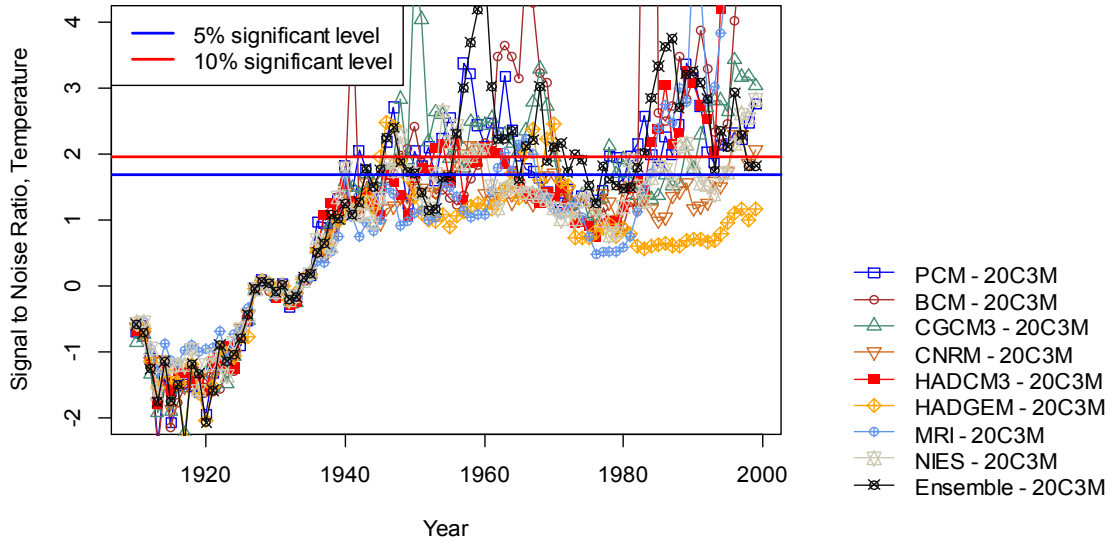

Figure 2.12 Signal to noise ratio (SNR) for the annual temperature in the SA. The blue line and the red lines are 5% and 10% significant level, respectively

By using the SNR results from the regions, the YODs are estimated with 90% confidence interval (Figure 2.13). With nine datasets (eight GCMs and one multi-model ensemble), nine results are obtained for each region. The majority of GCMs show YOD in three regions—RM,SA and SB. The YODs of RM fall around the late 1990's, the YODs of SA and SB fall in the mid 1980s. These results, once again, are likely to indicate the fact that the western U.S. has been affected the most by the impact of anthropogenic activity. Another important finding is that no YODs are found from any dataset for the CONUS. This can be due to the temperature variation in the 20 century remained statistically stationary for the CONUS, but some regions show significant changes in temperature due to the anthropogenic activities. This result can be supported by the annual average temperature of the CONUS (see Figure 2.5). There is an increase of 0.23 degrees Celsius

for 100 years but, this change can be not meaningful based on its p-value with 5% significant level. In other words, the average change in temperature in the CONUS is not significant.

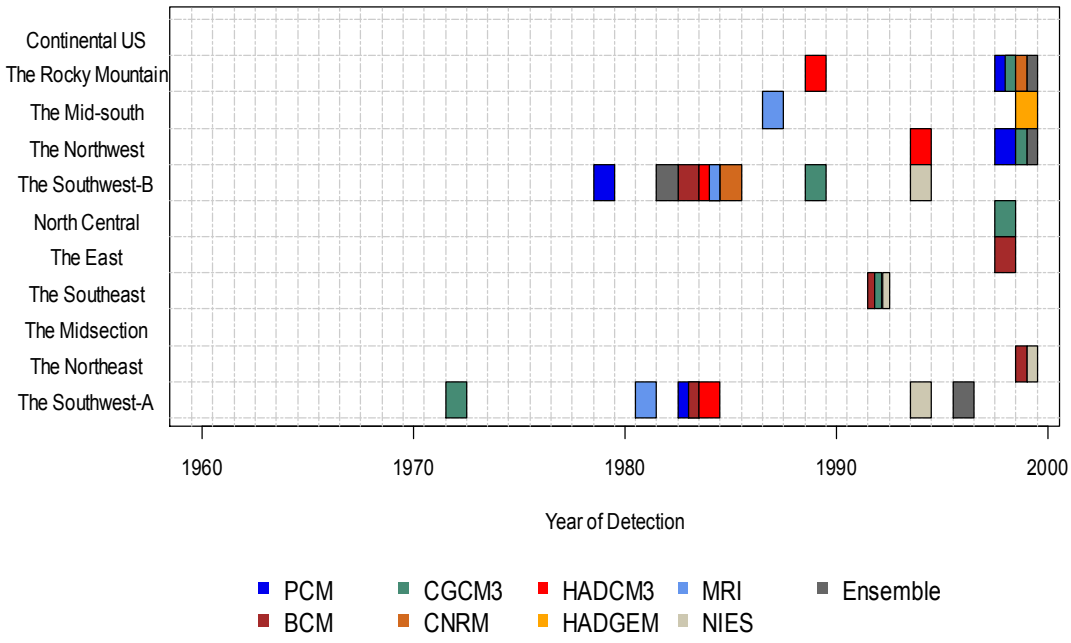

Figure 2.13 The YOD results corresponding to the regions, which are defined in this study (see Figure 2.2)

2.5.6 Sensitivity of YODs to Regional Clustering

As mentioned in the methodology section, the results can be different based on different regionalization of the data. In this section, the YODs are scrutinized in relation to different clustering results. Using three input variables—average temperature, longitude, and latitude, the categorization of five clusters is obtained as the new optimal K value. The new K-mean clustering results are shown in Figure 2.14.

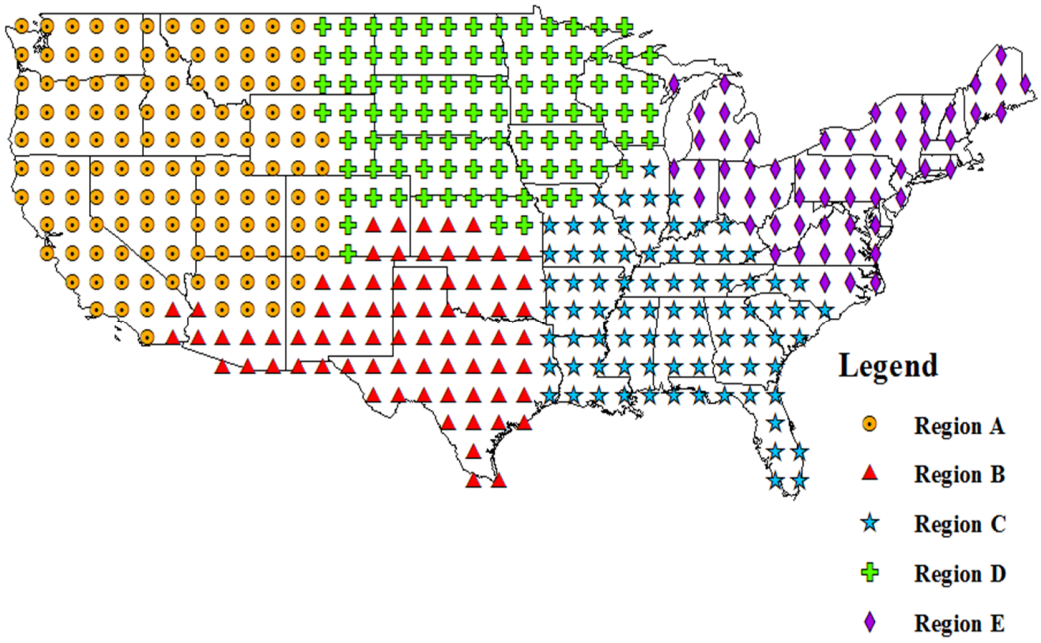

Figure 2.14 *K*-mean clustering results for sensitivity analysis

To distinguish from the original region names, the new regional areas are named as Region A – Region E, consecutively. Region A consists of NW, SA, the half of NE and a half of SB regions while region C is extended to SE and EA regions. Region D includes RM, NC and MI.

By using the newly-defined areas, YODs are estimated with a 90% confidence interval (Figure 2.15). In Figure 2.15, the majority of GCMs demonstrate YOD only in one region, region A. Although the majority of GCMs show YOD in region A, they are clearly distinctive from the YODs in Figure 2.13. Comparing YODs of the region A with the YODs of SA and SB in Figure 2.13, the average of YODs is delayed by approximately 10 years even including most of SA and SB in region A. Another salient point is that the meaningful results in the RM are not detected in Figure 2.15. We can conclude that as the

study area is expanded, the DOY gets delayed. Therefore, spatial discretization plays an important role in the regional D&A research.

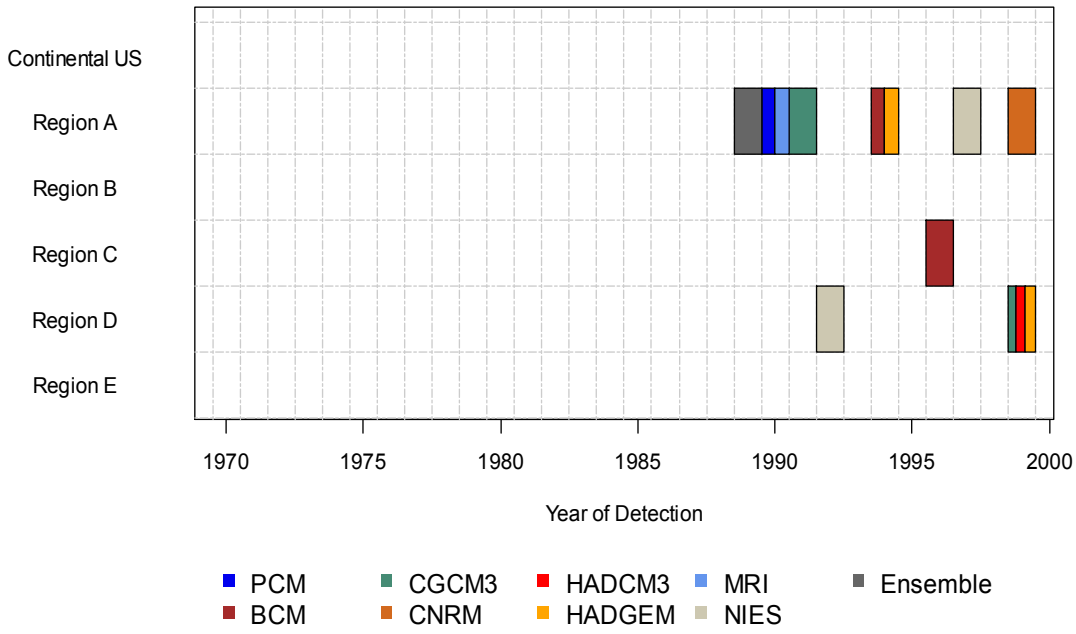

Figure 2.15 The YOD results corresponding to the regions, which are defined in Figure 2.14

2.6 Summary and Conclusion

The change in temperature magnitude for the CONUS and its cause are investigated in this chapter. The impact of anthropogenic activities on the temperature of the regions is analyzed by using the optimal fingerprint based D&A method. Data from eight global climate models and one multi-model ensemble are employed after statistical downscaling.

In conclusion, it is found that the observed trends temperature data for the CONUS over the 20th century lie inside the range expected from natural internal climate variability alone at 90% statistical confidence level for the all GCMs. However, some parts of the CONUS have demonstrated meaningful changes in temperature due to the impact of anthropogenic activities. The impact of anthropogenic activities particularly is greatest in the western U.S. (SA, and SB); the results of temperature changes in western U.S. are evident not only in the optimal fingerprint based detection and attribution analysis but also in the comparison of trend between observed and modeled data using the MK test.

It is important to note that the results for this study have a number of uncertainties. Even though officially guaranteed, the GCMs cannot be fully trusted (Hewitson BC and Crane RG, 1996); moreover, the uncertainties in the GCMs are unlikely to be completely eliminated despite the utilization of the downscaling method in this study.

CHAPTER 3. QUANTIFYING THE RELATIVE IMPACT OF CLIMATE AND ANTHROPOGENIC ACTIVITIES ON STREAMFLOW

3.1 Abstract

The objective of this study is to quantify the roles of climate impact and anthropogenic activities on streamflow conditions through historical streamflow records, in conjunction with trend analysis and hydrologic modeling. Four U.S. states, including Indiana, New York, Arizona and Georgia area, used to represent various levels of human activity based on population changes and diverse climate conditions. The Mann-Kendall trend analysis is first implemented to examine the magnitude of the changes in precipitation, streamflow and potential evapotranspiration for the four states. Four hydrologic modeling methods, including linear regression, hydrologic simulation, annual balance, and Budyko analysis are then used to quantify the impacts of climate change and human activities on streamflow. All four methods show that the impact of anthropogenic activities is more influential on streamflow at most gauging stations in all four states than climate impact is. Among the four methods used, the linear regression approach produces the best hydrologic output in terms of higher Nash-Sutcliffe coefficient. The methodology used in this study is also able to correctly highlight the areas with higher anthropogenic impact such as the modified channelized reaches in the northwestern part of Indiana. The results from this study show that population alone cannot capture all the changes caused by anthropogenic activities in a region. However, this approach provides a starting point towards understanding the role of individual anthropogenic activities on streamflow changes.

3.2 Introduction

Anthropogenic activities play a crucial role in the changes of hydrologic circulation (Kuchment, 2004). Due to increasing population and subsequent impacts of anthropogenic activities on the hydrologic cycle, there is a growing interest to learn how external forces such as anthropogenic activities affect hydrologic variables. As a result, a great amount of research has been ongoing to look at how the impact of anthropogenic activities affect hydro-climatic variables such as temperature (Allen and Stott, 2003; Hegerl et al., 1996; Santer et al., 2011), precipitation (Zhang et al., 2007), precipitation extremes (Min et al., 2011), and snow pack (Barnett et al., 2008; Pierce et al., 2008). The studies report critical changes due to anthropogenic influence; for example, Hegerl et al. (1996) conclude that the recent 30 year trend of global surface temperature are not explainable by natural variability. Furthermore, Zhang et al., (2007) argues that anthropogenic forces induce significant increases to observed precipitation in the Northern Hemisphere mid-latitudes, and decreases in the Northern Hemisphere subtropics. However, much of the research is implemented based on climate model outputs, which are reported to have various levels of uncertainty (Barnett et al., 1999).

In addition to hydro-climatic variables, streamflow generation is also the influence of anthropogenic activities as well as natural factors (Liu et al., 2010; A. Zhang et al., 2012). It is well acknowledged in the preceding literature that changes in climate variables and anthropogenic activities are the main contributors to the change of streamflow over time

(Vogel, 2011; Wagener et al., 2010; Wang et al., 2010). While the effects of anthropogenic activities have received relatively less attention (Tran and O'Neill, 2013), the roles of climatic influence on streamflow have been extensively well documented in the literature. For example, Karamouz et al. (2011) and Prudhomme et al. (2010) analyze the flood risk using a general circulation model. Similarly, Jung and Chang (2011), Raghavan et al. (2012) and Vaze et al. (2011) produce streamflow projections using climate models. Karl and Knight (1998) and McCabe and Wolock (2002) study the change of streamflow in the U.S. relating the change in streamflow to change in precipitation. On the other hand, as mentioned before, the magnitude of the impact of anthropogenic activities on streamflow has not yet fully reviewed. It is identified that the main anthropogenic activities influencing streamflow are urbanization, changes in agricultural practices, and construction of hydraulic structures. There are a few studies particularly focusing on these issues: e.g., Chelsea Nagy et al., (2012) and Huang et al., (2012) on the effects of urbanization; and Cruise et al., (2010) and Zheng et al., (2012) about changes in land use on hydrology

While many studies exist that quantify the effect of climate or landuse on streamflow, it is sometimes necessary to find how much of the streamflow is affected from anthropogenic activities versus climate effects. Such information may enable to develop mitigation strategies depending on whether climate or humans are primarily affecting the changes in streamflow.

Therefore, the objective of this study is to broaden the scope of understanding the dynamics of impacts from anthropogenic activities towards streamflow and to quantify the relative impacts of climate and anthropogenic activities on streamflow. More specifically, long-term streamflow records measured at United States Geological Survey (USGS) gauging stations from four different states are used to investigate the role of climate impact and anthropogenic activities.

3.3 Related Work

Several approaches including hydrologic simulation, mass balance and regression approach are applied in the recent studies to scrutinize the effects of climate impact and anthropogenic activities on streamflow Among the approaches, the hydrologic simulation approach is based on a hydrologic model as employed by (Bao et al., 2012; Jones et al., 2006; Ma et al., 2010; Wang et al., 2010; A. Zhang et al., 2012). Although this approach is technically sound, it needs a great amount of painstaking data gathering and an extensive amount of computational time to use a simulation model over large areas. On the other hand, the mass balance approach uses the water-energy balance over a long-term scale (Dooge J.C.I. et al., 1999, p. 199; Jones et al., 2006; Li et al., 2007; Ma et al., 2008; Milly, 1994; Wang and Hejazi, 2011). A typical example of this approach is the *Budyko* theory (Budyko, 1974) in which annual water balance is regarded as a manifestation of the competition between available water and available energy. However, the selection of appropriate governing equations is challenging; the simplicity of the

theory prevents it from being applied to diver catchemtns (Gentine et al., 2012). Another well-known approached is the regression approach, which uses a linear regression between predictor and predictand variables (Huo et al., 2008; Jiang et al., 2011; Tian et al., 2009; Wang et al., 2012; Ye et al., 2003). In the theory, the expected objective values are estimated using the independent variables, then, the differences from actual values are analyzed. Although convenient, this approach may not capture the true non-linear nature of the hydrologic system being analyzed.

Due to the diverse limitations of each approach, results obtained from a single approach are subject to produce imperfect results; a direct comparison of the results from the three approaches is necessary to find out their validity and reliability. To overcome the limitations of preceded studies, this study implements the four approaches in quantifying the relative effects of natural impact and anthropogenic activities on streamflow conditions.

3.4 Study Areas and Data

To accomplish the objective of this study, test beds with diverse climates as well as human activities are needed; thus, four states—New York, Indiana, Arizona and Georgia—are selected. Indiana and New York States have humid continental climate conditions, while Arizona and Georgia experience dry and humid subtropical climate conditions. The total annual average precipitation in New York and Indiana is

approximately 40 inches. The total annual average precipitation in Georgia is around 45 inches, and Arizona experiences the least amount of annual average precipitation of 12.7 inches. To study the role of human activities on streamflow, several methods can be considered;. one practical way is to look at the changes in population in the studied areas. Population change leads to change in landuse, which eventually affects the whole streamflow. The change in total population between 1950 and 2010 for the states is shown in Figure 3.1.

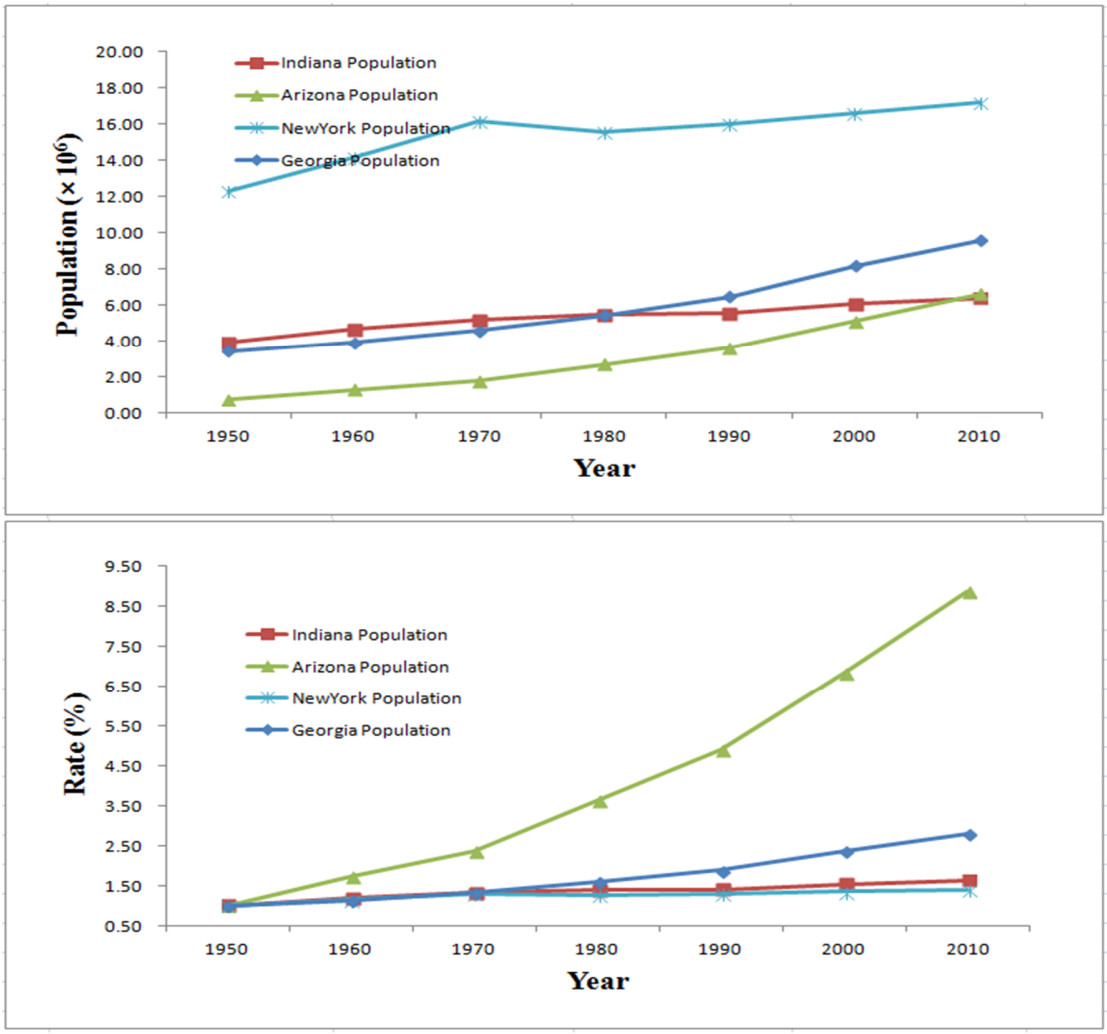

Figure 3.1 Population changes in the study areas (a) Absolute population per decade (b) Population rate based on the population in 1950

According to Figure 3.1, Indiana has the second largest population in 1950 following New York, but the population in Indiana is the smallest in 2010 compared to the other states. Between 1950 and 2010, Arizona has the highest rate of change in population with respect to the population in 1950, followed by Georgia. The magnitude in change of population for Indiana and New York is relatively small from 1950 to 2010. Another useful way to measure the human activities in a region is to follow the changes in the

urban area of the region; for example, Gibson (1998) describes that Phoenix (AZ) shows the highest rate (24.55 times) of change in urban area in the U.S. from 1950 to 1990. Among the four states, New York (NY) shows a slightly decreasing change, 0.98 times from 1950 to 1990. The rate of change in population for Atlanta (capitol of Georgia) and Indianapolis (capitol of Indiana) is 3.57 and 6.55, respectively.

With respect to the objectives of this study, New York, which is the most developed among the four states, has shown a fairly stable magnitude of the impact of anthropogenic activities. Arizona on the other hand represents a rapidly developing region between 1950 and 2010, followed by Georgia. While Indiana's population did not change during the same time period, its landuse change significantly due to growing agricultural activities in the state.

To fulfill the objective of this study, climate and streamflow data of the four states are gathered. Climate data mainly include precipitation, potential evapotranspiration (PET) and evaporation. Climate data are obtained from the Global Historical Climatology Network (GHCN) version 2 and the Climate Anomaly Monitoring System (CAMS) provided by the Climate Prediction Center (Fan and van den Dool, 2008). The GHCN + CAMS combination provides an observation-based reanalysis data at 0.5 degree spatial resolution and monthly time interval since January, 1948.

Furthermore, monthly streamflow data are obtained from the United States Geological Survey (USGS) National Water Information System (NWIS). Only the stations with continuous streamflow data from 1950 to 2010 are included in this study because not all stations have data for this period. A total of 103 streamflow stations, including 27 in Indiana, 27 in New York, 28 in Georgia and 21 in Arizona are used in the analysis. Compared to the stations in other states, streamflow stations in Arizona are fairly concentrated in the central part of the state. It is expected that this fact would not affect the results of this study as most of the development in Arizona over the last few decades has taken place in the central part; the results will reflect the effects of the development on the streamflow.

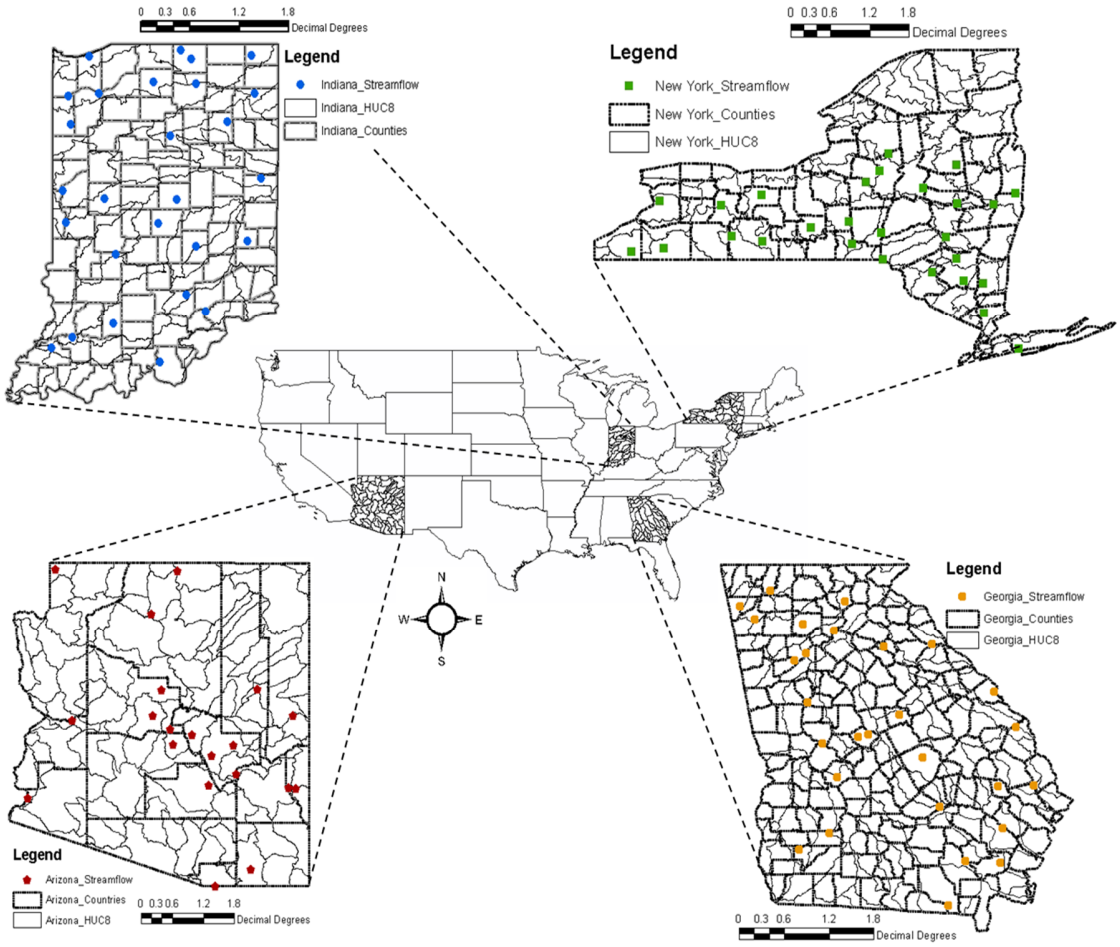

Figure 3.2 Location of the study areas and the streamflow gauges

3.5 Methodology

The effect of climate and anthropogenic factors on streamflow is not quantified in absolute terms, but it is quantified in relative terms based on the analysis of the data for two different periods. These include the 'natural period' from 1950 to 1979, and the 'impact period' from 1981 to 2010. A dataset of 30 years in each period is applied to overcome the limitation of a small sample size for statistical analysis. In a data analysis, changing points represent abrupt changes due to reservoir constructions or other factors

that directly affect the magnitude of a streamflow. As many changing points are detected around the year of 1980 when Pettitt Test (Pettitt, 1979) is applied to the streamflow data in this study, the data from 1980 is excluded from the overall analysis to reduce the distortion of the results due to the influence of the abrupt changes.

The methodology of this study mainly consists of three parts: trend analysis, hydrologic modeling and impact quantification. It is hypothesized that the streamflow increased in the impact period (1981-2010) compared to the natural period (1950-1979). To test this hypothesis, trend analysis is first performed to examine that the data at streamflow stations show an increasing trend. The analysis provides an indication of increasing or decreasing trend, which can then be investigated for possible climate or anthropogenic influence. Therefore, quantification of both the changes in magnitude as well as impacts is simultaneously needed.

Hydrologic modeling involves simulation using four different methods, including linear regression, hydrologic simulation, annual balance, and Budyko analysis. Results from hydrologic simulations are then used for calculating the amount of anthropogenic and climate impacts. Details of trend analysis, hydrologic simulation methods and the process of impact quantification are provided below.

3.5.1 Trend Analysis

The Mann-Kendall (MK) test (Kendall, 1955; Mann, 1945) is one of the popular non-parametric methods for analyzing trends in hydrologic variables (Hamed and Ramachandra Rao, 1998). Let S denotes MK test results, and can be acquired by the Equation (3-1) below.

$$S = \sum_{i=1}^{n-1} \sum_{j=i+1}^{n} \operatorname{sgn}(x_j - x_i) \tag{3-1}$$

$$\text{Where, } \operatorname{sgn}(x_j - x_i) = \begin{cases} +1, & x_j > x_i \\ 0, & x_j = x_i \\ -1, & x_j < x_i \end{cases},$$

n is the sample size and x is the target variable. Once n is greater than 8, S values will follow an approximate normal distribution (Zhang et al., 2011). The mean and variance of S is

$$E(S) = 0 \tag{3-2}$$

$$Var(S) = \frac{n(n-1)(2n+S)}{18} \tag{3-3}$$

Then, the Mann-Kendall Z is given by:

$$Z = \begin{cases} \dfrac{S-1}{\sqrt{Var(S)}} & for \;\; S > 0 \\ 0 & for \;\; S = 0 \\ \dfrac{S+1}{\sqrt{Var(S)}} & for \;\; S < 0 \end{cases} \qquad (3\text{-}4)$$

A positive Z-value means an increasing trend, and vice versa. It is also used to test the null hypothesis H_o that there is no significant trend. A significance level of 0.05 is used to test the null hypothesis of no trend in this study.

3.5.2 Hydrologic models

3.5.2.1 Linear Regression (LR)

Jiang et al. (2011) suggested a linear regression approach to estimate the monthly streamflow using a function of precipitation and PET. On a monthly time scale, groundwater storage may play some role in the generation of streamflow. However the original equation proposed by Jiang et al. (2011) does not have any term to represent this storage. As a result, Jiang et al.'s equation is modified by including an autoregressive (1) function of precipitation as presented in Equation (3-5).

$$Q_i = a_i \; P_i + b_i \; P_{i-1} + c_i \; PET_i + d_i \qquad (3\text{-}5)$$

Where, Q, P, and PET represent run-off, precipitation, and potential evapotranspiration, respectively for month i. Variables *a*, *b*, *c* and *d* are coefficients estimated by Least square estimation (LSE).

The coefficients are obtained for the above equation by using Q, P and PET for the natural period, and are then applied to estimate Q in the impact period. The calculated streamflow in the impact period can be considered to include the change in climate for the impact period while retaining the impact of anthropogenic activities from the natural period. The difference in the observed streamflow and the calculated streamflow will then yield the contribution from anthropogenic activities during the impact period. Equations (3-6) and (3-7) show how the climate impact and the impact of anthropogenic activities can be quantified by using the simulated and observed streamflow.

$$\Delta Q_{\text{climate}} = \left| \bar{O}_n - \bar{Q}_m \right| \qquad (3\text{-}6)$$

$$\Delta Q_{human} = \left| \bar{O}_m - \bar{Q}_m \right| \qquad (3\text{-}7)$$

$$\Delta Q_{total} = \Delta Q_{human} + \Delta Q_{\text{climate}} \qquad (3\text{-}8)$$

Where, ΔQ_{human} represents the average change in streamflow cause by human activities, and $\Delta Q_{climate}$ represents the average change in streamflow caused by climate impact, $\bar{O}_m$ represents the average observed monthly streamflow during the impact period, $\bar{Q}_m$

represents the average simulate monthly streamflow during the impact period, and $\bar{O}_n$ represents the average observed monthly streamflow during the natural period.

3.5.2.2 Hydrologic Simulation (HS)

Linear regression approach presents a very simple way of describing the relationship between climate variables and streamflow, which are non-linearly related. Therefore, a better way to describe the non-linear relationship between climate and streamflow is through a simulation model. Soil and Water Assessment Tool (SWAT), Variable Infiltration Capacity (VIC) and Hydrologic Engineering Center's Hydrologic Modeling System (HEC-HMS) can be regarded as representative hydrologic models that can be used for this purpose. However, a parsimonious runoff model is relatively more effective and computationally less intensive in simulating hydrology over larger spatial and temporal scales. Therefore, a parsimonious runoff model, called GR2M, which was proposed by Mouelhi et al. (2006) is used in this study. GR2M uses only two parameters: *X1*, and *X2,* where parameter *X1* governs the soil moisture accounting and *X2* is used for calculating the groundwater exchange. A genetic algorithm routine proposed by Sivanandam and Deepa (2007) is used to calibrated GR2M for X1 and X2 by using the observed data in the natural period from 1950-1979. Calibrated parameters are then used to create simulated streamflow for the impact period. The effects of climate impact and anthropogenic activities on streamflow are then calculated by using Equations (3-6) and (3-7), respectively.

3.5.2.3 Annual Balance (AB)

The annual balance concept was initially formulated by Li et al., (2007). While *LR* and *HS* are grounded on the monthly streamflow estimation, AB is based on the annual streamflow calculation. In this study, a modified form (Eq. (3-9)) of the original equation proposed by Parks and Madison (1985) is employed to estimate the annual streamflow. The original equation proposed by Parks and Madison (1985) only had the drainage area and precipitation term. Because evapotranspiration plays a major role on the overall water balance, it is added in the current study.

$$Q_k = 10^d \times DA^e \times P_k^f \times PET_k^g \qquad (3\text{-}9)$$

Where *DA* is the drainage area, *P* and *PET* are precipitation and potential evapotranspiration, respectively for the k^{th} year. Variables *d, e*, *f* and *g* are coefficients.

The methodology to compute the change in average flow due to climate impact and anthropogenic activities is similar to that for HS, where the coefficients for Eq. 9 are estimated by using the observed data in the natural period, and simulated streamflow is generated for the impact period. The change in streamflow due to climate impact and the climate impact are then computed by using Equation (3-6) and (3-7), respectively.

3.5.2.4 Budyko Analysis (BA)

Budyko (1974) suggested that the ratio of evaporation to precipitation is controlled by the ratio of PET to precipitation. Since then, governing equations for the Budyko hypothesis have been proposed by several scientists (Milly, 1994; Porporato et al., 2004; Zhang et al., 2001). Equation (3-10) proposed by Zhang et al (2001) is used in this study.

$$\frac{E}{P}=\frac{1+w(PET/P)}{1+w(PET/P)+(PET/P)^{-1}} \qquad (3\text{-}10)$$

where w is the plant-available water coefficient which ranges between 0.01 and 2.0 for grassland and forest, respectively. In this study, w is estimated by trial and error approach with increments in 0.001. Evaporation used in this study is calculated by using a water balance approach (Eq. 3-11).

$$P=E+Q+\Delta S \qquad (3\text{-}11)$$

where, P is precipitation, E is evaporation, Q is streamflow and ΔS is change in basin water storage.

In order to quantify the climate impact and the impact of anthropogenic activities by using Equation (3-10), Li et al. (2007) proposed Equations (3-12) ~ (3-15) as presented below.

$$\beta = \frac{1 + 2x + 3wx}{(1 + x + wx^2)^2} \quad (3\text{-}12)$$

$$\gamma = -\frac{1 + 2wx}{(1 + x + wx^2)^2} \quad (3\text{-}13)$$

$$\Delta Q_{\text{climate}} = \beta \Delta P + \gamma \Delta PET \quad (3\text{-}14)$$

$$\Delta Q_{total} = \left|\Delta Q_{\text{climate}}\right| + \left|\Delta Q_{\text{human}}\right| \quad (3\text{-}15)$$

where β is the sensitivity of streamflow to precipitation, γ is the sensitivity of potential evapotranspiration, x is the index of dryness (PET/P), and $\Delta Q, \Delta P, \Delta PET$ are the changes in streamflow, precipitation and potential evapotranspiration, respectively.

3.5.3 Quantifying the impacts

After ΔQ_{human} and $\Delta Q_{\text{climate}}$ are computed by the above four methodologies, the relative climate impact and the impact of anthropogenic activities can be quantified by using Equations (3-16) ~ (3-17) described below.

$$\text{Human Impact} = \frac{\Delta Q_{human}}{\Delta Q_{total}} \times 100(\%) \quad (3\text{-}16)$$

$$\text{Climate Impact} = \frac{\Delta Q_{\text{climate}}}{\Delta Q_{total}} \times 100(\%) \qquad (3\text{-}17)$$

3.6 Results

3.6.1 Trend Analysis

The trend in annual precipitation, potential evapotranspiration and streamflow data is analyzed by using the MK test. Figure 3.3 shows the MK test results using three different time periods representing the total period (1950-2010), natural period (1950-1979) and the impact period (1981-2010). It is clear that there are many locations which show different trends for natural and impact periods. While there is trend in the data at most stations, the significance of these trends need to be analyzed. The stations showing significant trends are presented in Figure 3.4 and the numbers of stations are presented in Table 3.1. The results in Figure 3.4 are quite similar to the results of Lins and Slack (1999), who evaluated the trends in streamflow at 395 climate-sensitive streamflow gauging stations in United States. Similar to Lins and Slack results, the stations showing the significant changes are in Indiana and New York. In contrast, Georgia does not have any gauging station that shows significant change in streamflow trend.

Many locations in New York and Arizona show significant trend for PET. The change in precipitation trend is significant at few locations in Indiana and New York. PET trends are assumed to be caused by the change of temperature since it is a main factor to determine the amount of PET. According to Karmeshu (2012), since the late 1970's, the

temperature in the U.S has been increasing at nearly twice the global rate, especially in the northern and western parts.

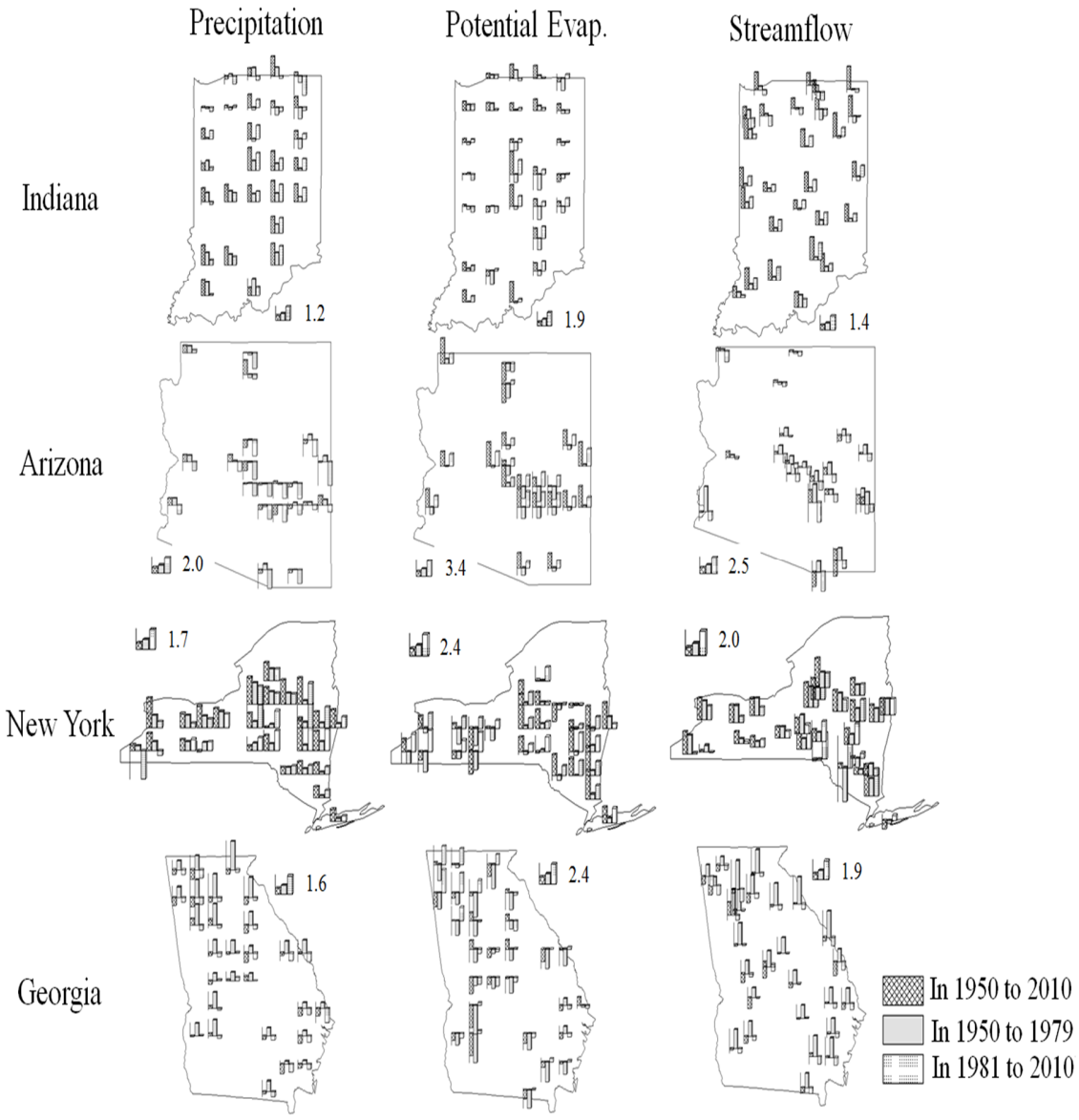

Figure 3.3 The results of Mann-Kendall analysis for precipitation, PET and streamflow for all study areas

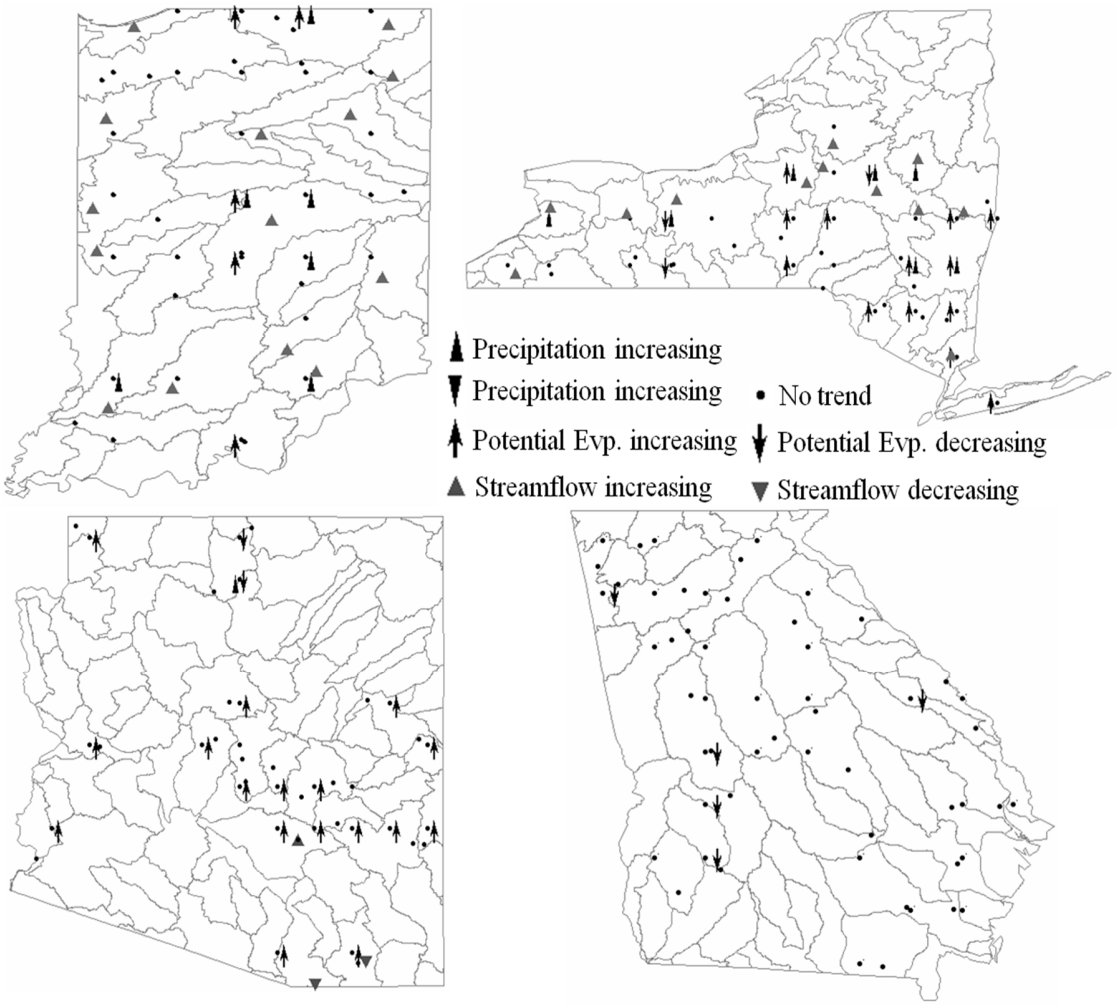

Figure 3.4 Location of significant Mann-Kendall trends for: (a) Indiana; (b) New York; (c) Arizona; and (d) Georgia

Table 3.1 Number of stations showing significant trend in each state at = 0.05

States (Total Stations)	Precipitation	Potential ET	Streamflow
Indiana (27)	6	5	14
New York (21)	7	16	12
Arizona (27)	1	19	3
Georgia (28)	0	5	0

3.6.2 Hydrologic Simulations

Four methodologies (LR, HS, AB and BA) are used in this study for simulating the hydrology in the four states. The results from each method are reported by using the Nash Sutcliffe Coefficient (NSC; Nash and Sutcliffe, (1970)).

$$NSC = 1 - \frac{\sum_{t=1}^{T}(O_t - Q_t)^2}{\sum_{t=1}^{T}(O_t - \overline{O}_t)^2} \qquad (3\text{-}18)$$

where O is observed monthly discharge, and Q is modeled monthly discharge. Nash–Sutcliffe efficiencies can range from $-\infty$ to 1. An efficiency of 1 (NSC = 1) corresponds to a perfect match of modeled discharge to the observed data. According to Moriasi et al. (2007), the accuracy of monthly simulations is satisfactory if the value of NCS is greater than 0.5. The average NSC value for all the three methods applied in this study is greater than 0.5 except for Arizona. The NSC values are low in Arizona because the amount of PET is larger than the amount of precipitation in this region (Table 3.2). Among all the methods, the LR produces the highest NSC for the four states. The NSC values are primarily computed for the natural period to make sure that the model is able to simulate hydrologic conditions based on climate impact, and produce reasonable outputs during this period. The values of NSC would be different if NSC was calculated for individual months or seasons. However the goal here is to compare the change in streamflow for two periods of 30 years. Thus, the accuracy using all the data taken together is investigated in this study.

Table 3.2 NSC values for three methods in the impact period

States	Methods		
	LRM	HSM	ABM
Indiana	0.733	0.491	0.653
New York	0.724	0.447	0.616
Arizona	0.603	0.298	0.304
Georgia	0.726	0.492	0.634

3.6.3 Quantification of Impacts

Equations (3-16) and (3-17) are used to quantify the impact from climate and human factors by comparing the average change in streamflow amount during impact period in relation to the natural period, based on two defined periods. Equation (3-6) and (3-7) give the average amounts of the human and climate impacts for the entire period. However, the human and climate impacts can be also acquired by using Equations (3-6) and (3-7) for annual data. Figure 3.5 shows the yearly estimates of climate impact and the impact of anthropogenic activities for the East Fork White River at Shoals (EFWRS), located in southern Indiana. The MK test results for the location show that the streamflow is significantly increased over 61 years (1950 ~ 2010) with 95 confidence interval. Figure 3.5 (a) demonstrates the degree of the impact of anthropogenic activities based on the time and Figure 3.5 (b) represents the degree of climate impact. Although the results may differ slightly depending on the methods, but overall the pattern is consistent among all

four methods. In addition, the impact of anthropogenic activities is somewhat growing over the entire period of analysis.

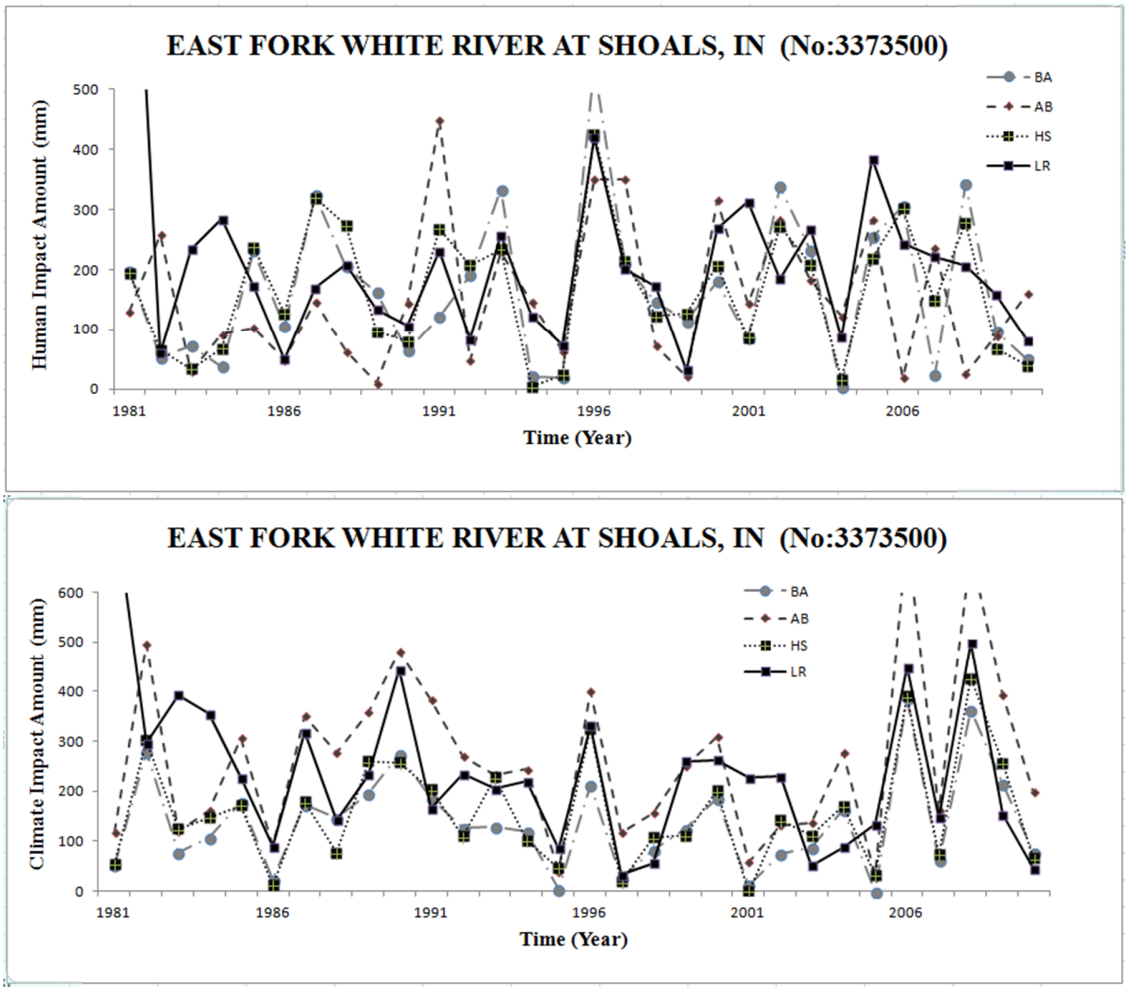

Figure 3.5 Climate impact and the impact of anthropogenic activities amounts for East Fork White River at Shoals gauging station in Indiana using the four methods. (LR- Linear Regression, HS- Hydrologic Simulation, AB- Annual Balance, BA- Budyko Analysis)

Figure 3.6 shows the relative role of anthropogenic impact and climate impact on streamflow in Indiana by using the four hydrologic modeling approaches. Both LR and HS show similar results because of their similarity in the overall concept. Even the results

from AB, which calculates the annual streamflow, show many similarities with the LR and HS results. In all four methods, the amount of the impact of anthropogenic activities is larger at many stations in Northwestern Indiana compared to other parts in the state. The streams in northwestern Indiana are significantly altered through construction of ditches, and this has contributed to increased flow in this region. Demonstration of the high impact of anthropogenic activities in northwestern part by all four methods proves that these methods are indeed able to capture the relative impact of anthropogenic activities on the overall streamflow.

However, these methods can only show significant the impact of anthropogenic activities if most of the anthropogenic activities occurred during the impact period. If the anthropogenic activities have been occurring over the entire period of record, the relative contribution of the impact of anthropogenic activities may get minimized in the final result. For example, Indianapolis (shown in Figure 3.6) is the most urbanized city in Indiana so the influence of anthropogenic activities on streamflow is expected to be larger in this area compared to other areas. However, the results for Indianapolis are contrary to what is expected. Thus, the results obtained in this study are dependent on how the natural and impact periods are defined, and the relative anthropogenic activities during these periods.

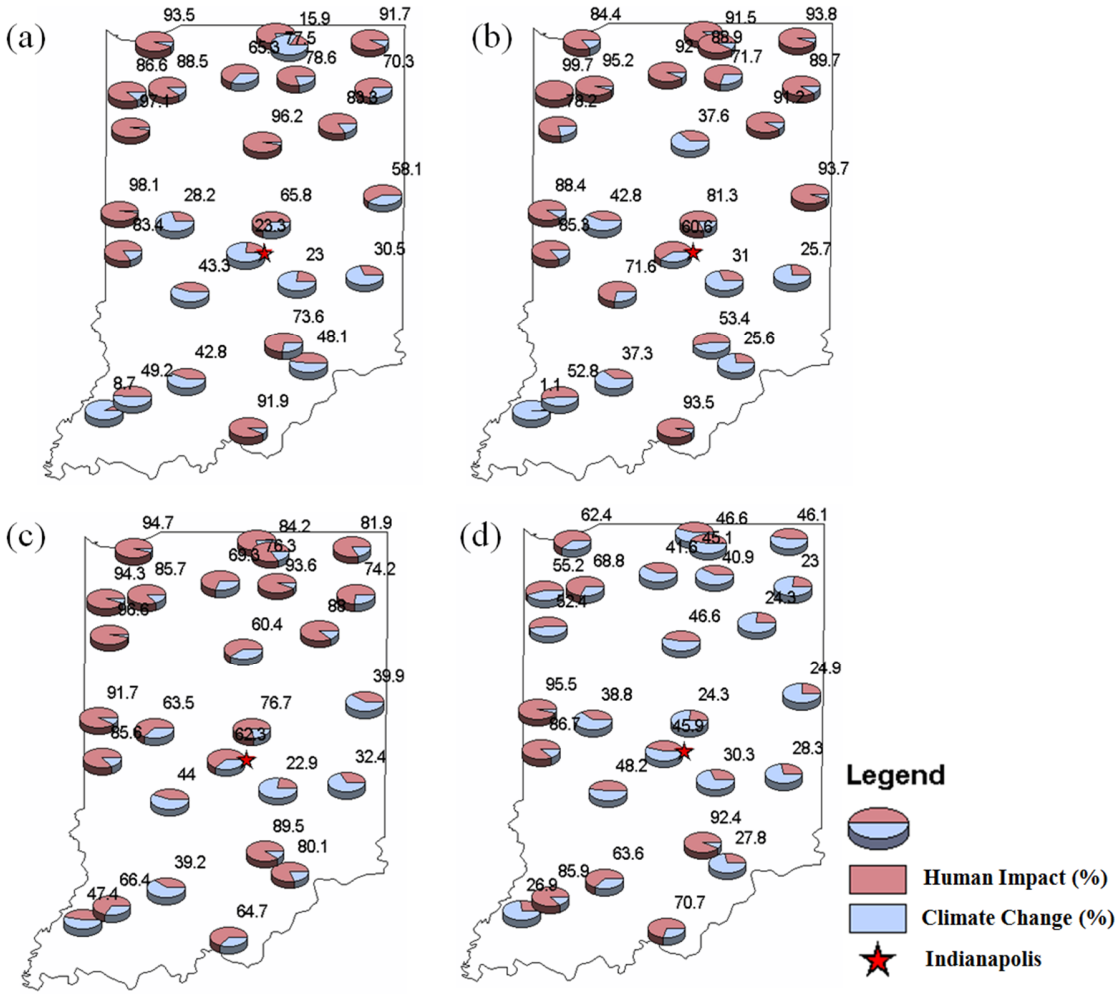

Figure 3.6 The results of human and climate impacts for Indiana using: (a) LR (Linear regression); (b) HS (Hydrologic simulation); (c) AB (Annual balance) and (d) BA (Budyko analysis)

The average anthropogenic and climate impacts for all the study areas using the four methods are shown in Figure 3.7. As mentioned in the previous paragraph, the amount of anthropogenic or climate impact varies across the whole state of Indiana. In contrast, New York State is characterized by relatively small variations in the results. Compared to Indiana, the influence of the impact of anthropogenic activities is prevalent in the whole state of New York. It is also noteworthy that very few stations demonstrates extreme

effect (defined as more than 80%) for anthropogenic or climate impact. The reason for absence of extreme results may again be due to the limitation of this research that assumes the data in the natural period as unaffected from the impact of anthropogenic activities. The population of New York State has been continuously increasing in both natural and impact periods (Figure 3.1), and therefore it is not possible to get the drastic impact of anthropogenic activities results during the impact period. Higher amount of the impact of anthropogenic activities may only be obtained if major population increase occurs during the impact period.

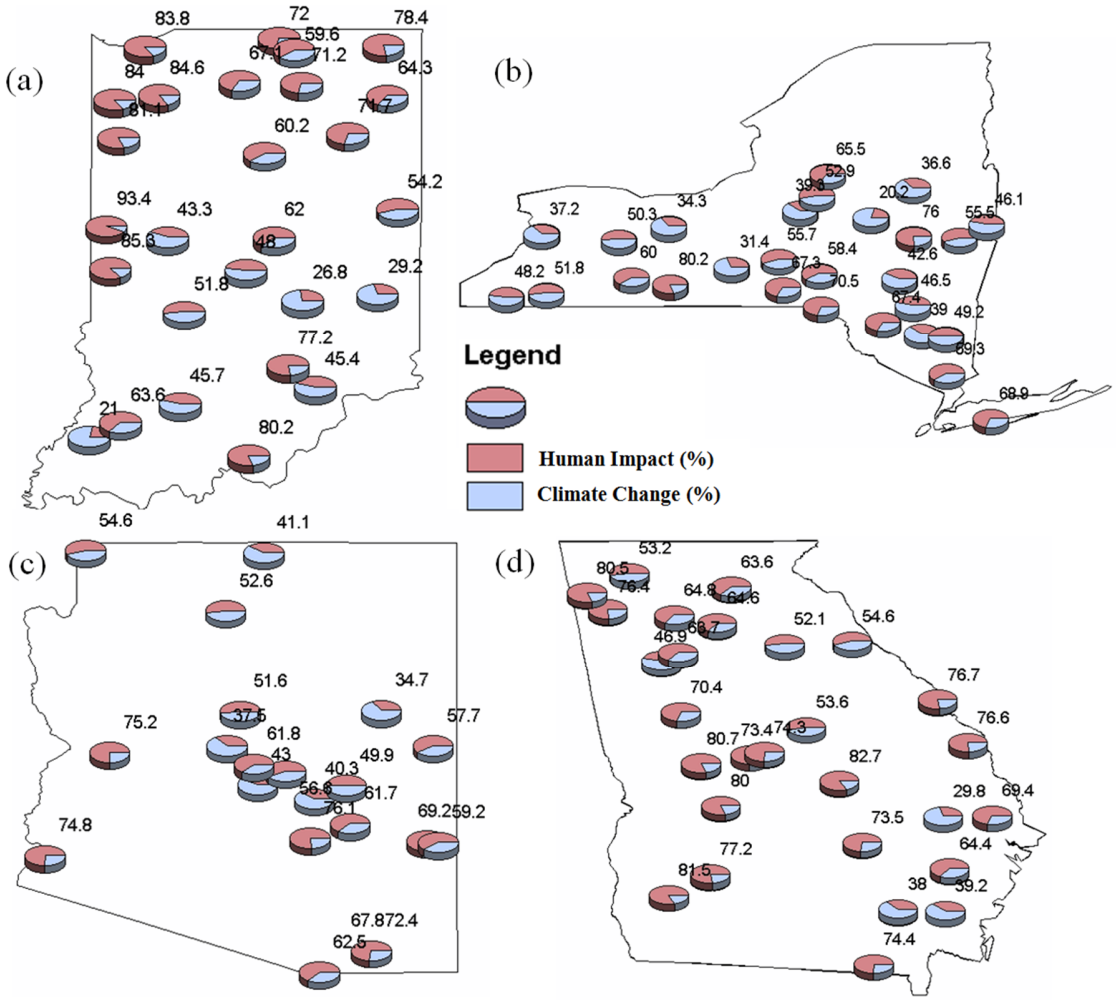

Figure 3.7 Average climate impact and the impact of anthropogenic activities from all four methods for: (a) Indiana; (b) New York; (c)Arizona; and (d) Georgia

Based on Figure 3.1, the population in Arizona and Georgia has been growing at a relatively steeper rate compared to Indiana and New York. If increasing population represents higher degree of the impact of anthropogenic activities, a higher amount of anthropogenic impact would be expected in both of these states. Interestingly, all methods used in this study produce relatively lower amount of the anthropogenic impact for Arizona. One possible reason for this may be significant changes in the PET in

Arizona over the study period. In the result of MK test, the increasing trend in PET is significant at more than 70% stations in Arizona. Therefore, even the climate impact is playing a significant role on the change of streamflow in Arizona. On the other hand, the impact of anthropogenic activities is significantly visible for most stations in Georgia. Only four out of 28 stations in Georgia show that the climate impact is higher than the impact of anthropogenic activities. The percentage of stations that show human and climate impact is presented in Table 3.3.

Table 3.3 Percentage of stations showing the climate impact and the impact of anthropogenic activities

	Indiana	New York	Arizona	Georgia
Anthropogenic impact	74.0 %	55.5 %	71.4 %	85.7 %
Climate Impact	26.0 %	44.5 %	28.6 %	14.3 %

The percentage of stations that show greater the impact of anthropogenic activities compared to climate impact is relatively higher for Arizona and Georgia compared to New York. These results demonstrate that anthropogenic activities plays a crucial role in the change of streamflow, and that approach of using population change as an indicator of anthropogenic activities is reasonable for Arizona and Georgia. In the case of Indiana, population has remained relatively flat for the last century, but most of the anthropogenic activity is in the form of agricultural expansion. Seventy four percent stations in Indiana show the higher impact of anthropogenic activities on streamflow compared to climate due to agricultural activities in the state. Although the population increase in the state of

New York is relatively slow compared to Arizona, the number of stations that show the higher impact of anthropogenic activities is greater than the number of stations showing climate impact. Therefore, the role of anthropogenic activities should get equal or more consideration in relation to climate impact when looking at the overall impact on the hydrologic system.

The use of trend analysis to study the effect of climate or other activities on streamflow is a standard practice adopted by many researchers (Chen et al., 2013; Wu et al., 2012; Zhang et al., 2008). The spatial distribution of the impact of anthropogenic activities (Figure 3.7) and significant trends in data (Figure 3.4) show that just looking at trends may not provide a complete picture of how the streamflow has been affected. For example, the northwestern part of Indiana does not show significant increasing or decreasing trend for most stations. It is known that the streamflow in this region is affected by channeling and ditch construction activities. This effect clearly emerges in the form of the higher impact of anthropogenic activities in the northwestern part of the state. Similarly, no significant trends in streamflow and precipitation are found for most stations in Georgia, but Figure 3.7d shows that streamflow at many stations in Georgia is affected by anthropogenic activities. In addition, stations show increasing precipitation trends in Figure 3.4 for all states tend to correspond well with climate impact locations in Figure 3.7.

3.7 Summary and Conclusions

The objective of this study was to investigate and quantify the relative amount climate impact and anthropogenic activities on the hydrology of four states, including Arizona, Georgia, Indiana and New York. The study area were selected to represent various anthropogenic activities, and included data for 103 stations from 1950 – 2010. Hydro-climatic variables including precipitation, PET and streamflow for all locations were first analyzed to examine their degree of change using the MK test. Four methods, including linear regression, hydrologic modeling, annual balance and Budyko analysis were used to quantify the relative amounts of anthropogenic and climate impact on streamflow.

Based on the NSC values (see Table 3.2), the linear regression method gives the best results for simulating the hydrology during the natural period. Although the NSC values for other methods are lower compared to the linear regression method, the overall pattern of relative anthropogenic and climate impacts is similar for all four methods as demonstrated by Figure 3.6 for Indiana (similar results for other states are not shown). While any method can be used to identify the locations affected by anthropogenic versus climate impact, taking the average of four methods in quantifying the impact provides more confidence in the results than the result obtained from just one method.

While the effect of climate on hydrologic system cannot be ignored, the results (Table 3.3) for the four states used in this study show that the percentage of stations that show impact of anthropogenic activities on streamflow is significantly higher compared to climate

impact. Therefore, the role of human activities should be given more attention when looking at future long-term forecasts, including extremes.

Anthropogenic activities can impact streamflow in several ways through urbanization, agricultural development, storm water management and construction of hydraulic structures, among others. In this study the change in population was used as an indicator of anthropogenic impact on streamflow assuming that an increasing population. While population increase can be related to streamflow change in some states (e.g., Georgia and New York in this study), this study has shown the impact of anthropogenic activities in some areas, e.g., Indiana in this study, is not directly related to population. Agricultural expansion in Indiana is caused by increased demand for corn or soy bean by non-Indiana residents and increase biofuel activities in the region. Therefore, a better approach would be to investigate the role of individual human activity such as urbanization, agricultural and hydraulic structures on streamflow.

The results from this study show that a just trend analysis may not give a complete picture of the streamflow changes that are affected by anthropogenic activities such as channelization. Therefore, a combination of trend analysis and any of the four methods should be used to investigate anthropogenic or climate impacts on streamflow.

The results also show that the approach adopted in this study for quantifying anthropogenic and climate impact is influenced by the temporal domain used for defining the natural and impact periods. Similarly, the relative development of anthropogenic

activities during the natural and impact periods also affect the results. For example, in urban areas that are undergoing development during both the natural and impact periods, the amount of the impact of anthropogenic activities will be relatively smaller than the areas that have seen most of the development during the impact period. Despite lower magnitude of the anthropogenic impact, the methods used in this study are still able to the show relative dominance of anthropogenic impact on streamflow for areas (e.g., Indianapolis in Indiana) that have seen steady development during both natural and impact period.

CHAPTER 4. THE EFFECT OF LAND USE CHANGE ON HIGH AND LOW FLOWS

4.1 Abstract

Land cover is a very important factor for hydrologic processes at the basin and regional scale. Therefore, understanding how the hydrologic system is affected by land cover change is significant for the overall management of water resources. The objective of this study is to investigate the effect of land cover change on the duration and severity of high and low flows by using the Soil Water Assessment Tool (SWAT) model and copulas. High and low flows are defined in terms of percentiles of streamflow. Two watersheds, which have different dominated land covers within the Ohio River basin, are employed to carry out this study. The results show that land cover change explicitly affects the duration and severity of both high and low flows. Increase in the forest area leads to a decrease in the duration and severity in high flow; its significant impact is observed in extreme high flows. The results also indicate that severity is occasionally affected more by the land cover change than the duration by land cover change in both high and low flows. In addition, at the basin scale, the change of forest area is likely to play a crucial role in determining runoff, compared to the change of urban area in both high flow and low flows.

4.2 Introduction

Land cover plays a major role in the overall behavior of a hydrologic system (Legesse et al., 2003). Understanding the effects of land cover change (LCC) on the hydrologic system is one of the crucial steps in the management of land use and water resources (Bulygina et al., 2013; Li et al., 2009). Numerous previous studies have investigated the impact of land cover condition on various hydrologic variables (Costa et al., 2003; Fang et al., 2013; Gebresamuel et al., 2010; Guo et al., 2008; He et al., 2008; Liu et al., 2009; Siriwardena et al., 2006; Zhang and Schilling, 2006; Zhou et al., 2013, 2012). The effect of land cover on a hydrologic system can vary under different geographic and climatic conditions. For instance, according to Beighley et al. (2003), who investigated the impacts of urbanization and climatic fluctuations on streamflow in the Atascadero Creek watershed located along the southern coast of California, found that an increase in impervious area induces a significant increase in streamflow. Similar results were found by Jennings and Jarnagin (2002) for Accotink Creek watershed in Virginia. Conversely, Chang (2003) found that urban growth is only projected to increase mean annual streamflow by less than 2% in the Conestoga River basin in Pennsylvania. Chang (2007) too found little or no effect of urbanization on streamflow for a watershed in the Portland Metropolitan Area.

According to Ma et al. (2009) and Mao and Cherkauer (2009), changes in forest area have the greatest impact on runoff; Ma et al. (2009) showed that reforestation causes a

decrease in mean annual streamflow in Kejie Watershed, China. Mao and Cherkauer (2009) show similar results in their study by investigating hydrologic impacts of land-use change on the water balance of three states including Minnesota, Wisconsin, and Michigan. In the results of Mao and Cherkauer (2009), deforestation leads to a 5–15% decrease in ET and a 10–30% increase in the total runoff. In contrast to their results, Beck et al. (2013) find that changes in forest area are not the major causes in the change of the streamflow; Beck et al. (2013) found no convincing change in streamflow conditions from the expansion of urban or forest area in 12 meso-scale humid tropical Purto Rican catchments.

These contradictory results found in the previous studies can be attributed to three major factors: the limitations of research methodologies such as limitation of hydrologic modeling; the differences in regions and scales of watersheds; and the limitations in establishing field experiments (Fang et al., 2013). Even when two watersheds share similar land cover characteristics overall, the differences in the spatial distribution of the land cover can produce varied hydrologic responses for the two systems. One way to understand the complex relationship between land cover and hydrology is through extensive field data collection and experimentation (Bathurst et al., 2011). While such efforts can be under taken for a small watershed, the same implementation for a larger watershed can be a very tedious and resource intensive. Similarly, the results acquired from a small watershed cannot be directly applied to a larger watershed. One way to overcome this limitation is through computational modeling.

Most previous studies including the ones mentioned above focus on effect of LCC on mean streamflow conditions. The effects of LCC on high/ low flow seemed to have received relatively less attention. Even studies focusing on high flows often concentrate on the changes in peak flow (Brath et al., 2006; Du et al., 2012; Wang and Melesse, 2006). Similarly, papers on the effects in low flow occasionally investigate the changes in flow magnitudes (Price et al., 2011; Savary et al., 2009). LCC can affect various aspects of high flow and low flow as well as maximum/minimum values. More specifically, it may contribute to the changes of the relationship between duration and severity in extreme flow. According to Javelle et al., (2003), besides instantaneous peak flow, the volume and duration of a flood event (high flow condition) should also be investigated for any flood analysis. Furthermore, the cumulative amount of streamflow is highly crucial in drought analysis (low flow condition), therefore, it is often used to define current drought situations (Ahn et al., 2012; Shukla and Wood, 2008). Thus, the overall objective of this study is to investigate the effects of LCC on duration and severity of high flow and low flow. To define the relationship between duration and severity, the copula method, which is widely used for studying multivariate distribution in hydrology (Li et al., 2009), is implemented in this study.

4.3 Study Areas and Data

4.3.1 Study area description

Two watersheds, White River Basin and Allegheny River Basin, in the Ohio River Basin in the United States (Figure 4.1) are selected as test beds for this study. These watersheds are selected primarily for their natural flow conditions, free from any upstream diversions and impoundments (United States Geological Survey (USGS), 2009). The White River Basin has a drainage area of 6,061 km^2 (2,341 $mile^2$) at East Fork White River in Seymour, IN streamflow gauge (USGS ID: 03365500); whereas the Allegheny River Basin has a drainage area of 4,163 km^2 (1,608 $mile^2$) at Allegheny River in Salamanca, NY streamflow gauge (USGS ID: 03011020). The climate condition for both study areas is characterized as humid continental. The average annual temperature and precipitation at White River Basin are 11.0 °C and 1020 mm, respectively, whereas the annual temperature and precipitation at Allegheny River Basin are 7.2 °C and 1130 mm, respectively.

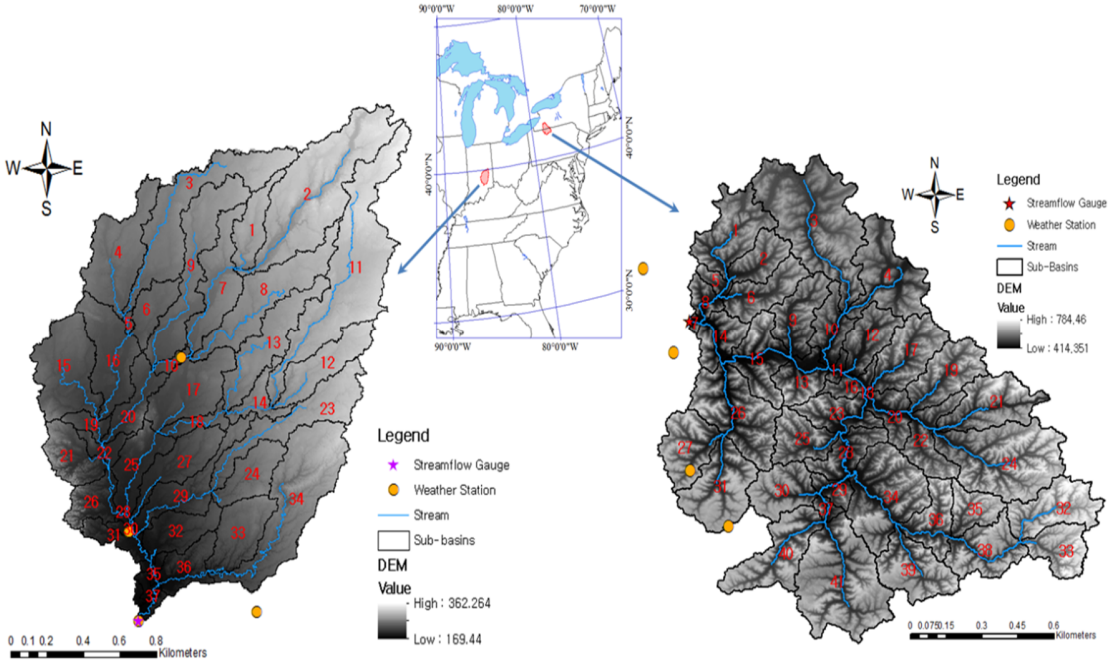

Figure 4.1 The study areas and locations of the observed gauges (The marked numbers in each study area represent the sub-basins)

4.3.2 Historical land cover

To study the effect of LCC, the decadal Historic Land Use data for Ohio River Basin 1930 – 1990 is employed in this study (Ray and Pijanowski, 2010). Compared with the national land cover database 2001 (NLCD 2001), which consists of 16 classifications for land cover information, the Historic Land Use has 4 classifications including urban, agricultural, forest and rangeland, and other land use. Table 4.1 shows the comparison of the land use descriptions of the Historic Land Use with the ones of the NLCD 2001.

Table 4.1 The land use description based on the NLCD 2001 and the Historic Land Use for the Ohio River Basin 1930 – 1990; the symbol numbers are also marked in each land cover data

	The Historic Land Use	The NLCD 2001
1	0 – Other Land Use	11 – Open Water 31 – Barren Land 90 – Woody Wetlands 95 – Emergent Herbaceous Wetland
2	1 – Urban	21 – Developed Open Space 22 – Developed Low Intensity 23 – Developed Medium Intensity 24 – Developed High Intensity
3	2 – Agriculture	81 – Pasture/Hay 82 – Cultivated Crops
4	3 – Forest and Rangeland	41 – Deciduous Forest 42 – Evergreen Forest 43 – Mixed Forest 52 – Scrub/Shrub 71 – Grassland/Herbaceous

Two different sets of the Historic Land Use—land of 1950s and land of 1990s—are used in this study and illustrated in Figure 4.2. From the 1950s to the 1990s, the land cover for White River Basin shows a 9.44 % decrease in agricultural area from 85.73 % to 76.29 %, and an increase in forest and rangeland area by 8.26 % and 1.18 %, respectively. The changes in land cover for Allegheny River Basin are relatively more pronounced; the forest and rangeland increased by 21.19 % from 60.78 % to 81.97 %, whereas the agricultural area decreased by 21.70 % from 34.20 % to 12.50 %. While the overall change in the urbanized area in both study areas is negligible, the LCC in both study areas can be characterized as change from agricultural land to forest and rangeland. The

percentage change in land cover for White River Basin and Allegheny River Basin is 9.44 % and 21.7 % of the entire area, respectively.

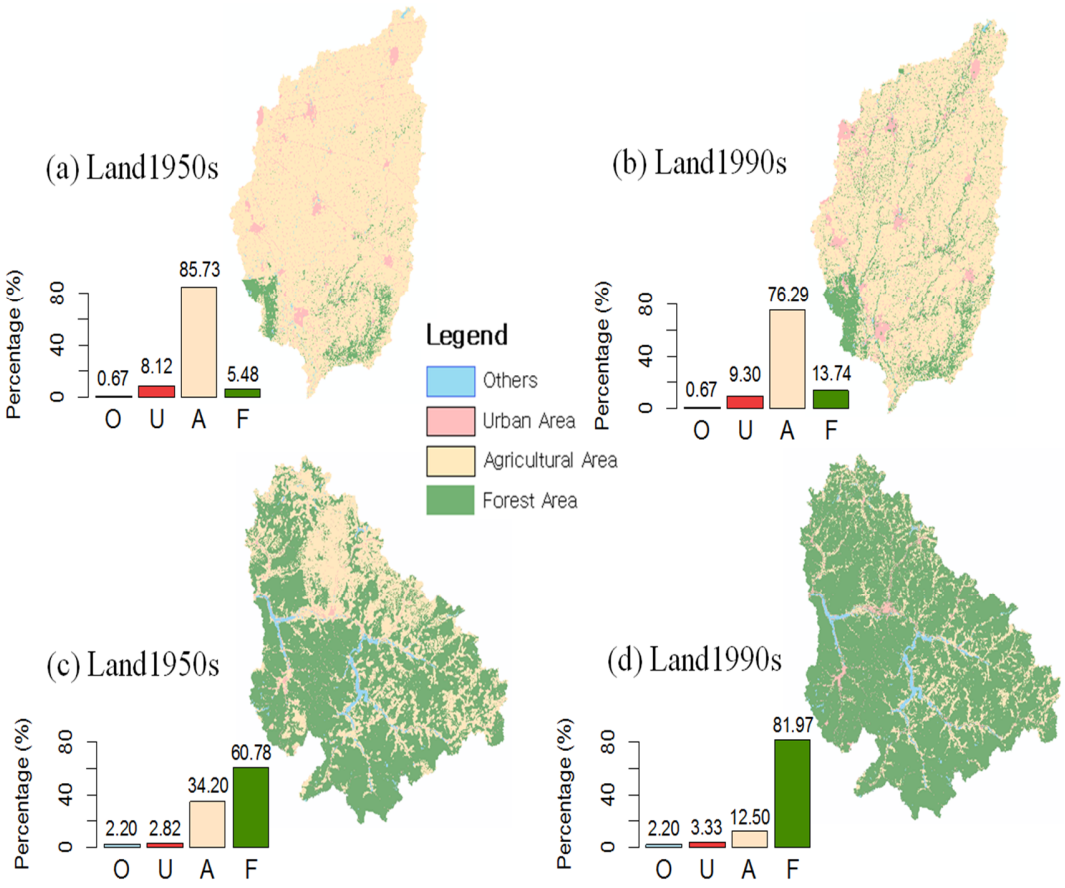

Figure 4.2 Land cover change in the study areas: (a) land cover 1950s for the White River Basin, (b) land cover 1990s for the White River Basin, (c) land cover 1950s for the Allegheny River Basin, (d) land cover 1990s for the Allegheny River Basin; O-others, U-urban area, A-agricultural area, and F- Forest and Rangeland

4.3.3 Data description

To investigate the effect of land cover change (LCC), hydrologic modeling using Soil Water Assessment Tool (SWAT) is performed. In addition to land use, 30m resolution digital elevation model (DEM) from the United States Geological Survey and the state soil geographic (STATSGO) are used. The SWAT model is driven by meteorological data including precipitation and temperature obtained from the National Climatic Data Center (NCDC) from 1952 to 1999. Climate data from a total of four stations in each study area as presented in Figure 4.1 is used in this study. Finally, the model is calibrated and validated for both watersheds by using gauged streamflow data from the United States Geological Survey (USGS).

4.4 Methodology

As the changes in precipitation are generally correlated with the changes of streamflow (Huang et al., 2013), a different trend between the two variables hint at the role of external factors such as LCC on streamflow. To investigate the trend in the data, the Mann-Kendall (MK) test (Kendall, 1955; Mann, 1945) is first employed. Then, to identify the land cover effect on streamflow, two different streamflow scenarios corresponding to land use conditions in 1950s and 1990s are independently generated by using the SWAT model. After the streamflows are generated, the durations and the severities are calculated in order to look at the effect of LCC on low and high streamflow

conditions. Finally, the copula method is applied to define the relationship between the duration and the severity of both low and high flow conditions. The details of each step in the methodology are provided in the following sub-sections.

4.4.1 Hydrologic model

SWAT model is an effective tool for assessing long-term impacts of land cover changes on surface hydrology (Fang et al., 2013; Guo et al., 2008). Furthermore, according to Borah and Bera (2003), SWAT is one of the encouraging models for long-term simulations in predominantly agricultural areas. Considering the above factors, the 2012 version of the SWAT model is adopted as a hydrologic model in this study.

4.4.1.1 Description of SWAT model

SWAT model is a process based basin-scale, continuous time and semi-distributed hydrologic model initially developed by the US Department of Agriculture (USDA) and Texas Experimental Station (TES) in the early 1990s (Du et al., 2013). SWAT conceptually sub-divides the watershed into sub-basins based on streamflow delineation using a DEM. These sub-basins are further delineated into hydrologic response units (HRUs) to capture the spatial heterogeneity in soil, land use and slope. For a given time step, hydrologic processes are calculated by using the water balance equation (Equation (4-1)) (Arnold et al., 1998).

$$SW_t = SW_{t-1} + \sum_{i=1}^{t}(P_i - Q_{surf,i} - ET_i - Q_{loss,i} - Q_{gw,i}) \qquad (4\text{-}1)$$

Where, SW_t is the soil water content at the end of day t, P is the precipitation, Q_{surf} is the surface runoff, ET is the evapotranspiration, Q_{loss} is percolation into deep aquifer and Q_{gw} is lateral subsurface flow, respectively; all units are in mm.

The Soil Conservation Service (SCS) curve number method is implemented for estimating surface runoff from daily precipitation. The Penman-Monteith method and variable storage method are selected to estimate evapotranspiration and perform channel flow routing, respectively.

4.4.1.2 Model calibration, validation and simulation

In the SWAT model, streamflow is generally affected by 27 parameters (Winchell et al., 2007). The limitations of manual calibration can be eliminated or overcome by using a sensitivity analysis (Franczyk and Chang, 2009). Through the global sensitivity analysis tool embedded in SWAT-CUP (Abbaspour et al., 2004), eight sensitive parameters for each study area are identified. This parameter sensitivity analysis is based on the multiple regression system, which regresses the Latin hypercube generated parameters against the objective function values. After the sensitive parameters are identified, model calibration is performed by the Sequential Uncertainty Fitting (SUFI-2) routine in the SWAT-CUP.

SUFI-2 has been recommended as a proper tool for calibration as well as for uncertainty analysis in the SWAT model (Abbaspour et al., 2007; Faramarzi et al., 2009; Rostamian et al., 2008; Setegn et al., 2010; Strauch et al., 2012). Model calibration is performed by using the Nash-Sutcliffe Efficiency (NSE; Eq. (4-2)) and the coefficient of determination (R^2; Eq. (4-3)) as performance indicators. The NSE and the R^2 are commonly used in the studies of hydrologic modeling (Han et al., 2012; Parajuli, 2010; Strauch et al., 2012).

$$NSE = 1 - \frac{\sum_{i=1}^{t}(O_i - S_i)^2}{\sum_{i=1}^{t}(O_i - \overline{O_i})^2} \quad (4\text{-}2)$$

$$R^2 = \frac{(\sum_{i=1}^{t}(O_i - \overline{O})(S_i - \overline{S}))^2}{\sum_{i=1}^{t}(O_i - \overline{O})^2 \sum_{i=1}^{t}(S_i - \overline{S})^2} \quad (4\text{-}3)$$

Where, O_i is observed streamflow and S_i is modeled streamflow at the *i*-th time step. The NSE can range from $-\infty$ to 1, whereas the R^2 can range from 0 to 1. The value of 1 in both cases corresponds to a perfect match between modeled streamflow and the observed data. Furthermore, a high-magnitude value of the NSE and the R^2 are preferred. According to Fang et al. (2013), NSE is recommended as an objective function in the parameters optimization rather than the R^2 since the NSE directly compares two variables instead of measuring the deviation from the best fit line as computed through R^2. Thus, the NSE is used for the objective function when the parameters are calibrated in this study.

Because two different land cover conditions (1950 and 1990) are used in this study, optimal values of the parameters can vary corresponding to these land covers. Accordingly, two different calibration and validation periods are employed for each study watershed ranging from the 1954 - 1959 for the 1950s scenario, and from 1994 - 1999 for the 1990s scenario. In both scenarios, the last year is used for validation. After calibration and validation, the SWAT model is used to simulate stream flow from 1952-1999 (2 years for warm-up) to produce flow corresponding to the 1950s and 1990s scenarios.

4.4.2 Definition and characteristics of high flow and low flow

After the streamflow corresponding to 1950s and 1990s scenarios is generated, low and high flow events are identified. There is no single criterion to define a low or high flow event. In the previous studies, various definitions are implemented for both high flow and low flow (Pyrce, 2004). In this study, low flow is defined as a period in which the flow is equal to or less than the assumed threshold streamflow, while high flow is defined as a period in which the flow is equal to or more than the assigned threshold streamflow (Dracup et al., 1980; Yevjevich, 1967; Zelenhasić and Salvai, 1987). The definition using the threshold level has been adopted in many research studies: for high flow, the Q95 in Arnell et al. (2014), Gudmundsson et al. (2011), and Rientjes et al. (2010); the Q90 in Dadaser-Celik and Stefan (2009), and van Lanen and Wanders (2011); and the Q85 in Giuntoli et al., (2013); while for low flow, the Q5 in Laaha and Blöschl (2007) and Wilby

and Harris (2006); the Q10 in Patil and Stieglitz, (2011), Pyrce (2004), and Smakhtin (2001); and the Q25 in Özdemir et al., (2007).

This study defines the high flow and the low flow using Q90 and Q10 thresholds of the observed streamflow from 1952 to 1999 (48 years). Table 4.2 shows the percentiles of the observed streamflow. While high flow is related to flood, low flow is associated with drought. In a flooding event, a shorter time interval is more crucial, thus daily streamflow is used for high flow. On the other hand, monthly streamflow is employed for low flow since a longer time interval is relatively important in a drought situation.

Table 4.2 The observed streamflow percentile (the unit is cubic meter per second)

Area	Time interval	Percentiles			
		5 %	10 %	90 %	95 %
White River Basin	Daily Streamflow	7.39	9.06	170.19	270.99
	Monthly Streamflow	8.09	10.359	186.95	222.023
Allegheny River Basin	Daily Streamflow	5.97	8.16	185.76	263.35
	Monthly Streamflow	6.71	10.72	165.59	199.56

To describe the temporal characteristics of high flow and low flow, the duration (D) and the severity (S) are calculated using the defined thresholds. The durations of high flow and low flow are the periods of continuous time over/under a defined threshold level. The

severities of high flow and low flow are the cumulative surplus or deficit above or below the threshold level, respectively. Figure 4.3 shows the definitions of the duration and the severity in high flow and low flow.

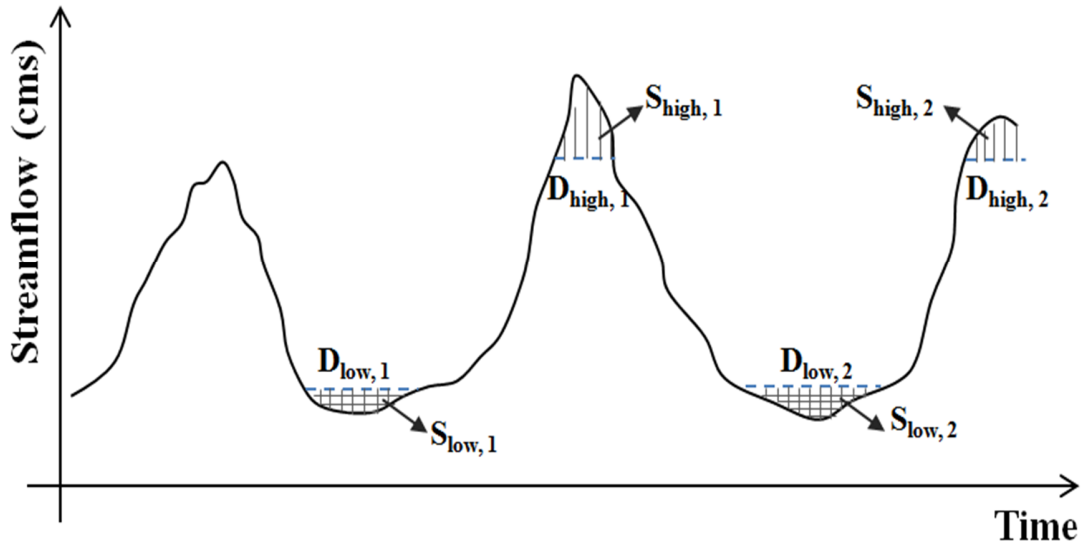

Figure 4.3 The definitions of the duration and the severity in high flow and low flow; (D – the duration, S – the severity, low – low flow, and high flow – high flow)

4.4.3 Copula approach

To investigate the relationship among the correlated variables, the joint distributions of the correlated multi-variables are used. However, the joint distributions have not been widely preferred owing to the fact that its best-fit marginal distributions for all the correlated variables must be identical. Using the copula originated by Sklar (1959), such limitations can be overcome in practical problems. The basic theorem of Sklar (1959) describes that there exists a copula function C which can merge the various marginal

distributions given the correlated marginal distributions. More information can be found in Joe (1997) and Nelsen (2006).

4.4.3.1 Archimedean copula

Among many families of copulas, the Archimedean copula is popular in hydrology due to its symmetric properties and tractability (Ariff et al., 2012; Fu and Butler, 2014; Zhang and Singh, 2006). With *m* variables, the Archimedean copula can be expressed as Eq. (4-4).

$$C(u) = \phi(\sum_{j=1}^{m} \phi^{-1}(u_j)) \quad (4\text{-}4)$$

Where, ϕ is the generator of the copula, which is a continuously decreasing function from $[0, 1]$ to $[0, \infty)$ such that $\phi(0) = \infty$ and $\phi(1) = 0$, and u_j is the CDF of *j* variable.

Using different forms of the generator ϕ, various families of Archimedean copula can be generated. According to Ariff et al. (2012), Archimedean copula has a total of 22 copula functions as its members, thus enabling its application in the analysis of a wide range of dependence levels, from negative to positive, for various hydrologic variables including duration and severity (Fu and Butler, 2014; Kao and Govindaraju, 2007). In this study, five popular Archimedean copula members are selected to describe the relationship between duration and severity: the Clayton copula (Kimeldori and Sampson, 1975); the

Frank copula (Frank, 1979); the Plackett copula (Plackett, 1965); the Galambos copula (Galambos, 1975); and the Gumbel-Hougaard copula (Gumbel, 1960). Table 4.3 shows brief information about the Archimedean bivariate copula families used in this study.

Table 4.3 Archimedean bivariate copula families used in this study

Family	$C_\phi(u,v)$	Scope of ϕ
Clayton	$(u^{-\phi}+v^{-\phi}-1)^{-1/\phi}$	$\phi \geq 0$
Flank	$-\frac{1}{\phi}\ln\left[1+\frac{(e^{-\phi u}-1)(e^{-\phi v}-1)}{(e^{-\phi}-1)}\right]$	$[-\infty,\infty]\{0\}$
Plackett	$\frac{1}{2}\frac{1}{\phi-1}[1+(\phi-1)(u+v)-[(1+(\phi-1)(u+v))^2-4\phi(\phi-1)uv]^{1/2}]$	$\phi \geq 0$
Galambos	$uv\exp[(-\ln u)^{-\phi}+(-\ln v)^{-\phi}]^{-1/\phi}$	$\phi \geq 0$
Gumbel-Hougaard	$\exp[-[(-\ln u)^{\phi}+(-\ln v)^{\phi}]^{1/\phi}]$	$\phi \geq 1$

The parameters of a copula function can be estimated by using various methods, including the Maximum Likelihood (ML) method, the Inference Function for Margins (IFM) method (Joe, 1997), the Canonical Maximum Likelihood (CML) method (Genest et al., 1995) and the non-parametric Kendall's tau method. According to Fu and Butler (2014), the IFM method show the best performance for analyzing overflow and flooding conditions compared with the others, and hence implemented in this study.

4.4.3.2 Goodness-of-fit test for copula function

Among the multiple copulas generated from a given dataset, the most suitable copula is selected based on the comparison of the estimated parametric probabilities (C_ϕ) with the empirical probabilities (C_{em}). This comparison is identified using the null hypothesis: $H_o : C_{em} \in C_\phi$ for a copula class C_ϕ against $H_1 : C_{em} \notin C_\phi$. To define the empirical copula, the method of Deheuvels (1981) is employed (Eq. (4-5))

$$C_{em} = \frac{1}{n} \sum_{i=1}^{n} I(U_i \leq u) \qquad (4\text{-}5)$$

Where, C_{em} is the empirical copula and I is the indicator function having 1 when the argument is true or 0 for false.

Two indices—the Crameŕ-von Mises (S_n) and the Kolmogorov-Smirnov statistics (T_n) —are applied to select the suitable copula family. The two indices are occasionally used for goodness of fit tests (Genest et al., 1995; Maity et al., 2013). The Crameŕ-von Mises statistic (Eq. (4-6)) is calculated based on the concept of the mean square error (MSE) whereas the Kolmogorov-Smirnov statistic (Eq. (4-7)) calculates the maximum distance between the empirical cumulative probability and the estimated cumulative probability. For the Kolomogorov-Smirnov statistic, 5% significance level is used.

$$S_n = \sum_{i=1}^{n} \{C_{em}(\hat{U}_i) - C_{\phi}(\hat{U}_i)\}^2 \quad (4\text{-}6)$$

$$T_n = \max_{u \in [0,1]^d} \left| \sqrt{n} \{C_{em}(u) - C_{\phi}(u)\} \right| \quad (4\text{-}7)$$

4.4.3.3 Sensitivity analysis using frequency analysis

As the LCCs, the impacts on the duration (*D*) and the severity (*S*) can be different. To examine which variable is affected more by the LCC, the change in the joint return period of the duration and the severity is used in this study. Using the duration and the severity, the joint frequency is estimated by using Eq. (4-8). This Equation (4-8) is adopted from the method of Zhang et al. (2012).

$$R_{\{S>s \text{ and } D>d\}} = \frac{\mu_t}{P(S > s \text{ and } D > d)} = \frac{\mu_t}{1 - F(s) - F(d) + F(s,d)} \quad (4\text{-}8)$$

Where, $F(s)$ is $P(S \le s)$, $F(d)$ is $P(D \le d)$, $F(s, d)$ is the joint distribution, and μ_t is the time interval calculated by using the theory of runs and Markov theorem (Shiau and Shen, 2001).

The return period for the *k* and *h* quantiles of the *D* and the *S* ($R_{\{S>h \text{ and } D>k\}}$) is calculated by using Eq. (4-8). If the *q* quantile is substituted for the probability of the *D* given that the *h* quantile for the *S* is fixed ($R_{\{S>h \text{ and } D>q\}}$), the difference ($Di_{du}^{1th}$) between $R_{\{S>h \text{ and } D>k\}}$

and $R_{\{S>h \text{ and } D>q\}}$ is only from the change of the *D*. Likewise, if the *w* quantile is substituted for the probability of the *S* given that the *k* quantile for the *D* is fixed ($R_{\{S>w \text{ and } D>k\}}$), the difference ($Di_{se}^{1th}$) between $R_{\{S>h \text{ and } D>k\}}$ and $R_{\{S>w \text{ and } D>k\}}$ is from the change of the *S*. Using this entire process, the differences (Di_{du}^{2nd}, Di_{se}^{2nd}) can be also calculated under different land cover conditions. Here, if the value of $\left|Di_{du}^{1th} - Di_{du}^{2nd}\right|$ is larger than the value of $\left|Di_{se}^{1th} - Di_{se}^{2nd}\right|$, the duration is affected more by LCC, and vice versa.

4.5 Results

4.5.1 Changes in observed precipitation, temperature and streamflow

As mentioned in the methodology, first the Mann-Kendall (MK) test (Kendall, 1955; Mann, 1945) is performed to study the trends in observed annual precipitation, temperature, and streamflow (Figure 4.4). In the White River Basin, streamflow shows a significant increasing trend based on 90 % confidence interval; whereas precipitation and temperature do not show any significant trend. Conversely, for Allegheny River Basin, precipitation shows a significant increasing trend, but the trends in temperature and the streamflow are not significant at 90% confidence level. Based on the trend analysis results, it is clear that the trend in streamflow in the two watersheds cannot be directly explained by the trends in climatic variables including precipitation and temperature. It

can be hypothesized that the changes in streamflow in the two watersheds is caused by the change in the land cover.

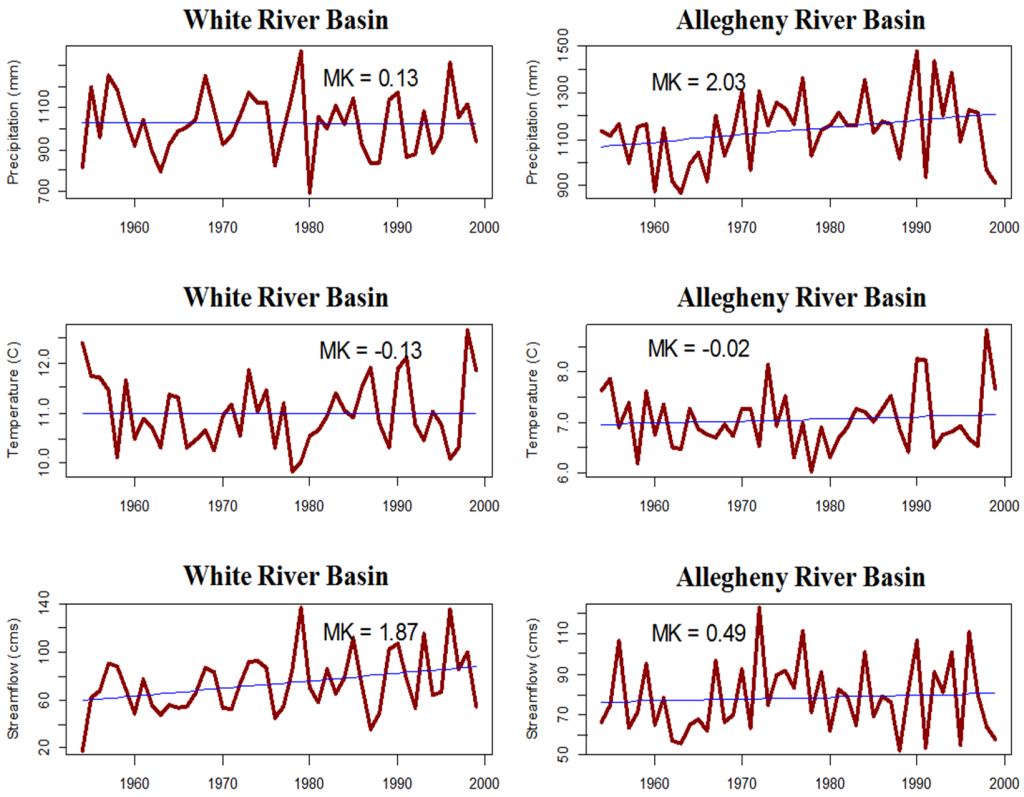

Figure 4.4 The changes of the annual variables depending on the study areas;(a) Precipitation (mm), (b) Temperature (°C), and (c) streamflow (cms). The results of MK test are denoted in each figure

4.5.2 Model calibration and validation

In order to exam the land cover condition in generating streamflow, the SWAT model is employed. Using the global sensitivity analysis tool in SWAT-CUP, the influential parameters are identified for the both study areas. The sensitive parameters for White River Basin are denoted in Table 4.4.

Table 4.4 The influential parameters for the both study area

Area	Abbreviation	Explanation
White River Basin	ALPHA_BF	Baseflow alpha factor
	CN2	Curve number
	CH_N2	Manning's 'n' value
	ESCO	Soil evaporation compesation factor
	GWQMN	Threshold depth of water in the shallow aquifer required for return flow to occur
	REVAPMN	Threshold depth of water in the shallow aquifer
	SOL_AWC	Available water capacity of the soil layer
	SOL_Z	Depth from soil surface to bottom of layer
Allegheny River Basin	ALPHA_BF	Baseflow alpha factor
	CN2	Curve number
	CH_N2	Manning's 'n' value
	GW_DELAY	Delay time for aquifer recharge
	CH_K2	Channel effective hydraulic conductivity
	OV_N	Manning's 'n' value for overland flow
	EPCO	Plant uptake compensation factor
	SMFMN	Melt factor on December 21

As mentioned in Section 4.4.1 and 4.4.2, use of two different types of land cover and two time intervals result in four calibration and validation results for each study area. Figure 4.5 shows the comparison of observed and simulated monthly streamflow corresponding to the land covers, while Table 4.5 shows the corresponding NSE and the R^2 values. Based on the performance criterion suggested by Moriasi et al. (2007), the SWAT simulations for the calibrations and the validations are within acceptable limits (NSE > 0.5). Overall, the NSE values are little higher for the White River Basin compared to the

ones for the Allegheny River Basin because the White River basin is more agricultural, which is the most suitable land use for SWAT simulations Borah and Bera (2003).

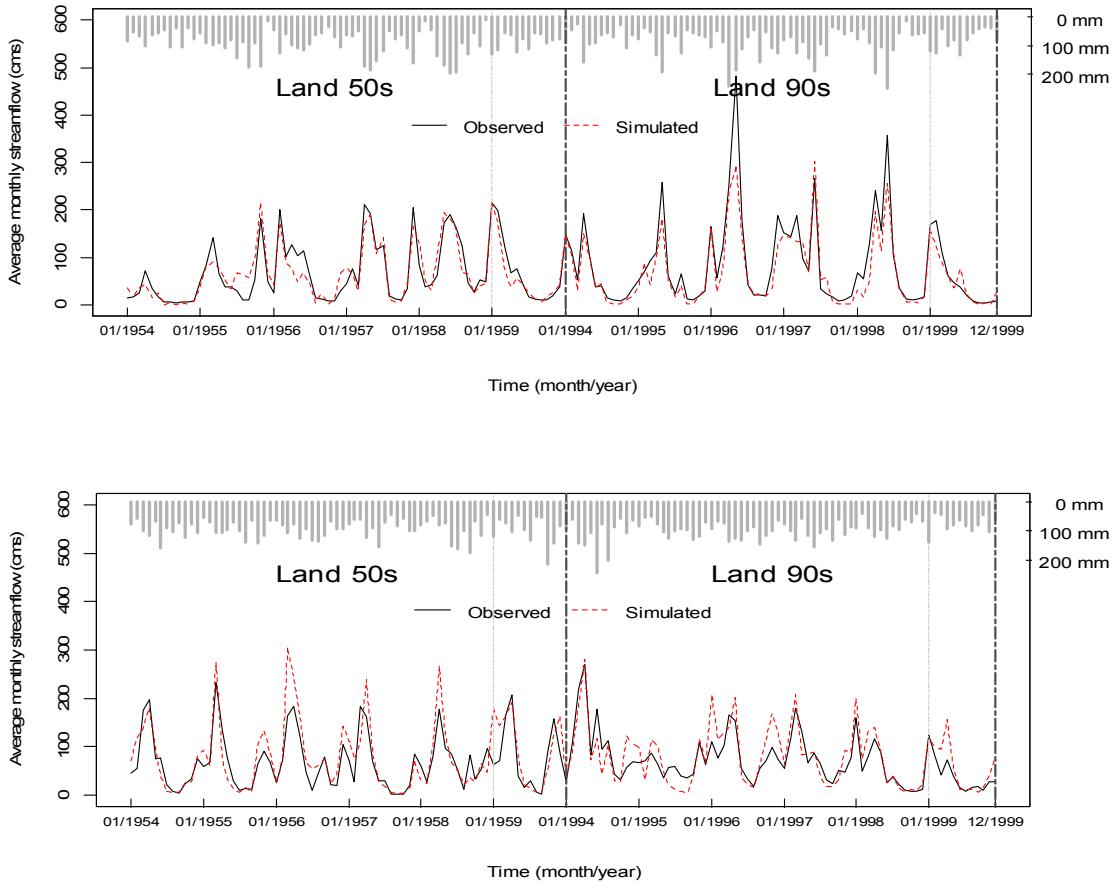

Figure 4.5 Comparison of observed and simulated streamflow corresponding to the land covers: (a) the results of the White River Basin and (b) the results of the Allegheny River Basin. The results of calibration and validation periods for each land cover are shown. And monthly precipitations are also denoted in the top of each figure.

Table 4.5 Results of calibration and validation in SWAT model

Area	Time intervals	Land cover	Calibration		Validation	
			NSE	R^2	NSE	R^2

White River Basin	Monthly	Land 50s	0.82	0.82	0.93	0.94
		Land 90s	0.86	0.88	0.83	0.83
	Daily	Land 50s	0.62	0.62	0.81	0.81
		Land 90s	0.73	0.74	0.66	0.68
Allegheny River Basin	Monthly	Land 50s	0.73	0.76	0.51	0.60
		Land 90s	0.73	0.74	0.64	0.83
	Daily	Land 50s	0.54	0.54	0.52	0.55
		Land 90s	0.55	0.57	0.63	0.70

4.5.3 The duration and the severity for high and low flows considering land cover

For the entire period (48 years from 1952 to 1999 including 2 years for a warm-up period), streamflow corresponding to two land cover conditions are generated using by the corresponding optimal parameters in the SWAT model as presented in Table 4.6 and Figure 4.6. As can be seen in Figure 4.6, there are a number of differences between the two simulated streamflow, considering the different land covers. In spite of the possibility of influence from the model performance to the biases (see Table 4-6), it is also viable to say that these can be also due to the change of land cover condition.

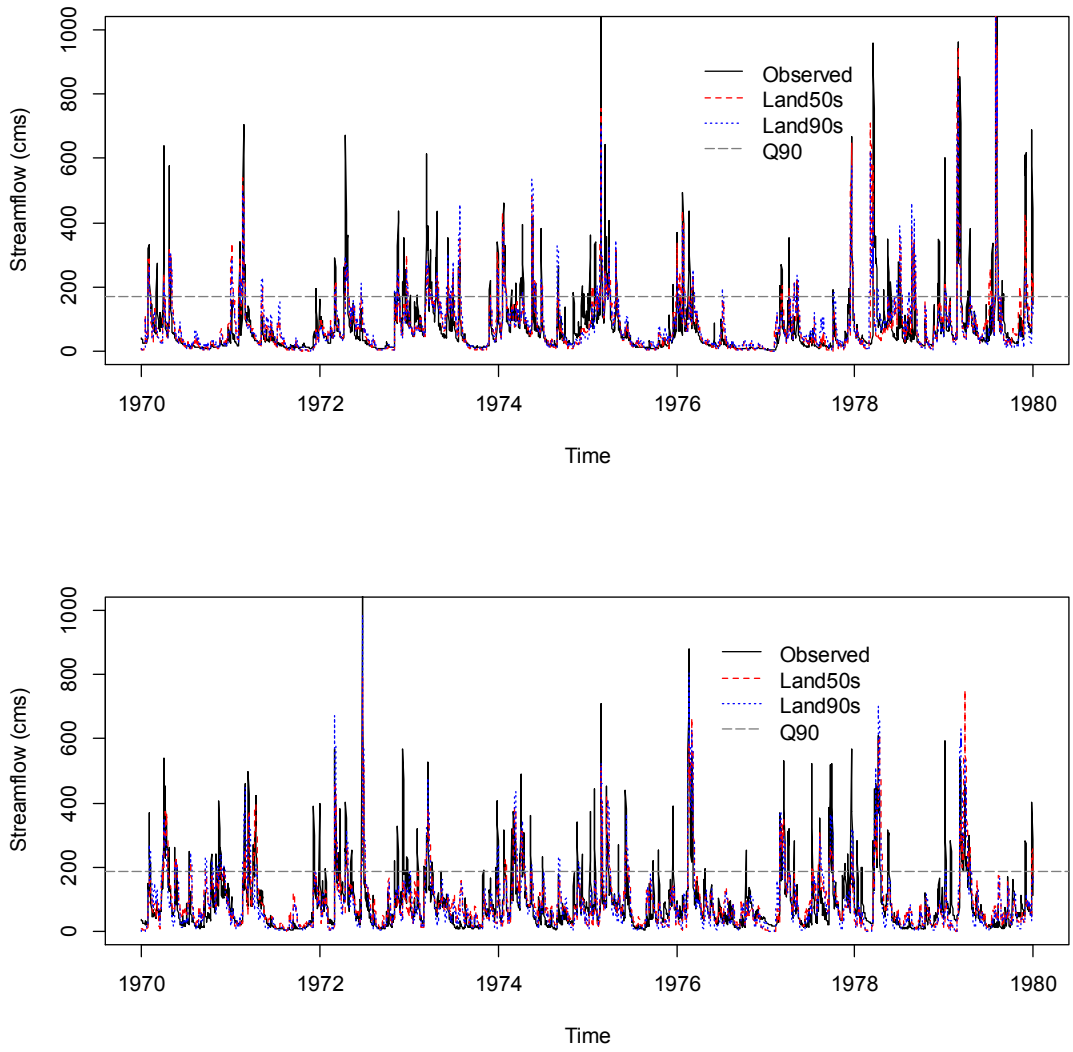

Figure 4.6 Comparison of the simulated and observed daily streamflow for 10 years (From 1970 to 1979): (a) the White River Basin and (b) the Allegheny River Basin

Table 4.6 The results of the parameters calibrated in SWAT model

Area	Abbreviation	Daily		Monthly	
		Land 50s	Land 90s	Land 50s	Land 90s
White	ALPHA_BF	0.753	0.195	0.809	0.723

River Basin	CN2	95.294	98.000	94.888	95.772
	CH_N2	0.251	0.289	0.192	0.135
	ESCO	0.936	0.921	0.802	0.999
	GWQMN	375.89	350.50	340.900	92.099
	REVAPMN	46.012	283.387	348.862	380.137
	SOL_AWC	0.046	0.067	0.262	0.048
	SOL_Z	1189.26	1248.02	1075.21	1239.34
Allegheny River Basin	ALPHA_BF	0.675	0.675	0.401	0.206
	CN2	96.023	97.342	90.841	96.581
	CH_N2	0.075	0.075	0.185	0.091
	GW_DELAY	75.00	225.00	2.93	0.375
	CH_K2	225.00	75.00	113.775	20.625
	OV_N	7.508	22.503	21.895	6.345
	EPCO	0.750	0.750	0.774	0.032
	SMFMN	5.00	15.00	0.945	4.745

The univariate distributions are adopted based on the previous studies (Ariff et al., 2012; Mirabbasi et al., 2012; Shiau and Modarres, 2009; Zhang et al., 2012): the Generalized Extreme Value (GEV) distribution is selected to fit the duration of high flow, the Weibull distribution is for the severity of high and low flows, and the exponential distribution is for the durations for low flow (summarized in Table 4.7). The parameters of the distributions are estimated by the maximum likelihood estimation (MLE). Figure 4.7 shows the fitted distributions for the duration and the severity of high flow as an example.

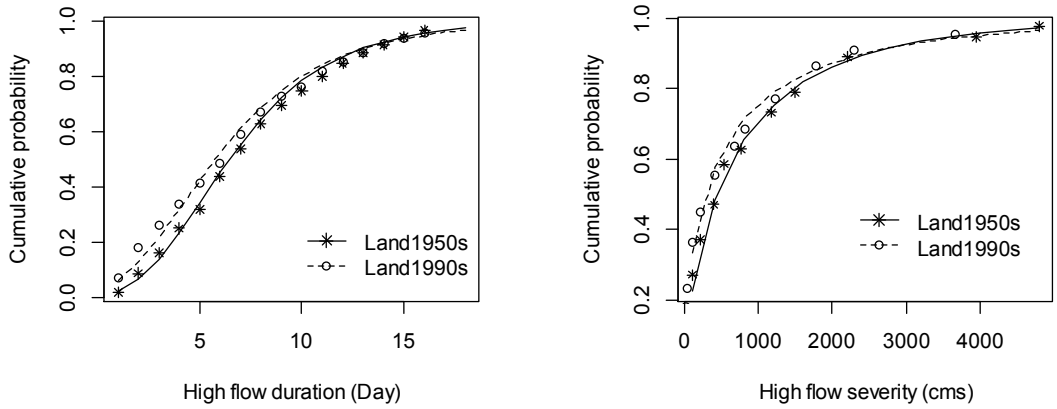

Figure 4.7 Observed high flow duration, severity and fitted distributions of the White River Basin corresponding to the simulated streamflows based on the land cover conditions

Table 4.7 The selected distributions for the duration and severity corresponding to the study areas

Area	High flow		Low flow	
	Duration	Severity	Duration	Severity
White River Basin	GEV dist.	Weibull dist.	Exponential dist.	Weibull dist.
Allegheny River Basin	Gamma dist.	Weibull dist.	Exponential dist.	Weibull dist.

4.5.4 Determination of the optimal copulas

The parameters for the copulas are estimated by the IFM method. Figure 4.8 represents the comparison between the empirical probabilities and the estimated probabilities based on the copula families. Except the Ali-Mikhail-Haq copula, most of the copulas are found to be suitable for the study datasets. To select the most suitable copula, two popular

criterion indices including S_n and T_n are used. The example results of S_n and T_n as well as the optimal values of copula parameter (ϕ) are presented in Table 4.8. As shown in Table 4.7, the Gumbel-Hougaard copula demonstrates the best performance for high flow in White River Basin. Similarly, the Gumbel-Hougaard copula produces the lowest values of Sn and Tn for low flows in the Allegheny River Basin. Based on these results, the Gumbel-Hougaard copula is selected as the appropriate copula for describing the joint probabilities corresponding to low and high flow conditions in this study.

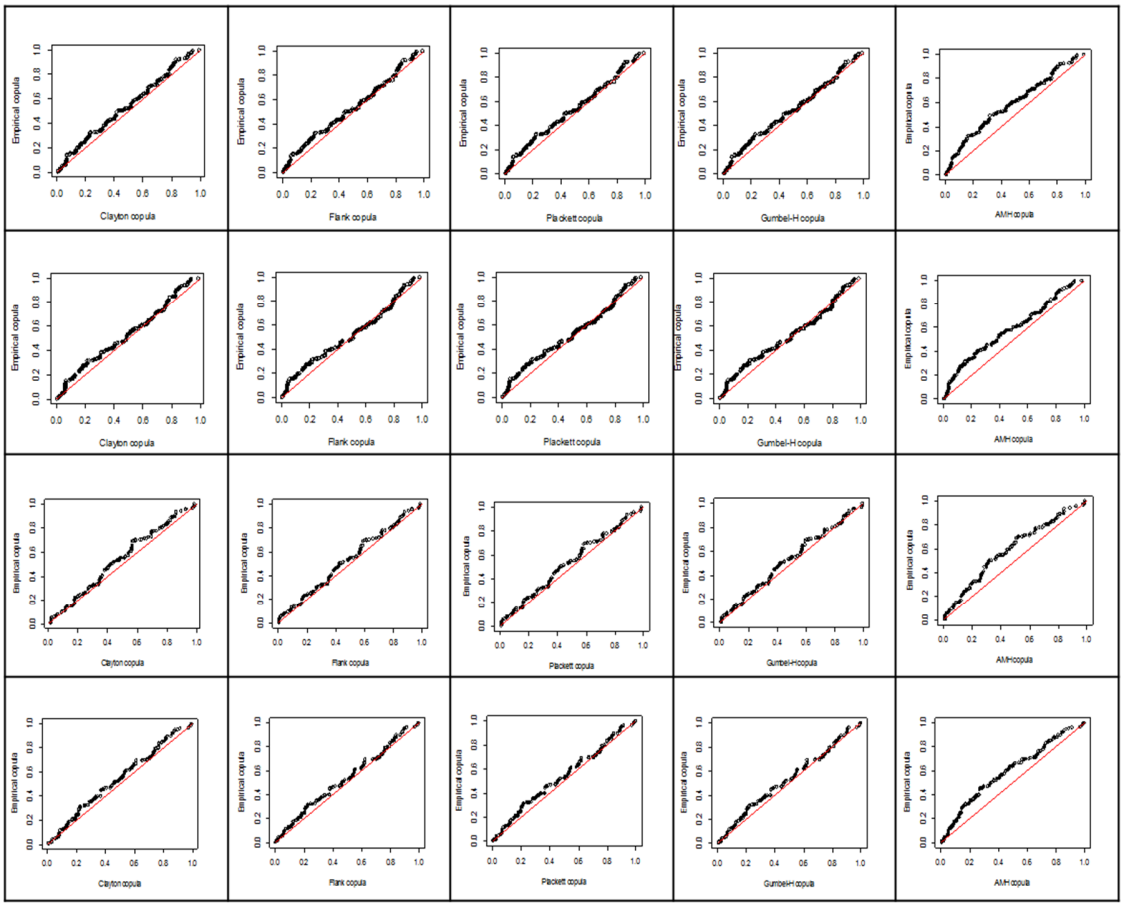

Figure 4.8 Comparison plots of the joint probabilities using the different copulas: first column- Clayton copula, second column- Frank copula, third column- Placket copula, fourth column- Gumbel-Hougaard copula, and fifth column-Ali-Mikhail-Haq copula, first

row- high flow of land 50s for the WS1, second row- high flow of land 90s for the WS1, third row- high flow of land 50s for the WS2, and fourth row- high flow of land 90s for the WS2

Table 4.8 The results of the copula applications in high flow of the White River Basin: T_n(max) for land 50s- 0.0986, and T_n(max) for land 90s- 0.0919

Copula families	Land cover	θ	S_n	T_n
Clayton	Land 50s	4.9822	0.42	0.06
	Land 90s	5.2613	0.49	0.06
Frank	Land 50s	15.5793	0.36	0.08
	Land 90s	19.2263	0.50	0.07
Plackett	Land 50s	67.5964	0.39	0.08
	Land 90s	83.9698	0.53	0.08
Gumbel-Hougaard	Land 50s	5.0147	*0.33*	0.08
	Land 90s	5.8768	*0.49*	0.08
Ali-Mikhail-Haq	Land 50s	1.0000	2.10	0.16
	Land 90s	1.0000	2.32	0.14

4.5.5 Land cover impact on high flow

With the Gumbel-Hougaard copula, the joint probability associated with high flow conditions including duration and severity is calculated. The contours of joint probabilities for high flow in White River Basin and Allegheny River Basin are presented in Figure 4.9. The solid black lines represent the probability contours for the high flow with regards to the 1950's land cover, the dashed red lines represent the probability contours for the high flow in the 1990's land cover. For both cases, contours corresponding to 1990 land cover are lower than the contours corresponding to the 1950

land cover for the same probability; the differences between the two lines are induced by land cover conditions because all other forcing data are unchanged. Based on these differences, it can be concluded that the LCC affects the duration and severity in high flow. However, the differences between the two contours are not pronounced at the low values for duration and severity (Probabilities < 30 %) for Allegheny River Basin compared to the White River Basin. This difference in joint probability contours is likely caused by the difference in dominant land cover conditions. As explained in Section 4.5.1, White River Basin is an agricultural-based watershed while Allegheny River Basin is a forest dominated watershed. For White River Basin, the forest area increased markedly from 5.48 % to 13.74 %. The land cover for Allegheny River Basin was already heavily forested at 60.78 %, and it increased to 81.97 %. Drawing from the two facts, the effects of LCC on high flow can be different. Many previous studies have concluded that deforestation leads to an increase of peak flow and runoff volume because of decreased infiltration into soil profile through deforestation. (Chu et al., 2010; Lin et al., 2009; Storck et al., 1998). Based on the results from this study, it is also possible to relate the changes in forest cover to the duration and severity in high flow conditions. Regardless of dominant land cover conditions, the increase in forest area may produce shorter duration less severe high flows. The markedly increase in forest area from non-forest area in the White River Basin especially has a greater impact on relatively longer lasting more severe high flows.

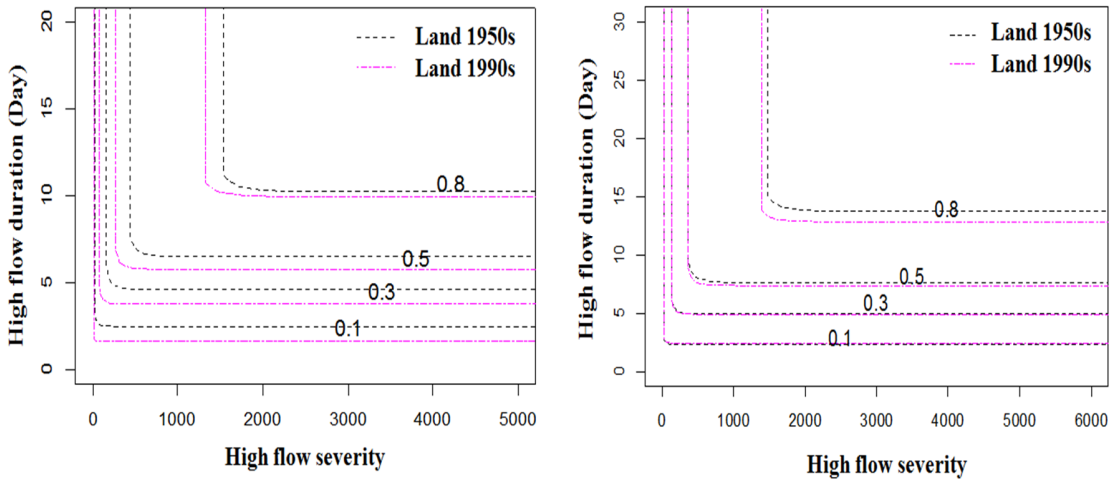

Figure 4.9 The contours of joint probabilities for high flow duration and severity (a) the White River Basin, and (b) the Allegheny River Basin

4.5.6 Land cover impact on low flow

Using the joint probability contours as described in the previous Section 4.5.5, the effect of LCC for both study areas is also analyzed for low flows using the Gumbel-Hougaard copula. (Figure 4.10). At a low probability value (less than 50%) for duration and severity, the land cover impacts show a completely different pattern. In White River Basin, an increase in forest area aggravates the duration and the severity; whereas an increase in forest area helps to alleviate the duration and severity of low flow in the Allegheny River Basin. This difference can be related to the pre-dominant land cover conditions; however, it is difficult to generalize the effects of land cover from this study. The severities in severe low flow (high probability, Probabilities > 70 %) are often alleviated by an increase in the forest area. It is possible that increased forest area is effective in reducing the severity of extreme low flow. Based on Figure 4.9 and 4.10, it can be concluded that the effect of LCC is more pronounced on high flow compared to

low flow. According to Bruijnzeel et al. (1990) and Ma et al. (2009), the infiltration characteristics of the forest play an important role in determining how the available water is partitioned between runoff and groundwater recharge; specifically, reforestation increases the baseflow, which in turn can contribute to streamflow during severe low flow conditions. The results from this study are similar Price et al. (2011), who also found that forest cover demonstrated a consistent, significant positive relationship with low flows, despite the higher evapotranspiration rates associated with forest cover.

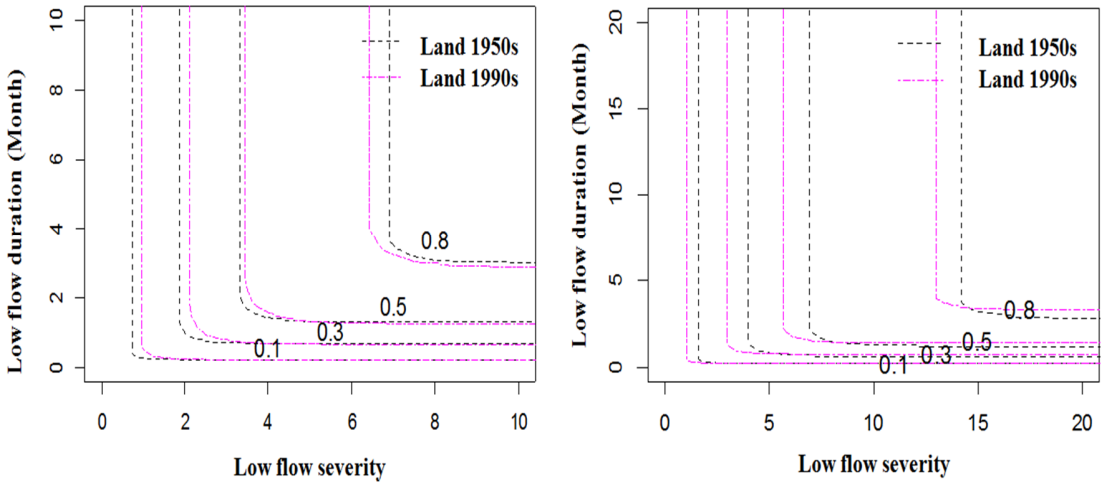

Figure 4.10 The contours of joint probabilities for low flow duration and severity (a) the WS1, and (b) the WS2

4.5.7 Comparison between increased urban and forest areas

At the watershed scale, not much change is visible in urban area for both study areas. From 1950 to 1990, the urban areas increased by 1.18 % and 0.51 % in White River Basin and Allegheny River Basin, respectively. However, one sub-basin in White River

watershed, which is closer to Indianapolis, did experience a relatively higher increase in urban area as shown in Figure 4.11.

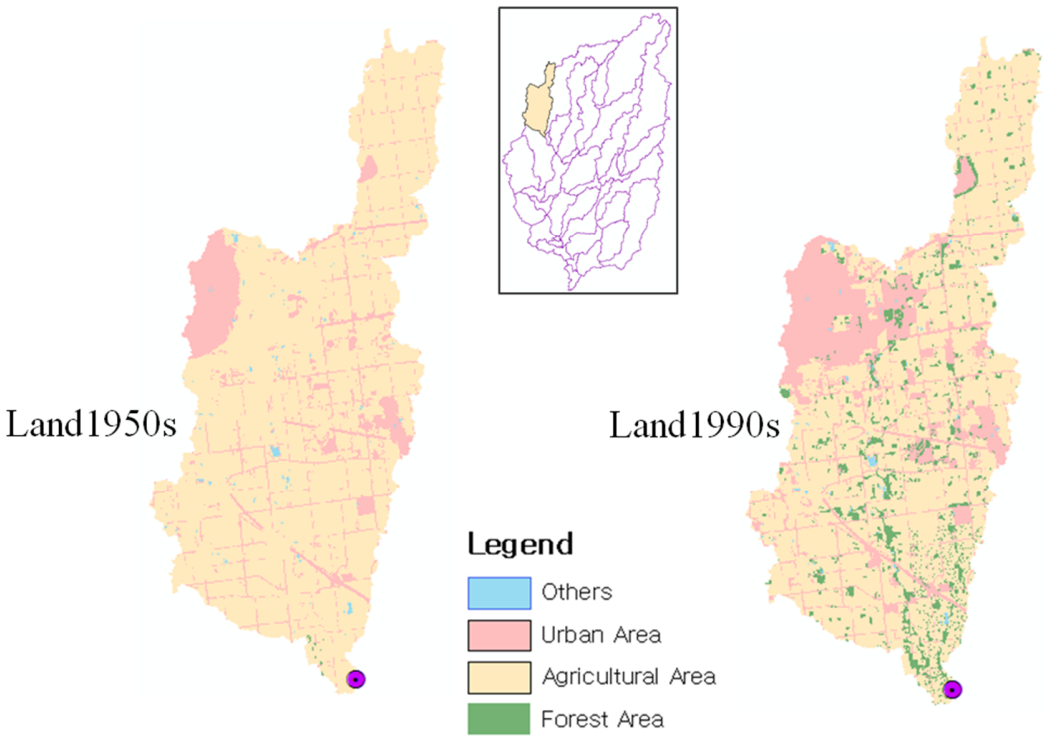

Figure 4.11 Land cover changes in one of sub-basins in the White River Basin, which shows the highest increase rate of the urbanization area

From the 1950s to the 1990s, the urban area of this sub-basin increased from 14.7 % to 23.58 (8.88 % increase). Moreover, it should be noted that the forest area in this sub-basin also increased from 0.04% in 1950 to 7.05% in 1990. The joint probability contours for both low and high flows are presented in Figure 4.12.

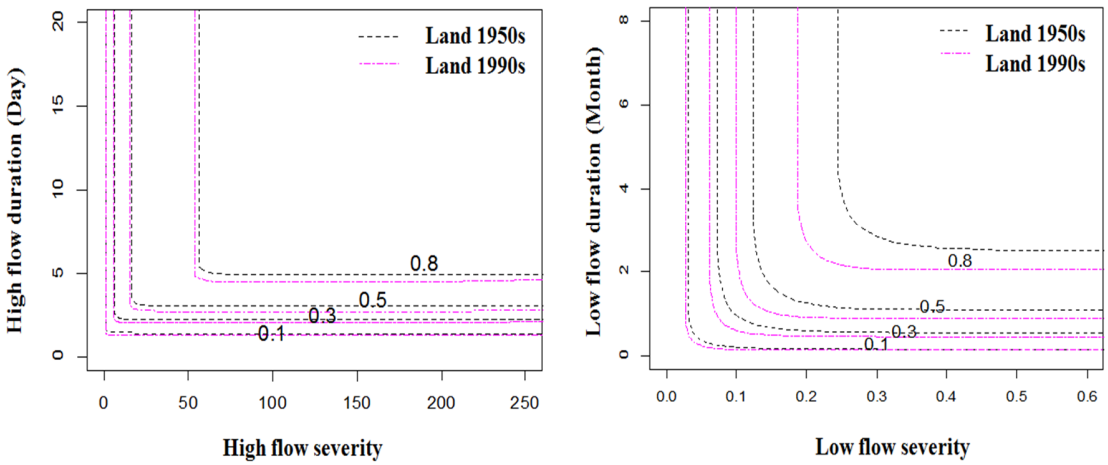

Figure 4.12 The contours of joint probabilities for the sub-basin (a) high flow, and (b) low flow

Despite both forest and urban covers increased at relatively the same rate between 1950 and 1990, the joint probability contour corresponding to 1900 land cover are lower compared to the contour corresponding to 1950 land cover for both high and flow flows. It indicates that the streamflow corresponding to 1990s' land has less severe shorter extreme flow conditions caused primarily by the increase in the forest cover. These results show that at the basin scale, the change in forest area plays a crucial role in the relationship between duration and severity for both high and low flows, compared to the changes in urban area. While this finding is interesting, it should be noted that the parameters that are used in simulating the hydrology of the sub-basin are obtained through calibration of streamflow at the watershed level, thus warranting further investigation.

4.5.8 Sensitivity of duration and severity to LCC

The return period (Eq. 4-8) is used to find whether duration or severity is more affected by LCC. Because the sensitivity of severity or duration can be affected by the magnitude of high and low flow, the flow data is categorized based on 10 and 70 percentiles: 10 percentile is used to represent the moderate high and low flow. 70 percentile is used to represent the severe high and low flow. The results are investigated when the 10 percentiles are changed. The results are shown in Table 4.9.

Table 4.9 The results of the sensitivity analysis

		$\left\|Di_{du}^{1th} - Di_{du}^{2nd}\right\|$	$\left\|Di_{se}^{1th} - Di_{se}^{2nd}\right\|$	Sensitive variable
White River Basin	Moderate high flow	5.87	11.33	Severity
	Severe high flow	24.06	26.27	Severity
	Moderate low flow	0.8	1.01	Severity
	Severe low flow	7.88	24.43	Severity
Allegheny River Basin	Moderate high flow	0.95	0.36	Duration
	Severe high flow	13.48	9.61	Duration
	Moderate low flow	0.68	0.97	Severity
	Severe low flow	6.75	20.93	Severity

Among eight cases, six cases reveal that the severities are affected more by LCC than durations. Based on these results, it is hard to conclude that one variable is more sensitive than the others. However, the results reveal that the severity is usually affected more by the LCC than the duration.

4.6 Summary and Conclusions

The objective of this study is to investigate the effects of LCC on the relationship between duration and severity of extreme in streamflow condition in two watersheds located within the Ohio River Basin in the United States. Two study areas are selected based on their dominant land cover conditions and degree of regulation. Hydro-climatic variables including precipitation, temperature and streamflow are first analyzed to examine their patterns of change using the MK test. SWAT model is then used to simulate streamflow considering land cover conditions. Using the extreme low and high values from the simulated data, the duration and the severity are calculated and then the copula function is applied to define the relationship between duration and severity.

The findings from this study show that LCC affects the duration and the severity in both high and low flows. Considering that the forest area increased in both study watersheds, the results show that the increase in forest area leads to the decrease of duration and severity in high flow; extreme high flow is particularly influenced by the increase in forest area. The results of the LCC effects are not consistent between two study areas for moderate low flow, but the study area show consistent results for severe low flow. This

indicates that the increase of forest is likely to be helpful for extreme drought condition. In addition, sensitivity of duration and severity is investigated by using frequency analysis (Eq. 4-8). Results show that the severity is affected more by the LCC than duration for both high flow and low flow. Finally, at the basin scale, the change is more affected by forest area than by urban area.

CHAPTER 5. SYNTHESIS

The results obtained by this dissertation agree with that anthropogenic activities are strongly influential to hydro- climatological variables. The major findings of this dissertation are described below.

5.1 Effect of Natural Variability versus Climate Change on Temperature

In chapter 2, the impact of anthropogenic activities on temperature is investigated and compared to the impact of natural variability. In conclusion, the observed trends of the entire CONUS over the 20th century lie inside the range expected from natural internal climate variability. However, some parts of the CONUS show meaningful changes in temperature due to anthropogenic activities. The impact of anthropogenic activities is greatest in the western U.S. (the SA, and the SB). Further analysis of the impact of anthropogenic activities on climate variables is needed for the regional water resources management.

5.2 Impact of Anthropogenic Activities versus Climate Impact on Streamflow

In chapter 3, the relative impacts of anthropogenic activities and climate change on the streamflow are quantified on four states: Arizona, Georgia, Indiana and New York. It is found that even though the effect of climate on streamflow cannot be disregarded, the results of impact of anthropogenic activities obtained here are significantly higher than the ones of climate impact. This result is a matter for consideration since much

research focuses only on climate change. This fact seems to show that anthropogenic activities including land cover change or the construction of hydrologic structures need to be considered as much as the consideration of climate change or more so when runoff is predicted.

5.3 The Effect of Land Cover Change on Hydrologic Variable

In chapter 4, the effect of land cover change on the relationship between duration and severity of extreme value in streamflow is investigated. As a result, it is explicitly that the land cover change affects the duration and the severity of both high and low flows. The increase in forest area leads to the decrease of duration and severity in high flow. Especially it impacts extreme high flow. While the effect of LCC is not consistent for moderate low flow, it shows the consistent result in severe low flow: It may indicate the increase of forest is helpful for extreme drought condition. In addition, the land cover change has a greater effect on severity than on duration for both high flow and low flow. Finally, at the basin scale, the duration and severity in high and low flow is more affected by the change of forest than by the change of urban area.

LIST OF REFERENCES

LIST OF REFERENCES

Abbaspour, K., Johnson, C., Van Genuchten, M.T., 2004. Estimating uncertain flow and transport parameters using a sequential uncertainty fitting procedure. Vadose Zone J. 3, 1340–1352.

Ahn, K.-H., Kim, Y.-O., Ahn, S.J., 2012. Manipulating Large-Scale Qualitative Meteorological Information for Drought Outlook. Mon. Weather Rev. 140.

Allen, M.R., Stott, P.A., 2003. Estimating signal amplitudes in optimal fingerprinting, part I: theory. Clim. Dyn. 21, 477–491. doi:10.1007/s00382-003-0313-9

Andreadis, K.M., Lettenmaier, D.P., 2006. Trends in 20th century drought over the continental United States. Geophys. Res. Lett. 33.

Ariff, N., Jemain, A., Ibrahim, K., Wan Zin, W., 2012. IDF relationships using bivariate copula for storm events in Peninsular Malaysia. J. Hydrol. 470, 158–171.

Arnell, N.W., Charlton, M.B., Lowe, J.A., 2014. The effect of climate policy on the impacts of climate change on river flows in the {UK}. J. Hydrol. 510, 424 – 435. doi:http://dx.doi.org/10.1016/j.jhydrol.2013.12.046

Arnold, J.G., Srinivasan, R., Muttiah, R.S., Williams, J.R., 1998. Large area hydrologic modeling and assessment part I: Model development1. JAWRA J. Am. Water Resour. Assoc. 34, 73–89.

Bao, Z., Zhang, J., Wang, G., Fu, G., He, R., Yan, X., Jin, J., Liu, Y., Zhang, A., 2012. Attribution for decreasing streamflow of the Haihe River basin, northern China: climate variability or human activities? J. Hydrol.

Barnett, T., Hasselmann, K., Chelliah, M., Delworth, T., Hegerl, G., Jones, P., Rasmusson, E., Roeckner, E., Ropelewski, C., Santer, B., others, 1999. Detection

and attribution of recent climate change: A status report. Bull. Am. Meteorol. Soc. 80, 2631–2659.

Barnett, T.P., Pierce, D.W., Hidalgo, H.G., Bonfils, C., Santer, B.D., Das, T., Bala, G., Wood, A.W., Nozawa, T., Mirin, A.A., Cayan, D.R., Dettinger, M.D., 2008. Human-Induced Changes in the Hydrology of the Western United States. Science 319, 1080–1083. doi:10.1126/science.1152538

Barnett, T.P., Pierce, D.W., Schnur, R., 2001. Detection of anthropogenic climate change in the world's oceans. Science 292, 270–274.

Bathurst, J.C., Iroumé, A., Cisneros, F., Fallas, J., Iturraspe, R., Novillo, M.G., Urciuolo, A., Bièvre, B. de, Borges, V.G., Coello, C., Cisneros, P., Gayoso, J., Miranda, M., Ramírez, M., 2011. Forest impact on floods due to extreme rainfall and snowmelt in four Latin American environments 1: Field data analysis. J. Hydrol. 400, 281 – 291. doi:http://dx.doi.org/10.1016/j.jhydrol.2010.11.044

Beck, H., Bruijnzeel, L., Van Dijk, A., McVicar, T., Scatena, F., Schellekens, J., 2013. The impact of forest regeneration on streamflow in 12 meso-scale humid tropical catchments. Hydrol. Earth Syst. Sci. Discuss. 10.

Beighley, R.E., Melack, J.M., Dunne, T., 2003. IMPACTS OF CALIFORNIA'S CLIMATIC REGIMES AND COASTAL LAND USE CHANGE ON STREAMFLOW CHARACTERISTICS1. JAWRA J. Am. Water Resour. Assoc. 39, 1419–1433.

Boé, J., Terray, L., Habets, F., Martin, E., 2007. Statistical and dynamical downscaling of the Seine basin climate for hydro-meteorological studies. Int. J. Climatol. 27, 1643–1655. doi:10.1002/joc.1602

Bonfils, C., Santer, B.D., Pierce, D.W., Hidalgo, H.G., Bala, G., Das, T., Barnett, T.P., Cayan, D.R., Doutriaux, C., Wood, A.W., Mirin, A., Nozawa, T., 2008. Detection and Attribution of Temperature Changes in the Mountainous Western United States. J. Clim. 21, 6404–6424. doi:10.1175/2008JCLI2397.1

Borah, D.K., Bera, M., 2003. SWAT model background and application reviews.

Brath, A., Montanari, A., Moretti, G., 2006. Assessing the effect on flood frequency of land use change via hydrological simulation (with uncertainty). J. Hydrol. 324, 141–153.

Bruijnzeel, L.A., others, 1990. Hydrology of moist tropical forests and effects of conversion: a state of knowledge review. Hydrol. Moist Trop. For. Eff. Convers. State Knowl. Rev.

Budyko (Ed.), 1974. Climate and life, English ed. ed. Academic Press.

Bulygina, N., Mclntyre, N., Wheater, H., 2013. A comparison of rainfall-runoff modelling approaches for estimating impacts of rural land management on flood flows. Hydrol. Res. 44.

Bureau, U.C., 2005. Statistical abstract of the United States. US Gov. Print. Off. US Gov. Print. Off.

Chang, H., 2003. Basin hydrologic response to changes in climate and land use: the Conestoga River basin, Pennsylvania. Phys. Geogr. 24, 222–247.

Chang, H., 2007. Comparative streamflow characteristics in urbanizing basins in the Portland Metropolitan Area, Oregon, USA. Hydrol. Process. 21, 211–222.

Chelsea Nagy, R., Graeme Lockaby, B., Kalin, L., Anderson, C., 2012. Effects of urbanization on stream hydrology and water quality: the Florida Gulf Coast. Hydrol. Process. 26, 2019–2030. doi:10.1002/hyp.8336

Chen, Z., Chen, Y., Li, B., 2013. Quantifying the effects of climate variability and human activities on runoff for Kaidu River Basin in arid region of northwest China. Theor. Appl. Climatol. 111, 537–545.

Chu, H.-J., Lin, Y.-P., Huang, C.-W., Hsu, C.-Y., Chen, H.-Y., 2010. Modelling the hydrologic effects of dynamic land-use change using a distributed hydrologic model and a spatial land-use allocation model. Hydrol. Process. 24, 2538–2554.

Collier, J.C., Zhang, G.J., 2007. Effects of increased horizontal resolution on simulation of the North American monsoon in the NCAR CAM3: an evaluation based on surface, satellite, and reanalysis data. J. Clim. 20, 1843–1861.

Costa, M.H., Botta, A., Cardille, J.A., 2003. Effects of large-scale changes in land cover on the discharge of the Tocantins River, Southeastern Amazonia. J. Hydrol. 283, 206–217.

Cruise, J.F., Laymon, C.A., Al-Hamdan, O.Z., 2010. Impact of 20 Years of Land-Cover Change on the Hydrology of Streams in the Southeastern United States1. JAWRA J. Am. Water Resour. Assoc. 46, 1159–1170. doi:10.1111/j.1752-1688.2010.00483.x

Dadaser-Celik, F., Stefan, H.G., 2009. Stream Flow Response to Climate in Minnesota.

Deheuvels, P., 1981. An asymptotic decomposition for multivariate distribution-free tests of independence. J. Multivar. Anal. 11, 102–113.

Déqué, M., Rowell, D.P., Lüthi, D., Giorgi, F., Christensen, J.H., Rockel, B., Jacob, D., Kjellström, E., Castro, M. de, Hurk, B. van den, 2007. An intercomparison of regional climate simulations for Europe: assessing uncertainties in model projections. Clim. Change 81, 53–70. doi:10.1007/s10584-006-9228-x

Dooge J.C.I., Bruen M., Parmentier B., 1999. A simple model for estimating the sensitivity of runoff to long-term changes in precipitation without a change in vegetation. Adv. Water Resour. 23, 153–163. doi:10.1016/S0309-1708(99)00019-6

Dracup, J.A., Lee, K.S., Paulson, E.G., 1980. On the definition of droughts. Water Resour. Res. 16, 297–302.

Du, J., Qian, L., Rui, H., Zuo, T., Zheng, D., Xu, Y., Xu, C.-Y., 2012. Assessing the effects of urbanization on annual runoff and flood events using an integrated hydrological modeling system for Qinhuai River basin, China. J. Hydrol. 464–465, 127 – 139. doi:http://dx.doi.org/10.1016/j.jhydrol.2012.06.057

Du, J., Rui, H., Zuo, T., Li, Q., Zheng, D., Chen, A., Xu, Y., Xu, C.-Y., 2013. Hydrological simulation by SWAT model with fixed and varied parameterization approaches under land use change. Water Resour. Manag. 27, 2823–2838.

Fang, X., Ren, L., Li, Q., Zhu, Q., Shi, P., Zhu, Y., 2013. Hydrologic Response to Land Use and Land Cover Changes within the Context of Catchment-Scale Spatial Information. J. Hydrol. Eng. 18, 1539–1548.

Fan, Y., van den Dool, H., 2008. A global monthly land surface air temperature analysis for 1948–present. J. Geophys. Res. Atmospheres 113, n/a–n/a. doi:10.1029/2007JD008470

Faramarzi, M., Abbaspour, K.C., Schulin, R., Yang, H., 2009. Modelling blue and green water resources availability in Iran. Hydrol. Process. 23, 486–501.

Franczyk, J., Chang, H., 2009. The effects of climate change and urbanization on the runoff of the Rock Creek basin in the Portland metropolitan area, Oregon, USA. Hydrol. Process. 23, 805–815.

Frank, M.J., 1979. On the simultaneous associativity ofF (x, y) andx+y- F (x, y). Aequationes Math. 19, 194–226.

Fu, G., Butler, D., 2014. Copula-based frequency analysis of overflow and flooding in urban drainage systems. J. Hydrol. 510, 49 – 58. doi:http://dx.doi.org/10.1016/j.jhydrol.2013.12.006

Galambos, J., 1975. Order statistics of samples from multivariate distributions. J. Am. Stat. Assoc. 70, 674–680.

Gebresamuel, G., Singh, B.R., Dick, Ø., 2010. Land-use changes and their impacts on soil degradation and surface runoff of two catchments of Northern Ethiopia. Acta Agric. Scand. Sect. B–Soil Plant Sci. 60, 211–226.

Genest, C., Ghoudi, K., Rivest, L.-P., 1995. A semiparametric estimation procedure of dependence parameters in multivariate families of distributions. Biometrika 82, 543–552.

Gentine, P., D'Odorico, P., Lintner, B.R., Sivandran, G., Salvucci, G., 2012. Interdependence of climate, soil, and vegetation as constrained by the Budyko curve. Geophys. Res. Lett. 39, n/a–n/a. doi:10.1029/2012GL053492

Ghosh, P., Brand, W.A., 2003. Stable isotope ratio mass spectrometry in global climate change research. Int. J. Mass Spectrom. 228, 1–33.

Ghosh, S., Mujumdar, P.P., 2008. Statistical downscaling of GCM simulations to streamflow using relevance vector machine. Adv. Water Resour. 31, 132–146. doi:10.1016/j.advwatres.2007.07.005

Gibson, C., 1998. Population of the 100 largest cities and other urban places in the United States: 1790-1990. US Bureau of the Census Washington, DC.

Gillett, N.P., Zwiers, F.W., Weaver, A.J., Stott, P.A., 2003. Detection of human influence on sea-level pressure. Nature 422, 292–294. doi:10.1038/nature01487

Giorgi, F., Francisco, R., 2000. Evaluating uncertainties in the prediction of regional climate change. Geophys. Res. Lett. 27, 1295–1298.

Giorgi, F., Mearns, L.O., 2002. Calculation of Average, Uncertainty Range, and Reliability of Regional Climate Changes from AOGCM Simulations via the "Reliability Ensemble Averaging" (REA) Method. J. Clim. 15, 1141–1158. doi:10.1175/1520-0442(2002)015<1141:COAURA>2.0.CO;2

Giuntoli, I., Renard, B., Vidal, J.-P., Bard, A., 2013. Low flows in France and their relationship to large-scale climate indices. J. Hydrol. 482, 105–118.

Gleick, P.H., others, 1993. Water in crisis: a guide to the world's fresh water resources. Oxford University Press, Inc.

Gordon, L., Dunlop, M., Foran, B., 2003. Land cover change and water vapour flows: learning from Australia. Philos. Trans. R. Soc. Lond. B. Biol. Sci. 358, 1973–1984.

Goudie, A., 2013. The human impact on the natural environment: past, present and future.

Gudmundsson, L., Tallaksen, L.M., Stahl, K., 2011. Spatial cross-correlation patterns of European low, mean and high flows. Hydrol. Process. 25, 1034–1045. doi:10.1002/hyp.7807

Gumbel, E.J., 1960. Distributions des valeurs extrêmes en plusieurs dimensions. Publ Inst Stat. Univ Paris 9, 171–173.

Guo, H., Hu, Q., Jiang, T., 2008. Annual and seasonal streamflow responses to climate and land-cover changes in the Poyang Lake basin, China. J. Hydrol. 355, 106–122.

Hamed, K.H., Ramachandra Rao, A., 1998. A modified Mann-Kendall trend test for autocorrelated data. J. Hydrol. 204, 182–196. doi:10.1016/S0022-1694(97)00125-X

Han, E., Merwade, V., Heathman, G.C., 2012. Implementation of surface soil moisture data assimilation with watershed scale distributed hydrological model. J. Hydrol. 416, 98–117.

Hansen, J., Ruedy, R., Sato, M., Imhoff, M., Lawrence, W., Easterling, D., Peterson, T., Karl, T., 2001. A closer look at United States and global surface temperature change. J. Geophys. Res. Atmospheres 106, 23947–23963. doi:10.1029/2001JD000354

Hegerl, 2007. Climate Change 2007: The Physical Science Basis. Cambridge University Press, Cambridge, UK and New York, NY.

Hegerl, G.C., von Storch, H., Hasselmann, K., Santer, B.D., Cubasch, U., Jones, P.D., 1996. Detecting Greenhouse-Gas-Induced Climate Change with an Optimal Fingerprint Method. J. Clim. 9, 2281–2306. doi:10.1175/1520-0442(1996)009<2281:DGGICC>2.0.CO;2

Hegerl, G., Zwiers, F., 2011. Use of models in detection and attribution of climate change. Wiley Interdiscip. Rev. Clim. Change 2, 570–591. doi:10.1002/wcc.121

He, H., Zhou, J., Zhang, W., 2008. Modelling the impacts of environmental changes on hydrological regimes in the Hei River Watershed, China. Glob. Planet. Change 61, 175–193.

Hewitson BC, Crane RG, 1996. Climate downscaling: techniques and application. Clim. Res. 07, 85–95.

Hidalgo, H.G., Das, T., Dettinger, M.D., Cayan, D.R., Pierce, D.W., Barnett, T.P., Bala, G., Mirin, A., Wood, A.W., Bonfils, C., Santer, B.D., Nozawa, T., 2009. Detection and Attribution of Streamflow Timing Changes to Climate Change in the Western United States. J. Clim. 22, 3838–3855. doi:10.1175/2009JCLI2470.1

Huang, J.-C., Lin, C.-C., Chan, S.-C., Lee, T.-Y., Hsu, S.-C., Lee, C.-T., Lin, J.-C., 2012. Stream discharge characteristics through urbanization gradient in Danshui River, Taiwan: perspectives from observation and simulation. Environ. Monit. Assess. 184, 5689–5703.

Huang, X., Zhao, J., Li, W., Jiang, H., 2013. Impact of climatic change on streamflow in the upper reaches of the Minjiang River, China. Hydrol. Sci. J. 1–11.

Huo, Z., Feng, S., Kang, S., Li, W., Chen, S., 2008. Effect of climate changes and water-related human activities on annual stream flows of the Shiyang river basin in arid north-west China. Hydrol. Process. 22, 3155–3167. doi:10.1002/hyp.6900

Hyndman, R.J., Koehler, A.B., 2006. Another look at measures of forecast accuracy. Int. J. Forecast. 22, 679–688. doi:10.1016/j.ijforecast.2006.03.001

Intergovernmental Panel on Climate Change, 2007. Fourth Assessment Report: Climate Change 2007: The AR4 Synthesis Report. Geneva: IPCC.

IPCC Technical Paper VI: Climate Change and Water [WWW Document], n.d. . Clim. Change Today. URL http://climatechangetoday.wordpress.com/documentsreports/the-intergovernmental-panel-on-climate-change-ipcc-docs/ipcc-technical-paper-vi-climate-change-and-water/ (accessed 5.21.13).

Javelle, P., Ouarda, T.B., Bobée, B., 2003. Spring flood analysis using the flood-duration–frequency approach: application to the provinces of Quebec and Ontario, Canada. Hydrol. Process. 17, 3717–3736.

Jennings, D.B., Jarnagin, S.T., 2002. Changes in anthropogenic impervious surfaces, precipitation and daily streamflow discharge: a historical perspective in a mid-Atlantic subwatershed. Landsc. Ecol. 17, 471–489.

Jiang, S., Ren, L., Yong, B., Singh, V.P., Yang, X., Yuan, F., 2011. Quantifying the effects of climate variability and human activities on runoff from the Laohahe basin in northern China using three different methods. Hydrol. Process. 25, 2492–2505. doi:10.1002/hyp.8002

Joe, H., 1997. Multivariate Models and Multivariate Dependence Concepts, Chapman & Hall/CRC Monographs on Statistics & Applied Probability. Taylor & Francis.

Johnson, F., Sharma, A., 2012. A nesting model for bias correction of variability at multiple time scales in general circulation model precipitation simulations. Water Resour. Res. 48, n/a–n/a. doi:10.1029/2011WR010464

Jones, R.N., Chiew, F.H.S., Boughton, W.C., Zhang, L., 2006. Estimating the sensitivity of mean annual runoff to climate change using selected hydrological models. Adv. Water Resour. 29, 1419–1429. doi:10.1016/j.advwatres.2005.11.001

Jung, I.-W., Chang, H., 2011. Assessment of future runoff trends under multiple climate change scenarios in the Willamette River Basin, Oregon, USA. Hydrol. Process. 25, 258–277. doi:10.1002/hyp.7842

Kao, S.-C., Govindaraju, R.S., 2007. Probabilistic structure of storm surface runoff considering the dependence between average intensity and storm duration of rainfall events. Water Resour. Res. 43.

Karamouz, M., Noori, N., Moridi, A., Ahmadi, A., 2011. Evaluation of floodplain variability considering impacts of climate change. Hydrol. Process. 25, 90–103. doi:10.1002/hyp.7822

Karl, T.R., Knight, R.W., 1998. Secular Trends of Precipitation Amount, Frequency, and Intensity in the United States. Bull. Am. Meteorol. Soc. 79, 231–241. doi:10.1175/1520-0477(1998)079<0231:STOPAF>2.0.CO;2

Karl, T.R., Knight, R.W., Easterling, D.R., Quayle, R.G., 1996. Indices of Climate Change for the United States. Bull. Am. Meteorol. Soc. 77, 279–292. doi:10.1175/1520-0477(1996)077<0279:IOCCFT>2.0.CO;2

Karmeshu, N., 2012. Trend Detection in Annual Temperature & Precipitation using the Mann Kendall Test–A Case Study to Assess Climate Change on Select States in the Northeastern United States.

Kendall, M.G., 1955. Rank correlation methods. C. Griffin.

Kimeldori, G., Sampson, A., 1975. Uniform representations of bivariate distributions. Commun. Stat. Methods 4, 617–627.

Kittel, T., Giorgi, F., Meehl, G., 1997. Intercomparsion of regional biases and doubled CO2-sensitivity of coupled atmosphere-ocean general circulation model experiments. Clim. Dyn. 14, 1–15.

Klink, C.A., Moreira, A.G., 2002. Past and current human occupation, and land use. Cerrados Bras. Ecol. Nat. Hist. Neotropical Savanna 69–90.

Knutson, T.R., Zeng, F., Wittenberg, A.T., 2013. Multi-Model Assessment of Regional Surface Temperature Trends: CMIP3 and CMIP5 20th Century Simulations. J. Clim. doi:10.1175/JCLI-D-12-00567.1

Kuchment, L.S., 2004. The Hydrological Cycle and Human Impact on it. Water Resour. Manag.

Laaha, G., Blöschl, G., 2007. A national low flow estimation procedure for Austria. Hydrol. Sci. J. 52, 625–644.

Leemans, R., Eickhout, B., 2004. Another reason for concern: regional and global impacts on ecosystems for different levels of climate change. Glob. Environ. Change 14, 219–228.

Legesse, D., Vallet-Coulomb, C., Gasse, F., 2003. Hydrological response of a catchment to climate and land use changes in Tropical Africa: case study South Central Ethiopia. J. Hydrol. 275, 67–85.

Li, L.-J., Zhang, L., Wang, H., Wang, J., Yang, J.-W., Jiang, D.-J., Li, J.-Y., Qin, D.-Y., 2007. Assessing the impact of climate variability and human activities on streamflow from the Wuding River basin in China. Hydrol. Process. 21, 3485–3491. doi:10.1002/hyp.6485

Lins, H.F., Slack, J.R., 1999. Streamflow trends in the United States. Geophys. Res. Lett. 26, 227–230. doi:10.1029/1998GL900291

Lin, Y.-P., Verburg, P.H., Chang, C.-R., Chen, H.-Y., Chen, M.-H., 2009. Developing and comparing optimal and empirical land-use models for the development of an urbanized watershed forest in Taiwan. Landsc. Urban Plan. 92, 242–254.

Liu, D., Chen, X., Lian, Y., Lou, Z., 2010. Impacts of climate change and human activities on surface runoff in the Dongjiang River basin of China. Hydrol. Process. 24, 1487–1495. doi:10.1002/hyp.7609

Liu, X., Ren, L., Yuan, F., Singh, V., Fang, X., Yu, Z., Zhang, W., 2009. Quantifying the effect of land use and land cover changes on green water and blue water in northern part of China. Hydrol. Earth Syst. Sci. 13.

Li, Y., Zhu, L., Zhao, X., Li, S., Yan, Y., 2013. Urbanization Impact on Temperature Change in China with Emphasis on Land Cover Change and Human Activity. J. Clim. 26, 8765–8780. doi:10.1175/JCLI-D-12-00698.1

Li, Z., Liu, W., Zhang, X., Zheng, F., 2009. Impacts of land use change and climate variability on hydrology in an agricultural catchment on the Loess Plateau of China. J. Hydrol. 377, 35–42.

Lubowski, R., Vesterby, M., Bucholtz, S., 2009. AREI Chapter 1.1: Land Use. Econ. Res. Serv. Httpwww Ers Usda Govpublicationsareieib16chapter111 Retrieved 03–09.

Lu, J., Sun, G., McNulty, S.G., Amatya, D.M., 2005. A COMPARISON OF SIX POTENTIAL EVAPOTRANSPIRATION METHODS FOR REGIONAL USE IN THE SOUTHEASTERN UNITED STATES1. JAWRA J. Am. Water Resour. Assoc. 41, 621–633.

MacKay, D.J.C., 2003. Information Theory, Inference and Learning Algorithms. Cambridge University Press.

Ma, H., Yang, D., Tan, S.K., Gao, B., Hu, Q., 2010. Impact of climate variability and human activity on streamflow decrease in the Miyun Reservoir catchment. J. Hydrol. 389, 317–324. doi:10.1016/j.jhydrol.2010.06.010

Maity, R., Ramadas, M., Govindaraju, R.S., 2013. Identification of hydrologic drought triggers from hydroclimatic predictor variables. Water Resour. Res. 49, 4476–4492.

Mann, H.B., 1945. Nonparametric Tests Against Trend. Econometrica 13, 245–259. doi:10.2307/1907187

Mao, D., Cherkauer, K.A., 2009. Impacts of land-use change on hydrologic responses in the Great Lakes region. J. Hydrol. 374, 71–82.

Ma, X., Xu, J., Luo, Y., Prasad Aggarwal, S., Li, J., 2009. Response of hydrological processes to land-cover and climate changes in Kejie watershed, south-west China. Hydrol. Process. 23, 1179–1191.

Ma, Z., Kang, S., Zhang, L., Tong, L., Su, X., 2008. Analysis of impacts of climate variability and human activity on streamflow for a river basin in arid region of northwest China. J. Hydrol. 352, 239–249. doi:10.1016/j.jhydrol.2007.12.022

McCabe, G.J., Wolock, D.M., 2002. A step increase in streamflow in the conterminous United States. Geophys. Res. Lett. 29, 38–1–38–4. doi:10.1029/2002GL015999

Meehl, G.A., Arblaster, J.M., Lawrence, D.M., Seth, A., Schneider, E.K., Kirtman, B.P., Min, D., 2006. Monsoon regimes in the CCSM3. J. Clim. 19, 2482–2495.

Milly, P.C.D., 1994. Climate, soil water storage, and the average annual water balance. Water Resour. Res. 30, 2143–2156. doi:10.1029/94WR00586

Min, S.-K., Zhang, X., Zwiers, F.W., Hegerl, G.C., 2011. Human contribution to more-intense precipitation extremes. Nature 470, 378–381.

Mirabbasi, R., Fakheri-Fard, A., Dinpashoh, Y., 2012. Bivariate drought frequency analysis using the copula method. Theor. Appl. Climatol. 108, 191–206.

Mondal, A., Mujumdar, P.P., 2012. On the basin-scale detection and attribution of human-induced climate change in monsoon precipitation and streamflow. Water Resour. Res. 48, n/a–n/a. doi:10.1029/2011WR011468

Moriasi, D., Arnold, J., Van Liew, M., Bingner, R., Harmel, R., Veith, T., 2007. Model Evaluation Guidelines for Systematic Quantification of Accuracy in Watershed Simulations. Trans. ASABE 50, 885–900.

Mouelhi, S., Michel, C., Perrin, C., Andréassian, V., 2006. Stepwise development of a two-parameter monthly water balance model. J. Hydrol. 318, 200–214. doi:10.1016/j.jhydrol.2005.06.014

Nash, J.E., Sutcliffe, J.V., 1970. River flow forecasting through conceptual models part I — A discussion of principles. J. Hydrol. 10, 282–290. doi:10.1016/0022-1694(70)90255-6

Nelsen, R.B., 2006. An Introduction to Copulas, Springer Series in Statistics. Springer.

Özdemir, A.D., Karaca, Ö., ERKUŞ, M.K., 2007. Low Flow Calculation to Maintain Ecological Balance in Streams, in: International Congress on River Basin Management, Antalya.

Parajuli, P.B., 2010. Assessing sensitivity of hydrologic responses to climate change from forested watershed in Mississippi. Hydrol. Process. 24, 3785–3797.

Parks, B., Madison, R.J., 1985. Estimation of selected flow and water-quality characteristics of Alaskan streams (No. WRI - 84-4247). United States Geological Survey.

Patil, S., Stieglitz, M., 2011. Hydrologic similarity among catchments under variable flow conditions. Hydrol. Earth Syst. Sci. 15.

Percival, D.B., Walden, A.T., 1993. Spectral analysis for physical applications : multitaper and conventional univariate techniques / Donald B. Percival and Andrew T. Walden. Cambridge University Press, Cambridge ; New York, N.Y., U.S.A.

Peters, G.P., Marland, G., Le Quéré, C., Boden, T., Canadell, J.G., Raupach, M.R., 2011. Rapid growth in CO2 emissions after the 2008-2009 global financial crisis. Nat. Clim. Change 2, 2–4.

Peterson, T.C., Vose, R.S., 1997. An Overview of the Global Historical Climatology Network Temperature Database. Bull. Am. Meteorol. Soc. 78, 2837–2849. doi:10.1175/1520-0477(1997)078<2837:AOOTGH>2.0.CO;2

Pettitt, A.N., 1979. A Non-Parametric Approach to the Change-Point Problem. J. R. Stat. Soc. Ser. C Appl. Stat. 28, 126–135. doi:10.2307/2346729

Pierce, D.W., Barnett, T.P., Hidalgo, H.G., Das, T., Bonfils, C., Santer, B.D., Bala, G., Dettinger, M.D., Cayan, D.R., Mirin, A., Wood, A.W., Nozawa, T., 2008. Attribution of Declining Western U.S. Snowpack to Human Effects. J. Clim. 21, 6425–6444. doi:10.1175/2008JCLI2405.1

Pierce, D.W., Barnett, T.P., Santer, B.D., Gleckler, P.J., 2009. Selecting global climate models for regional climate change studies. Proc. Natl. Acad. Sci. 106, 8441–8446. doi:10.1073/pnas.0900094106

Plackett, R.L., 1965. A class of bivariate distributions. J. Am. Stat. Assoc. 60, 516–522.

Pongratz, J., Reick, C., Raddatz, T., Claussen, M., 2008. A reconstruction of global agricultural areas and land cover for the last millennium. Glob. Biogeochem. Cycles 22.

Porporato, A., Daly, E., Rodriguez-Iturbe, I., 2004. Soil water balance and ecosystem response to climate change. Am. Nat. 164, 625–632. doi:10.1086/424970

Postel, S.L., Daily, G.C., Ehrlich, P.R., 1996. Human Appropriation of Renewable Fresh Water. Science 271, 785–788. doi:10.1126/science.271.5250.785

Price, K., Jackson, C.R., Parker, A.J., Reitan, T., Dowd, J., Cyterski, M., 2011. Effects of watershed land use and geomorphology on stream low flows during severe drought conditions in the southern Blue Ridge Mountains, Georgia and North Carolina, United States. Water Resour. Res. 47.

Prudhomme, C., Wilby, R.L., Crooks, S., Kay, A.L., Reynard, N.S., 2010. Scenario-neutral approach to climate change impact studies: Application to flood risk. J. Hydrol. 390, 198–209. doi:10.1016/j.jhydrol.2010.06.043

Pyrce, R., 2004. Hydrological low flow indices and their uses. Watershed Sci. CentreWSC Rep.

Quintana Seguí, P., Ribes, A., Martin, E., Habets, F., Boé, J., 2010. Comparison of three downscaling methods in simulating the impact of climate change on the hydrology of Mediterranean basins. J. Hydrol. 383, 111–124. doi:10.1016/j.jhydrol.2009.09.050

Raghavan, S.V., Vu, M.T., Liong, S.-Y., 2012. Assessment of future stream flow over the Sesan catchment of the Lower Mekong Basin in Vietnam. Hydrol. Process. 26, 3661–3668. doi:10.1002/hyp.8452

Ray, D.K., Pijanowski, B.C., 2010. A backcast land use change model to generate past land use maps: application and validation at the Muskegon River watershed of Michigan, USA. J. Land Use Sci. 5, 1–29.

Rientjes, T., Haile, A., Mannaerts, C., Kebede, E., Habib, E., 2010. Changes in land cover and stream flows in Gilgel Abbay catchment, Upper Blue Nile basin–Ethiopia. Hydrol. Earth Syst. Sci. Discuss. 7, 9567–9598.

Rostamian, R., Jaleh, A., Afyuni, M., Mousavi, S.F., Heidarpour, M., Jalalian, A., Abbaspour, K.C., 2008. Application of a SWAT model for estimating runoff and sediment in two mountainous basins in central Iran. Hydrol. Sci. J. 53, 977–988.

Santer, B.D., Mears, C., Doutriaux, C., Caldwell, P., Gleckler, P.J., Wigley, T.M.L., Solomon, S., Gillett, N.P., Ivanova, D., Karl, T.R., Lanzante, J.R., Meehl, G.A., Stott, P.A., Taylor, K.E., Thorne, P.W., Wehner, M.F., Wentz, F.J., 2011. Separating signal and noise in atmospheric temperature changes: The importance of timescale. J. Geophys. Res. Atmospheres 116, n/a–n/a. doi:10.1029/2011JD016263

Santer, B.D., Mears, C., Wentz, F.J., Taylor, K.E., Gleckler, P.J., Wigley, T.M.L., Barnett, T.P., Boyle, J.S., Brüggemann, W., Gillett, N.P., Klein, S.A., Meehl, G.A., Nozawa, T., Pierce, D.W., Stott, P.A., Washington, W.M., Wehner, M.F., 2007. Identification of human-induced changes in atmospheric moisture content. Proc. Natl. Acad. Sci. 104, 15248–15253. doi:10.1073/pnas.0702872104

Santer, B.D., Mikolajewicz, U., Brüggemann, W., Cubasch, U., Hasselmann, K., Höck, H., Maier-Reimer, E., Wigley, T.M.L., 1995. Ocean variability and its influence on the detectability of greenhouse warming signals. J. Geophys. Res. Oceans 100, 10693–10725. doi:10.1029/95JC00683

Savary, S., Rousseau, A.N., Quilbé, R., 2009. Assessing the effects of historical land cover changes on runoff and low flows using remote sensing and hydrological modeling. J. Hydrol. Eng. 14, 575–587.

Scanlon, B.R., Jolly, I., Sophocleous, M., Zhang, L., 2007. Global impacts of conversions from natural to agricultural ecosystems on water resources: Quantity versus quality. Water Resour. Res. 43.

Sen, P.K., 1968. Estimates of the Regression Coefficient Based on Kendall's Tau. J. Am. Stat. Assoc. 63, 1379–1389. doi:10.1080/01621459.1968.10480934

Setegn, S.G., Srinivasan, R., Melesse, A.M., Dargahi, B., 2010. SWAT model application and prediction uncertainty analysis in the Lake Tana Basin, Ethiopia. Hydrol. Process. 24, 357–367.

Shiau, J.-T., Modarres, R., 2009. Copula-based drought severity-duration-frequency analysis in Iran. Meteorol. Appl. 16, 481–489.

Shiau, J.-T., Shen, H.W., 2001. Recurrence analysis of hydrologic droughts of differing severity. J. Water Resour. Plan. Manag. 127, 30–40.

Shukla, S., Wood, A.W., 2008. Use of a standardized runoff index for characterizing hydrologic drought. Geophys. Res. Lett. 35.

Siriwardena, L., Finlayson, B.L., McMahon, T.A., 2006. The impact of land use change on catchment hydrology in large catchments: The Comet River, Central Queensland, Australia. J. Hydrol. 326, 199–214.

Sivanandam, S.N., Deepa, S.N., 2007. Introduction to Genetic Algorithms, 2008th ed. Springer.

Sklar, A., 1959. Fonctions de Répartition À N Dimensions Et Leurs Marges. Université Paris 8.

Smakhtin, V., 2001. Low flow hydrology: a review. J. Hydrol. 240, 147–186.

Storck, P., Bowling, L., Wetherbee, P., Lettenmaier, D., 1998. Application of a GIS-based distributed hydrology model for prediction of forest harvest effects on peak stream flow in the Pacific Northwest. Hydrol. Process. 12, 889–904.

Strauch, M., Bernhofer, C., Koide, S., Volk, M., Lorz, C., Makeschin, F., 2012. Using precipitation data ensemble for uncertainty analysis in SWAT streamflow simulation. J. Hydrol. 414, 413–424.

Theil, H., 1950. A rank-invariant method of linear and polynomial regression analysis, 3; confidence regions for the parameters of polynomial regression equations, in: Proceedings KNAW.

Tian, F., Yang, Y., Han, S., 2009. Using runoff slope-break to determine dominate factors of runoff decline in Hutuo River Basin, North China. Water Sci. Technol. J. Int. Assoc. Water Pollut. Res. 60, 2135–2144. doi:10.2166/wst.2009.578

Tran, L.T., O'Neill, R.V., 2013. Detecting the effects of land use/land cover on mean annual streamflow in the Upper Mississippi River Basin, {USA}. J. Hydrol. 499, 82 – 90. doi:http://dx.doi.org/10.1016/j.jhydrol.2013.06.041

United States Geological Survey (USGS), 2009. Water-Resources Data for the United States Water Year 2007.

Van Aalst, M.K., 2006. The impacts of climate change on the risk of natural disasters. Disasters 30, 5–18.

Van Lanen, H.A., Wanders, N., 2011. High Flows in the 21st Century: Analysis with a Simple Conceptual Hydrological Model Using the Input of 3 GCMS (A2 Scenario). WATCH.

Vaze, J., Davidson, A., Teng, J., Podger, G., 2011. Impact of climate change on water availability in the Macquarie-Castlereagh River Basin in Australia. Hydrol. Process. 25, 2597–2612. doi:10.1002/hyp.8030

Vogel, R., 2011. Hydromorphology. J. Water Resour. Plan. Manag. 137, 147–149. doi:10.1061/(ASCE)WR.1943-5452.0000122

Wagener, T., Sivapalan, M., Troch, P.A., McGlynn, B.L., Harman, C.J., Gupta, H.V., Kumar, P., Rao, P.S.C., Basu, N.B., Wilson, J.S., 2010. The future of hydrology: An evolving science for a changing world. Water Resour. Res. 46, n/a–n/a. doi:10.1029/2009WR008906

Wang, D., Hejazi, M., 2011. Quantifying the relative contribution of the climate and direct human impacts on mean annual streamflow in the contiguous United States. Water Resour. Res. 47, n/a–n/a. doi:10.1029/2010WR010283

Wang, J., Hong, Y., Gourley, J., Adhikari, P., Li, L., Su, F., 2010. Quantitative assessment of climate change and human impacts on long-term hydrologic response: a case study in a sub-basin of the Yellow River, China. Int. J. Climatol. 30, 2130–2137. doi:10.1002/joc.2023

Wang, S., Yan, Y., Yan, M., Zhao, X., 2012. Quantitative estimation of the impact of precipitation and human activities on runoff change of the Huangfuchuan River Basin. J. Geogr. Sci. 22, 906–918. doi:10.1007/s11442-012-0972-8

Wang, X., Melesse, A.M., 2006. EFFECTS OF STATSGO AND SSURGO AS INPUTS ON SWAT MODEL'S SNOWMELT SIMULATION1. JAWRA J. Am. Water Resour. Assoc. 42, 1217–1236.

Whitney, G.G., 1996. From Coastal Wilderness to Fruited Plain: A History of Environmental Change in Temperate North America from 1500 to the Present. Cambridge University Press.

Wilby, R.L., Harris, I., 2006. A framework for assessing uncertainties in climate change impacts: Low-flow scenarios for the River Thames, UK. Water Resour. Res. 42.

Wilcox, R.R., 2001. Fundamentals of Modern Statistical Methods: Substantially Improving Power and Accuracy. Springer Verlag.

Wilks, D.S., 2006. Statistical Methods in the Atmospheric Sciences: An Introduction, International Geophysics Series. Elsevier Academic Press.

Winchell M., Srinivasan, R., Di Luzio, M., 2007. ArcSWAT interface for SWAT2005 - User's Guide.

Wood, A.W., Leung, L.R., Sridhar, V., Lettenmaier, D.P., 2004. Hydrologic Implications of Dynamical and Statistical Approaches to Downscaling Climate Model Outputs. Clim. Change 62, 189–216. doi:10.1023/B:CLIM.0000013685.99609.9e

Wu, C.S., Yang, S.L., Lei, Y., 2012. Quantifying the anthropogenic and climatic impacts on water discharge and sediment load in the Pearl River (Zhujiang), China (1954–2009). J. Hydrol. 452–453, 190–204. doi:10.1016/j.jhydrol.2012.05.064

Xu, R., Wunsch, D., I., 2005. Survey of clustering algorithms. IEEE Trans. Neural Netw. 16, 645–678. doi:10.1109/TNN.2005.845141

Yang, G., Bowling, L.C., Cherkauer, K.A., Pijanowski, B.C., Niyogi, D., 2010. Hydroclimatic response of watersheds to urban intensity: an observational and modeling-based analysis for the White River Basin, Indiana. J. Hydrometeorol. 11, 122–138.

Ye, B., Yang, D., Kane, D.L., 2003. Changes in Lena River streamflow hydrology: Human impacts versus natural variations. Water Resour. Res. 39, n/a–n/a. doi:10.1029/2003WR001991

Yevjevich, V.M., , Colorado State University., Hydrology and Water Resources Program., 1967. An objective approach to definitions and investigations of continental hydrologic droughts. Colorado State University, Fort Collins.

Zelenhasić, E., Salvai, A., 1987. A method of streamflow drought analysis. Water Resour. Res. 23, 156–168.

Zhang, A., Zhang, C., Fu, G., Wang, B., Bao, Z., Zheng, H., 2012. Assessments of Impacts of Climate Change and Human Activities on Runoff with SWAT for the Huifa River Basin, Northeast China. Water Resour. Manag. 26, 2199–2217. doi:10.1007/s11269-012-0010-8

Zhang, B., Govindaraju, R.S., 2000. Prediction of watershed runoff using Bayesian concepts and modular neural networks. Water Resour. Res. 36, 753–762. doi:10.1029/1999WR900264

Zhang, L., Dawes, W.R., Walker, G.R., 2001. Response of mean annual evapotranspiration to vegetation changes at catchment scale. Water Resour. Res. 37, 701–708. doi:10.1029/2000WR900325

Zhang, L., Singh, V., 2006. Bivariate flood frequency analysis using the copula method. J. Hydrol. Eng. 11, 150–164.

Zhang, Q., Li, J., Chen, Y.D., Chen, X., 2011. Observed changes of temperature extremes during 1960–2005 in China: natural or human-induced variations? Theor. Appl. Climatol. 106, 417–431. doi:10.1007/s00704-011-0447-3

Zhang, Q., Xiao, M., Singh, V.P., Li, J., 2012. Regionalization and spatial changing properties of droughts across the Pearl River basin, China. J. Hydrol. 472, 355–366.

Zhang, X., Zhang, L., Zhao, J., Rustomji, P., Hairsine, P., 2008. Responses of streamflow to changes in climate and land use/cover in the Loess Plateau, China. Water Resour. Res. 44.

Zhang, X., Zwiers, F.W., Hegerl, G.C., Lambert, F.H., Gillett, N.P., Solomon, S., Stott, P.A., Nozawa, T., 2007. Detection of human influence on twentieth-century precipitation trends. Nature 448, 461–465.

Zhang, Y.-K., Schilling, K., 2006. Increasing streamflow and baseflow in Mississippi River since the 1940s: Effect of land use change. J. Hydrol. 324, 412–422.

Zheng, J., Yu, X., Deng, W., Wang, H., Wang, Y., 2012. Sensitivity of Land-Use Change to Streamflow in Chaobai River Basin. J. Hydrol. Eng. 18, 457–464.

Zhou, F., Xu, Y., Chen, Y., Xu, C.-Y., Gao, Y., Du, J., 2013. Hydrological response to urbanization at different spatio-temporal scales simulated by coupling of CLUE-S and the SWAT model in the Yangtze River Delta region. J. Hydrol. 485, 113–125.

Zhou, T., Wu, J., Peng, S., 2012. Assessing the effects of landscape pattern on river water quality at multiple scales: A case study of the Dongjiang River watershed, China. Ecol. Indic. 23, 166–175. doi:10.1016/j.ecolind.2012.03.013

VITA

VITA

Kuk Hyun Ahn was born in Chungju, Republic of Korea (South Korea). He graduated with a B.S in Department of Civil Engineering in 2007 from University of Seoul, Seoul, Korea. He received his M.S. degree in Civil and Construction Engineering from Seoul National University, Seoul, Korea in 2010. He joined the graduate program in Civil Engineering at Purdue University in 2011 and received Doctor of Philosophy degree in December, 2014.